Shahid Mehmood

Experimental and Theoretical Investigation of Thermophysical Properties of Platinum Alloys in the Solid and the Liquid Regions

DOCTORAL THESIS

For obtaining the academic degree of

Doktor der technischen Wissenschaften

Doctoral Programme of Technical Sciences
Technical Physics

Graz University of Technology

Supervisor:

Univ.-Prof. Dipl.-Ing. Dr.techn. Gernot Pottlacher

Institute of Experimental Physics Graz, Austria

April 2012

Deutsche Fassung:
Beschluss der Curricula-Kommission für Bachelor-, Master- und Diplomstudien vom 10.11.2008
Genehmigung des Senates am 1.12.2008

EIDESSTATTLICHE ERKLÄRUNG

Ich erkläre an Eides statt, dass ich die vorliegende Arbeit selbstständig verfasst, andere als die angegebenen Quellen/Hilfsmittel nicht benutzt, und die den benutzten Quellen wörtlich und inhaltlich entnommene Stellen als solche kenntlich gemacht habe.

Graz, am ……. ……..
(Unterschrift)

Englische Fassung:

STATUTORY DECLARATION

I declare that I have authored this thesis independently, that I have not used other than the declared sources / resources, and that I have explicitly marked all material which has been quoted either literally or by content from the used sources.

……. ……..
date (signature)

Dedicated To My Parents, Teachers and Family

Abstract (English)

Platinum and copper along with their alloys have been used in a broad range of applications like jewellery, coinage, electrical and electronic devices and many others. Their thermophysical properties such as density, heat capacity, thermal conductivity and surface tension play an important role in casting processes and are required as input data for casting simulation. The goal of this work is to investigate these properties by different methods and to simulate and predict these properties through modeling. Platinum, copper and six platinum alloys namely: Pt95Co05, Pt95Ru05, Pt96Cu04, Pt68Cu32, Pt50Cu50 and Pt25Cu75 were investigated within this work by pulse heating technique and compared with the results of fem Schwaebisch Gmuend, Germany by DSC and dilatometry, respectively.

The pulse heating technique delivers thermophysical properties of electrically conducting materials in the solid and the liquid phase. Samples are resistively volume heated as part of a fast capacitor discharge circuit, heating rates up to 10^8 $K \cdot s^{-1}$ are achieved and the samples reach the liquid phase about 30 µs after starting the experiment. Time resolved electrical measurements with sub-µs resolution allow the calculation of specific heat capacity and temperature dependencies of electrical resistivity, enthalpy, and density of these alloys in the solid and liquid phases. Thermal conductivity and thermal diffusivity as a function of temperature are estimated from resistivity data using the Wiedemann-Franz-law for temperature regions between several hundreds of degrees below and above the corresponding solidus and liquidus temperatures.

Model calculations for specific heat and thermal conductivities of three alloy series (PtCu, FeNi and CuNi) in the solid (up to melting point) and liquid region have been performed respectively to get a deeper insight of their thermodynamical behavior based on temperature-dependent experimental data obtained by an ohmic pulse heating technique. For such calculations it is of special importance to choose model functions which are both physically relevant and numerically robust.

The specific heat at constant volume is calculated for the alloy series including both lattice and electronic contribution to it. The lattice contribution is done at high

temperature using Dulong- Petit law whereas electronic contribution is calculated using band structure calculation or Sommerfeld approximation.

Three different models namely: T_o, q and η model, are proposed for the prediction of effective thermal conductivities of alloy series taking into account the thermal conductivities of the constituents, the temperature, and a fit parameter. It is observed that the values of the effective thermal conductivity predicted by the models are in agreement with the experimentally determined thermal conductivities by the pulse heating technique within maximum deviations of 10%.

Abstract (Deutsch)

Platin und Kupfer sowie deren Legierungen werden in einem weiten Anwendungsgebiet z.B. in der Schmuckindustrie, für Münzen und für elektronische Bauteile verwendet. Thermophysikalische Eigenschaften wie Dichte, spezifische Wärmekapazität, Temperaturleitfähigkeit und Oberflächenspannung haben einen wesentlichen Einfluss auf Gießprozesse und werden als Eingangsparameter für Gusssimulationen benötigt. Das Ziel dieser Arbeit ist es diese thermophysikalischen Eigenschaften experimentell zu untersuchen und darüber hinaus mit verschiedenen Modellen diese Eigenschaften auch vorherzusagen. Platin, Kupfer und sechs Platin Kupfer Legierungen: Pt95Cu05, Pt95Co05, Pt96Cu4, Pt68Cu32, Pt50Cu50 und Pt25Cu75 wurden in dieser Arbeit mit Hilfe der Ohm´schen Pulsheiztechnik untersucht und die Ergebnisse mit DSC und Dilatometriemessungen, durchgeführt am fem in Schwäbisch Gmünd, Deutschland, verglichen.

Die Pulsheiztechnik liefert thermophysikalische Eigenschaften von elektrisch leitenden Materialien in fester und flüssiger Phase. Die Proben werden durch den elektrischen Widerstand volumsgeheizt und sind ein Teil eines schnellen Kondensatorentladungskreises. Mit Heizraten von 10^8 K/s werden die Drahtproben innerhalb von 30 µs nach dem Start des Experiments bis in die flüssige Phase geheizt. Zeitaufgelöste elektrische Messungen mit sub-µs Zeitauflösung von Strom und Spannung erlauben die Ermittlung spezifischer Wärmekapazität, elektrischem Widerstand, Enthalpie und Dichte der obengenannten Proben ab Funktion der Temperatur in der festen und der flüssigen Phase. Wärmeleitfähigkeit und Temperaturleitfähigkeit als Funktion der Temperatur werden mit Hilfe des Wiedemann-Franz Gesetzes aus den elektrischen Daten in einem Temperaturbereich unterhalb und oberhalb des Schmelzens abgeschätzt.

Modellrechnungen für spezifische Wärmekapazität und Temperaturleitfähigkeit für 3 Serien von Legierungen (PtCu, FeNi und CuNi) im festen bis zum Schmelzen und in der flüssigen Phase basierend auf den experimentellen Daten wurden durchgeführt. Für solche Berechnungen ist es besonders wichtig Modellfunktionen zu wählen die einerseits physikalisch relevant und andererseits numerisch robust sind.

Die spezifische Wärmekapazität bei konstanten Volumen wird für diese Legierungen berechnet wobei sowohl Gitter als auch elektronische Beiträge berechnet werden. Der Gitterbeitrag wird bei hohen Temperaturen abgeschätzt unter Verwendung des Dulong-Petit Gesetzes, die elektronischen Beiträge werden abgeschätzt über Bandstrukturrechnungen einerseits und andererseits über die Sommerfeldnäherung. Der Unterschied zwischen den experimentell erhaltenen c_p Werten und den theoretisch erhaltenen c_v Werten rührt eventuell von anharmonischen Gittereffekten her.

Drei verschiedene Modelle und zwar das T_o, dass *q* und das η Modell wurden für die Vorhersage der thermischen Leitfähigkeiten von Legierungsserien vorgeschlagen, wobei dafür die thermischen Leitfähigkeiten der Konstituenten, die Temperatur und ein Fit-Parameter berücksichtigt wurden. Es wird beobachtet, dass die Werte der durch die Modelle vorhergesagten thermischen Leitfähigkeiten in Übereinstimmung mit dem experimentell durch die Pulsheizung ermittelten Daten innerhalb von 10% liegt.

Declaration

This dissertation is submitted to the Institute of Experimental Physics, Graz University of Technology, Graz Austria, in partial fulfillment of the requirement for the degree of Doctor of Technical Sciences.
The thesis is entitled:

Experimental and Theoretical Investigation of Thermophysical Properties of Platinum Alloys in the Solid and the Liquid Regions

written by Shahid Mehmood and has been approved by the Institute of Experimental Physics, Graz University of Technology, Graz Austria.

The final copy of this thesis has been examined by the under signed authority, and find that both the content and the form meet acceptable presentation standards of scholarly work in the above mentioned discipline.

_____

Univ. Prof. Dip.-Ing. Dr. tech. Gernot Pottlacher

Date _____

Contents

CHAPTER 5

Thermophysical Properties and Data Evaluation

CHAPTER 6

Experimental Results and Discussions

CHAPTER 10

Uncertainty Analysis

Chapter 1

Introduction

In the last few decades, metal and alloy industry has enhanced its effort to improve product quality and raise production processes. In particular, casting and moulding processes have been improved tremendously. Fast computers and finite-element casting simulations are commonly used for better understanding and control of the solidification process of metals. The success of these numerical simulations is dependent on the precise knowledge of thermophysical properties of metals and alloys. Thermophysical properties, such as thermal conductivity, thermal diffusivity, specific heat or density change in the solid, liquid, or mushy zones, are important parameters for the accuracy of casting simulations. These properties are well known for many pure metals, but not for the innumerable different alloys. For most alloys, thermophysical properties cannot be found in literature. Therefore, measurements have to be carried out in order to achieve the highest possible accuracy of numerical simulations.

Two different techniques have been used to measure thermophysical properties of Pt alloys to support and develop models for the casting industry. The first one is a conventional steady state technique at fem, Schwaebisch Gemünd Germany and other is a pulse heating technique at TUG Graz, Austria. At fem DTA and dilatometric measurements were performed with a Netzsch STA 449C and Netzsch DIL 402C with a heating rate of 20 K/min and 5 K/min respectively from room temperature to a maximum temperature of about 1600 K. The results are extended by both techniques and compared. The electrical pulse heating technique has been used to measure thermophysical properties of a wide range of electrically conducting elements in the solid and liquid states. With this technique, better results have been obtained for both pure metals as well as for alloys of technical interest.

The dynamic technique was used because static techniques, which are capable of greater precision, fail at high temperatures. Compared to steady-state or quasi-steady-state techniques, the dynamic technique has a number of advantages to offer, particularly at higher temperatures and in the liquid state. This is where problems such as increased heat transfer, chemical reactions, evaporation, loss of mechanical strength, etc. may have a

significant impact on the quality of the acquired data. These limitations can be overcome by making the experimental measurement duration short enough. Despite the high heating rate (on the order of 10^8 $K \cdot s^{-1}$), the measured results agree well with data obtained by static and quasistatic methods.

The data obtained by our measurements are of great interest for the metalworking industry, i.e. as input data for computer simulations to model liquid metal processing operations such as casting or welding. The data are used to understand and design processing equipment and facilities such as the growth of single crystals from the melt, to obtain more accurate phase diagrams, for better assessment of potential accidents in the design of safer nuclear reactors, for aerospace techniques, or just for fundamental materials research reasons and in jewellery industry.

Platinum is a precious element and its alloys are commonly used in jewellery. Platinum-jewellery is usually produced by investment casting starting from wax models. Platinum is much more difficult to cast than other jewellery alloys like silver or gold because of its high melting temperature, large shrinkage during freezing, low thermal conductivity, high surface tension and high viscosity. As a result, casters are confronted with relatively high reject rates. Hence to resolve these difficulties, a detailed study of thermophysical properties of solid and liquid platinum and its alloys is done within the present work. These thermophysical properties, mainly of the melting transition and the subsequent liquid phase will be used as input data for casting simulations. The investigated materials are pure platinum, pure copper, PtCu series, PtCo and PtRu, their compositions with the corresponding solidus and liquidus temperatures along with their densities are shown in Table 1.1. The compositions are given in weight percent as shown in the binary phase diagrams of Figure 1.1, Figure 1.2 and Figure 1.3 which are actually redrawn from Hansen and calculated by ThermoCalc SNOB1 database [1, 2].

1.1. Introduction to Samples

The platinum alloy samples were prepared by vacuum induction melting and casting into copper molds. Rods of 3 mm in diameter and a length of 80 mm were prepared and drawn to wires of 0.5 mm in diameter.

Table 1.1. Properties of investigated alloys. T_s and T_l are solidus and liquidus temperatures and d is density at room temperature [3].

Metal / Alloy	T_s / K	T_l / K	d / $kg.m^{-3}$
Pt	2042		21450 [4]
Pt96Cu04	1976	1986	20350
Pt68Cu32	1639	1686	14742
Pt50Cu50	1519	1540	12519
Pt25Cu75	1415	1460	10406
Pt95Co05	1949	1964	19869
Pt95Ru05	2013	2025	20720
Cu	1356		8960 [5]

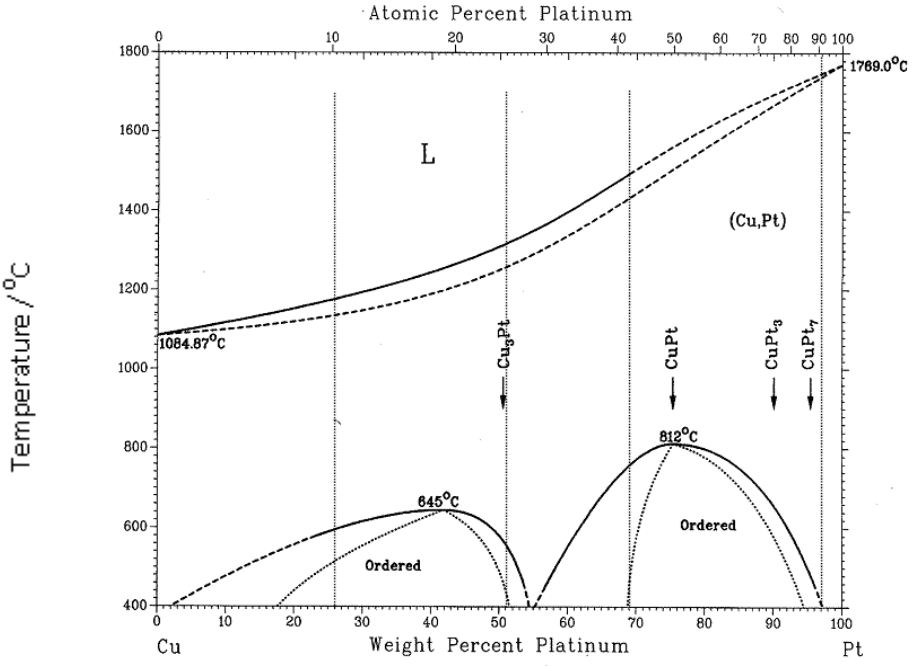

Figure 1.1. Binary phase diagram (weight percent) of investigated alloys, Pt96Cu04, Pt68Cu32, Pt50Cu50 and Pt25Cu75 redrawn from Hansen [1]. The vertical dashed lines indicate the compositions and corresponding solidus and liquidus values of investigated alloys.

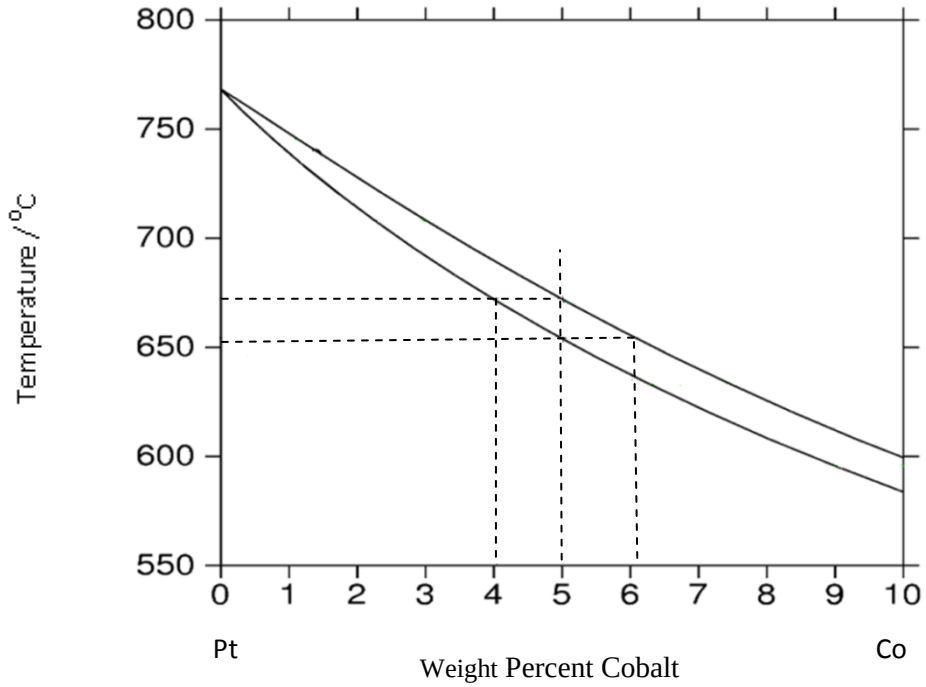

Figure 1.2. Binary phase diagram (weight percent) of investigated alloy, Pt95Co05 [2]. The vertical dashed lines indicate the compositions and corresponding solidus and liquidus values of investigated alloys.

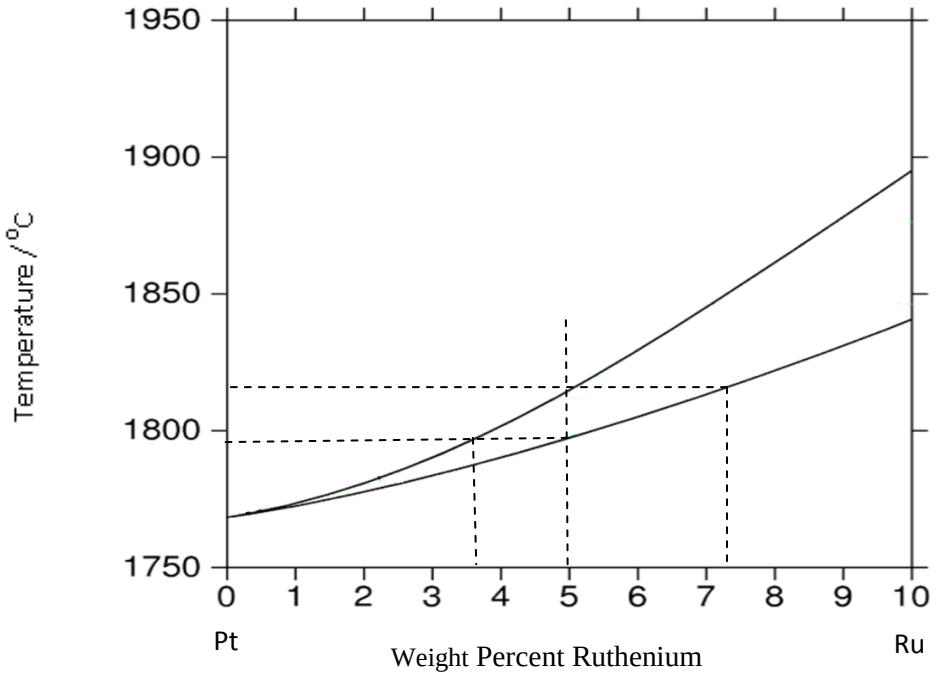

Figure 1.3. Binary phase diagram (weight percent) of investigated alloy, Pt95Ru05 [2]. The vertical dashed lines indicate the compositions and corresponding solidus and liquidus values of investigated alloys.

1.2. Common Properties of Investigated Alloyed Metals

Copper, platinum, ruthenium and cobalt have distinct characteristics. Some of the prominent properties of these metals are given in the following paragraphs:

Copper is a versatile metal of reddish-brown colour and a well known transition metal. The intrinsic properties of copper such as excellent electrical and thermal conductivity, high reflectivity, malleability and ductility make it a good material choice for a wide range of industrial applications like jewellery, coinage, decorative elements in architecture, electrical and electronic devices, contact paths on electrical circuit boards, capacitor components and plating among many others. It can easily be formed into a variety of shapes, from ingots to wire, coins, sheets, or rods. It is resistant to weak acids, but will dissolve in strong acids. Copper resists better to atmospheric corrosion than iron does. Copper, after silver, is an excellent conductor of electricity [6].

On the other hand platinum is a precious metal and belongs to the group of platinum metals. Pure platinum is a high density silvery-whitish lustrous ductile metal with low electrical resistivity and comparatively low thermal conductivity. Its crystal structure is face-centered cubic (f.c.c.). It is shiny, forge and workable and founds in the crust of the earth with a frequency of approximately 0.001 part per million (ppm). Platinum is attacked neither by oxygen nor by water and is insoluble in all acids with the exception of aqua regia or melted alkalis. Platinum is employed as material in large areas of the thermodynamic temperature scale ITS-90 in platinum resistance thermometers. Platinum is used in many fields such as in weights and standard measures, in the electronic industry it is used for electric contacts which can be exposed to high temperatures and its alloys are commonly used in jewellery [7].

Ruthenium is a hard transition metal belonging to the platinum group and has a silvery white colour with seven isotopes. The most common use of it is to improve certain properties of the alloys. When alloyed with gold it increases the stability of gold in the jewelry. Ruthenium is very effective in hardening platinum and palladium for making electrical contacts which are highly wear resistant. Ruthenium is utilized in the production of turbine blades in jet engines. Ruthenium as a catalyst can be used to remove hydrogen sulfide from oil refineries. In research on solar energy, ruthenium complexes are used because they can absorb light in the entire visible spectrum. One of

the recent important usages of ruthenium is its anti-cancer property. It is more effective on certain tumors than the complexes of platinum. It is a very toxic metal and can affect human skin very strongly [8].

Cobalt is a bluish steel-gray coloured brittle metal with many uses in science and industry. Pure cobalt is not found in nature, but compounds of cobalt are common. It is only malleable when alloyed with other metals. Cobalt possesses natural magnetic properties. When alloyed with aluminum, iron and nickel it shows a high coercive force (‘‘alnico” metal). Whereas when alloyed with iron it acts as soft magnet, in which cobalt increases the Curie temperature and the saturation magnetization of iron. Cobalt is also alloyed with 95% platinum for jewelry purposes, producing an alloy that is suitable for fine detailed casting which is weakly magnetic.

Addition of cobalt in an alloy increases the solidus temperature and enhances hot hardness and temperature resistance. Alloys of cobalt are offering exceptional hardness hence exhibit corrosion and wear resistance and find applications in cutting and machining tools. Cobalt alloys are also used for dental prosthetics because of its light weight and resistance to corrosion. Its high temperature resistance also makes it a suitable material for components of turbochargers. Glass with 0.5% Co is very suitable for camera lenses. Alloys of cobalt are well established in high-temperature gas turbine industry, Co-60 is used as an agent against cancer in radiotherapy (‘‘cobalt therapy”). Longtime exposure to cobalt powder may cause allergic reaction and chronic bronchitis. Cobalt is an essential element for life on earth, and is important for both humans and animals [9, 10].

1.3. Employed Thermophysical Parameters

Thermal Conductivity and Heat Capacity

There are many situations in design or in process modeling where it would be useful to know thermal conductivity and specific heat of the material being used, and how these would change as a function of temperature. Despite the broad scientific and technological interest, heat capacity and thermal conductivity at very high temperatures are very difficult to measure because of experimental problems.

Thermal conductivity controls the magnitude of the temperature gradients which occur in components during manufacturing. In structural components which are subjected to thermal cycling, these temperature gradients produce thermal stresses. Thermal conductivity controls the size of the desired microstructure, since transformation depends on cooling rate and temperature.

Thermal conductivity depends upon many factors such as the thermal conductivities of constituent phases, their corresponding volume fractions, the contact areas, distribution within the medium, the shape of particles and the type of packing.

Thermal conductivity of alloys is modeled in this research work in terms of easily measureable parameters. Three different models namely: T_0-model, q-model and η-model are proposed for the prediction of effective thermal conductivities of binary alloy series as a function of temperature, while taking into account the thermal conductivities of the constituents and a fit parameter.

A suitable model of thermal conductivity should help to improve the design of material and the understanding of heat treatment, solidification and welding processes, design of material structures and components, and prediction of thermo-mechanical fatigue. Some models are primarily intended to reproduce known data. In other cases the purpose is to make a prediction outside the range of knowledge or to establish details in a physical mechanism. Whatever the purpose may be, we would like to know how accurately the model can account for the real situation. The original motivation of the author was to estimate thermal conductivity of a range of alloys in the liquid region of the material. The models presented here are developed using a previously developed model that was used for non conducting materials but here it has been modified for conducting materials like metals and alloys.

An exact theoretical estimation of the high temperature heat capacity of transition metals has largely been lacking. It has been called into question recently whether such estimation in terms of existing theories of electrons and lattice vibrations is at all adequate. In fact, the analysis is difficult because simple analytic models give a linear temperature dependence of the electronic heat capacity and the low-order anharmonic effects, which are insufficient at high temperatures. Furthermore, experimental data are uncertain near the melting temperature, and are sometimes not sufficient. Despite all of

this, experiments have improved considerably during the last decade. For example, the uncertainty in the experimentally determined c_p values of many transition metals in the liquid region is less than 5%, and also data on the bulk modulus and the thermal expansion are available accurately enough to use for a meaningful analysis.

Theoretical models are usually concerned with a fixed volume V_o (volume at 298 K), thus nullify the effects due to the thermal expansion. The quantity c_v is generally evaluated by subtracting a term from c_p that accounts for the expansion of the solid. In this work we shall specifically be concerned with specific heat at fixed volume V_o of some transition metals, up to their melting temperature. We selected PtCu, FeNi and CuNi series, shown in Table 1.1, Table 1.2 and Table 1.3 for model calculation and compared them with their experimentally evaluated c_p values. To estimate lattice contribution in the high temperate range, Dulong-Petit law is applied. Whereas electronic contribution is done by electron density of states (DOS) determination applying band structure calculations. The shape of the electron density of states of the solid (bcc) phase, with a deep and broad minimum around the Fermi level, stabilizes the solid relative to the liquid and pushes up the melting temperature.

Speed of Sound and Bulk Modulus

The speed of sound is an important thermodynamic parameters and accurate measurements of the speed of sound c can be used to study the equation of state of a fluid. Conventionally, knowledge of the equation-of-state is obtained from (p, V, T) measurements which inherently have a number of significant systematic errors, some but not all of which may be reduced by more sophisticated experimental techniques [11]. The speed of sound information may be utilized to evaluate any proposed form of equation of state or assist in the optimization of an existing (p, V, T) surface for a particular application. Several different techniques for measurement of c in the fluid phase have been evolved. In this work, speed of sound measurements from Hixson et al has been exploited to evaluate many additional thermodynamics properties such as: adiabatic bulk modulus, adiabatic compressibility, specific heats ratio, isothermal bulk modulus, isothermal compressibility, Grüneisen gamma and specific heat at constant volume [12].

It is well known that adequate knowledge of the temperature dependence of the bulk modulus $B_T(T)$ is necessary for understanding the thermodynamic and anharmonic

properties of the crystal. Recently, many researchers have made various efforts to exploit thermodynamic properties of materials under the effect of high temperatures [13-15]. In these studies, thermodynamic properties such as the temperature dependence of the volume thermal expansivity and bulk modulus of materials from room temperature to the melting temperature with different approximations are considered. In the present work, a relation is derived for the bulk modulus which can be obtained from pulse heating data and that relation can also be used to estimate internal energy and work done on / by the sample material if the bulk modulus is known.

Table 1.2. Properties of the investigated alloys, mass-fraction of iron (other constituent is nickel) determined by means of EDAX 111, sum of impurities (P, S, Si, C etc.) less than 0.5%. T_s and T_l are solidus and liquidus temperatures and d is density at room temperature [16].

No.	Mass % Fe	T_s / K	T_l / K	d / $kg{\cdot}m^{-3}$
1	0	1726		8900
2	18.6	1712	17I5	8734
3	41.7	1707	1710	8583
4	48.5	1709	1715	8328
5	62.7	1717	1727	8000
6	79.9	1740	1755	8038
7	89.0	1763	1777	8150
8	100	1808		7850

Table 1.3. Properties of investigated alloys, mass fraction of copper (other is Ni). T_s and T_l are solidus and liquidus temperatures and d is density at room temperature [17].

No.	Mass % Cu	T_s / K	T_l / K	d / $kg{\cdot}m^{-3}$
1	0	1726		8900
2	85	1417	1447	8913
3	70	1472	1520	8965
4	55	1528	1576	8902
5	45	1599	1638	8945
6	20	1656	1678	8953
7	100	1356		8960

1.4. Aim of the Present Work

The primary aim of this work is to investigate and compare the thermophysical properties of Pt alloys by different techniques and support casting industry by delivering them input data for casting simulations. The secondary aim is to perform model calculations, such as determination of thermal conductivity in terms of easily measurable parameters for example temperature, thermal conductivity of constituents of binary alloy in liquid phase with the addition of some empirical coefficient, exponent or adjustable parameter; whose value can be determined through the application of regression analysis to laboratory data. To determine theoretically the heat capacity of experimentally investigated alloys in high temperature region close to the solidus points using existing theories and models is another aim of this work.

References

[1] Hansen M, 1958 *Constitution of Binary Alloys*. Metallurgy and Metallurgical Engineering Series, ed. R.F. Mehl New York: McGraw-Hill.

[2] *Thermo-Calc Software AB,* Stockholm, Sweden, SGTE Nobel Metal Alloys Database (SNOB), Version 1.1.

[3] Massalski T B, 1986 *Binary alloy phase diagrams* vol.1+2 Metals Park, Ohio: American Society of metals.

[4] Wilthan B, Cagran C, Seifter A and Pottlacher G 2004 *Thermophysical properties of solid and liquid platinum.* Thermochimica Acta,. **415**(1–2): pp 47-54.

[5] Cagran C, Seifter A and Pottlacher G, 2000 *Thermophysical properties of solid and liquid copper.* Schriften des Forschungszentrums Jülich, Science Energy Technology **1**: pp763-766.

[6] *ASM Handbook, Properties and Selection: Nonferrous Alloys and Special-Purpose Materials,* 1999 vol. 2, ASM International, ASM Handbook on CD-ROM, ASM International and The Dialog Corporation,) pp 759.

[7] Pottlacher G, 2010 High *Temperature Thermophysical Properties of 22 Pure Metal* Graz, Austria: Keiper pp 82-87.

[8] http://www.mapsofworld.com/referrals/metals/platinum/ruthenium.html

[9] Per Enghag 2004 *Encyclopedia of the Elements: Technical Data - History - Processing - Applications* Wiley-VCH.

[10] Lars Friberg Gunnar Nordberg Bruce A. Fowler, Monica Nordberg, 2007 *Handbook on the Toxicology of Metals* Academic Press, 3rd edition.

[11] Knobler CM, 1983 *Twixt Cup And Lip: Do Equation-Of-State Measurements Really Tell Us Anything Useful About Intepmjlewlar Forces Pure and Applied. Chemistry*, **55**, 455.

[12] Hixson R S and Winkler M A and Hodgdon M L, 1990 *Sound speed and thermophysical properties of liquid iron and nickel.* Physical Review B, **42**(10): pp 6485-6491.

[13] Kumar M and Upadhyay S P, 1994 *Analysis of the Thermal Expansion Coefficient and Its Temperature Dependence for Alkali Halides.* physica status solidi (b), **181**(1): pp 55-61.

[14] Munish K, 1995 *High pressure equation of state for solids.* Physica B: Condensed Matter, **212**(4): pp 391-394.

[15] Rajiv K P, 1998 *Study of temperature dependence of interatomic separation and bulk modulus for ionic solids.* Journal of Physics and Chemistry of Solids,. **59** (6–7): pp 1157-1160.

[16] Seifter A, Pottlacher G, Jäger H, Groboth G and Kaschnitz E, 1998 *Measurements of thermophysical properties of solid and liquid Fe-Ni alloys.* Berichte der Bunsengesellschaft für physikalische Chemie, **102**(9): pp. 1266-1271.

[17] Hüpf T, Cagran C, Kaschnitz E and Pottlacher G, 2010 *Thermophysical Properties of Five Binary Copper–Nickel Alloys.* International Journal of Thermophysics, **31**(4): pp 966-974.

Chapter 2

Thermal Conductivity

The knowledge of thermophysical properties of metals as a function of temperature has become important with the widespread interest in thermal processes. Precise measurements of the thermal conductivity of alloys are difficult to make and are very time-consuming. To make laboratory measurements into a useful, simple mathematical form of interest which can be used under all environmental conditions of temperature and pressure would be prohibitive in terms of time and expense. Consequently, a lot of effort has been made to formulate a simple physical model for the prediction of thermal conductivities of binary alloys. The objective of this work is to develop a model for the determination of the thermal conductivity of alloys as a function of temperature and in terms of simple parameters. Before going into elaborative discussion, it is quite reasonable to discuss the heat transfer mechanism and different factors involved in the thermal conductivity process.

2.1. Mechanisms of Heat Transfer

Thermodynamics defines heat as a transfer of energy across the boundary of a system as a result of a temperature difference. According to this definition, heat by itself is an energy transfer process and it is therefore redundant to use the expression ‘heat transfer’. Heat has no option but to transfer and the expression ‘heat transfer’ reinforces the incorrect concept that heat is a property of a system that can be ‘transferred’ to another system. Heat is the transfer of energy due to a temperature gradient; mechanisms of heat transfer are possible under certain circumstances and can be divided into three categories: conduction, convection and radiation [1]. In many cases, these three modes of heat transfer happen in the same time but it is important to differentiate them for better understanding. A brief description of each mechanism is given below [2].

2.1.1. Conduction

In a conduction process heat transfers by direct contact at the molecular level from the more energetic particles of a substance to the adjacent less energetic ones as a result of interactions between the particles. Conduction can take place in solids, liquids or gases but in gases and liquids conduction is due to the collisions and diffusion of the molecules during their random motion. When a fast molecule hits a slow molecule, the energy is transferred from the former to the latter. In case of solids, it is due to the combination of vibrations of the molecules in a lattice and the energy transport by free electrons. In metals, at high temperature, lattice vibrations are much less efficient than electrons. Regardless of these details, the rate of heat conduction obeys a mathematical law that is not hard to guess [3].

According to this law, the rate of heat conduction $\frac{dQ}{dt}$ through a material is proportional to the temperature difference *dT* across the material and the heat transfer area *A*, but is inversely proportional to the thickness *dx* of the material. That is:

$$\frac{dQ}{dt} = \lambda A \frac{dT}{dx} \tag{2.1}$$

The constant of proportionality λ is called thermal conductivity of the material and is defined as, "The rate of heat transfer through a unit thickness of material per unit area per unit temperature difference''. The equation (2.1) is called, "Fourier's law of heat conduction" after J. Fourier, who expressed it for the first time in his heat transfer text in 1822. The thermal conductivity λ, is characterized as an ability of a substance to conduct heat, which in turn is dependent on the atomic structure of the substance. Thermal conduction can involve electrons, ions, and/or phonons. Electrons and ions move from a point of higher temperature to a point of lower temperature, thereby transporting heat. Due to the lighter weight of electron than ions, electrons move much more easily. In crystals, the thermal agitation of atoms creates spontaneously vibrational waves and the amplitude of these waves increases as the temperature rises, these elastic waves are called phonons in the Einstein model. Einstein postulated the creation and existence of phonons at a large amount in the hot part of a solid, these phonon are partially eliminated in the

cold part. He also postulated their wave-particle duality. For a lattice such as one defined by a metal or a crystal, the vibration waves at a certain frequency υ and at temperature T give the energy state of the phonon: $E = h\ \upsilon$, where h is the Planck constant. Energy transport can be thought as a consequence of a series of phonon collisions, in these collisions, energy is transferred between phonons by changes in the vibration frequency. Between two successive collisions of a phonon, the phonon traverses some random distances and the algebraic mean of these distances is thus defined as the mean free path l. The longer the mean free path, the faster the energy can be transmitted and hence the greater the thermal conductivity would be. Metals conduct heat and electricity by electrons because they have plenty of free electrons. A nonmetal like diamond conducts heat by phonons because it does not have free electrons and its low atomic weight intensifies the lattice vibrations. Usually, electrons provide the best heat transfer via conduction and therefore normally good thermal conductors are also good electrical conductors. For example, typical $\lambda(T)$ values in metals are hundreds times higher than in that of nonmetals like solids, liquids and gases [4].

2.1.2. Convection

In a fluid (liquid and gas), the transfer of heat occurs due to the bulk motion of a fluid and this leads to a more complex situation which is called convection. Convection is the mechanism of heat transfer between a solid surface and the adjacent liquid or gas which is in motion. The whole process has combined effects of conduction and convection.
The rate of convection depends on the heat capacity of the fluid and some possible forces acting on it. Newton's law of cooling describes the rate of heat transfer by convection as follows:

$$\frac{dQ_{convec}}{dt} = pA(T_s - T_\infty) \tag{2.2}$$

Where p is the convection heat transfer coefficient in $W \cdot m^{-2} \cdot K^{-1}$, A is the surface area, through which convection heat transfer takes place, T_S is the surface temperature and T_∞ is the temperature of the fluid which is sufficiently far from the surface. Due to close

proximity the fluid temperature on its surface equals the surface temperature of the solid at which convection process is being done. The convection heat transfer coefficient p does not depend on the fluid but is an experimentally determined parameter whose value depends on all the factors influencing convection such as surface geometry, the nature of fluid motion, properties of the fluid and the bulk fluid velocity [5]. It is important to note here that when thermal conductivity measurements are carried out on liquids, the heat flux ΔQ can have significant contributions from convection and gives erroneously high values for thermal conductivity (and also for thermal diffusivity). Consequently, it is important to control those factors of errors and usually it is done by minimizing convection through:

(i) Precise control of the sample temperature

(ii) Ensuing that the surface temperature of the liquid is marginally higher than the base of the sample.

On the other hand, most metals melt at very high temperatures and in practice it is very difficult to provide the necessary precise control of temperature under these conditions. Therefore, new techniques have been developed and used in recent years like transient and non-steady state methods to carry out measurements on liquid metals and alloys. In these techniques the measurements are carried out so rapidly that the entire experiment is done before the onset of convection [6].

Many different types of convection occur in our daily life,, e.g. if the fluid is forced to move by a pump or a blower, then this type of convection is known as forced convection. The simplest illustration of this case is the use of the fan: the fan increases the motion of air and as a result the convection process increases. If the fluid motion is due to difference in density, the convection is known as natural or free convection. An example of free convection could be the use of a heater in a room [7].

2.1.3. Radiation

The emission of energy as electromagnetic waves due to changes in the interatomic configuration of a body or system is known as radiation. All surfaces/bodies (solids, liquids and gases) emit or absorb radiant heat due to the difference in temperature from their surroundings. If the bodies are separated by empty space then the only possible heat transfer mechanism is radiation/electromagnetic waves. Unlike conduction and convection, the transfer of energy by radiation does not require the presence of an intervening medium. In fact, energy transfer by radiation is fastest (at the speed of light) and it suffers no attenuation in a vacuum [3]. For these emitted radiation the dominant wavelength decreases with increasing temperature of the body. The higher the temperature is, the greater the rate of emission of radiant energy per unit area of the surface. Radiation is a volumetric phenomenon and all solids, liquids and gases emit, absorb or transmit radiation to varying degrees. However, in solids, radiation is usually considered to be a surface phenomenon because the radiation emitted by the interior regions of solid materials can never reach the surface and are absorbed internally, whereas the radiations incident on such bodies are usually absorbed within a few microns from the surface. The maximum rate of radiation that can be emitted from a surface at an absolute temperature is given by Stefan-Boltzmann law as:

$$\frac{dQ_{\max}}{dt} = \sigma A T_s^4 \tag{2.3}$$

Where $\sigma = 5.67\times10^{-8}\ W\cdot m^{-2}\cdot K^{-4}$, is the Stefan-Boltzmann constant. The ideal surface that emits radiation at this maximum rate is called a black body, and the radiation emitted by a black body is called black body radiation. The radiations emitted by all real surfaces/bodies are less than the radiations emitted by a black body at the same temperature and the modified relation for them can be expressed as:

$$\frac{dQ_{\max}}{dt} = \sigma \varepsilon A T_s^4 \tag{2.4}$$

Where ε, is the emissivity of the real surface and the ratio of the actual emissive power E of a body to the emissive power of a blackbody $E_{blackbody}$ is defined as the surface emissivity $\varepsilon = E / E_{blackbody}$. The emissive property, whose value is in the range $0 \leq \varepsilon \leq 1$ is a measure of how close the real surface is to a black body whereas for a black body $\varepsilon = 1$ [5]. The following Table 2.1 presents some values of emissivity for different materials in a different range of temperature. It is seen experimentally that the blacker a material is, the closer its emissivity to 1. The emissivity also depends on roughness and the oxidation state of the material.

The prevention and control of radiation is more difficult than that of convection and conduction. The most effective way, in general, against radiation is to set a radiation shield mirror around the sample. A radiation shield is a material of high thermal conductivity which is in thermal contact with the fixture. This shield cannot, however, be perfect and the heat loss by radiation must be taken into account.

Table 2.1. Emissivity data for material in different states [4].

MATERIAL	°C	EMISSIVITY
G-10 Epoxy Resin	---	0.95
Glass	20-100	0.94-0.91
Carbon:		
Filament	1000-1400	0.53
Graphite	0-3600	0.7-0.8
Lamp Black	20-400	0.96
Soot Applied to Solid	50-1000	0.96
Soot with Water Glass	20-200	0.96
Aluminum:		
Polished	50-500	0.04-0.06
Rough Surfaces	20-50	0.06-0.07
Strongly Oxidized	55-500	0.2-0.3
Oxidized	200	0.11

2.2. Theory of Thermal Conductivity

A flow of heat occurs wherever there is a thermal gradient in a crystal in a direction opposite to that of the gradient. So if there is a thermal gradient $\frac{dT}{dx}$ along the x-direction and J_x is the resulting heat flux density then:

$$J_x = \frac{dQ}{Adt} = -\lambda \frac{dT}{dx} \tag{2.5}$$

Equation (2.5) shows that the process of thermal energy transfer is a random process [8]. The energy transfer process is not so simple like the entrance of heat energy from one end of the specimen and proceed directly in a straight path to the other end, instead, the energy diffuses through the specimen, suffering frequent collisions. If energy would be transmitted directly through the specimen without deflection, then the expression for energy transfer would only dependent on difference in temperature ΔT between the two ends of the specimen regardless of the length of the specimen. But the actual expression, due to the random nature of the conductivity process, for the thermal flow includes temperature gradient and mean free path. The heat, as discussed earlier, may be propagated in the materials by several independent agents in metal, for example, the heat is carried both by electrons and by lattice waves (phonons). These electrons provide an additional contribution to the thermal conductivity, which can therefore be much greater than in non–metals in which only phonons contribute [9]. However, in poor metals such as bismuth or in metals containing large amount of impurities (alloys), the lattice conductivity may be important. Since there are no mobile electrons in insulators, so heat is transmitted entirely by phonons.

2.2.1 Thermal Conductivity in Insulators

A theory of thermal conductivity by phonons in insulators was developed in 1914 by Debye. Debye argued that the thermal conductivity by phonon can be expressed as:

$$\lambda = \frac{1}{3} c_v \, l \, v_{ph} \tag{2.6}$$

Where λ is the thermal conductivity, v_{ph} *is* the mean thermal speed of phonon c_v is the heat capacity at constant volume *l is* the mean free path between randomized collisions. This expression is derived though for an ideal Maxwell-Boltzmann gas, but it is also good for a gas of phonons by providing that the velocity v_{ph} is referred to an average phonon velocity in the crystal. The problem of determining the lattice thermal conductivity is essentially the determination of the mean free path *l* of phonon in the crystal because the sound velocity and the specific heat are comparatively easily measurable. It has been seen that thermal conductivity depends strongly on temperature because the mean free path *l* depends strongly on temperature, whereas the phonon velocity v_{ph} is found to be essentially insensitive to temperature.

The mean free path *l* is determined by three important collision processes in solids;

(a) The collision of phonons with other phonons.

(b) The collision of phonons with imperfections in crystal such as impurities and dislocations.

(c) The collision of phonons with the external boundaries of the sample.

By considering the collision of type (a) where the phonon scatters from each other due to anharmonic interaction; this collision becomes particularly important because at high temperature the atomic displacements are quite large. In that particular range of temperature, the mean free path is inversely proportional to temperature that is $l \approx 1/T$. Since the larger the temperature is, the greater the number of phonon collisions with the other phonons would be. Defects, impurities and crystal imperfections also scatter phonons because they partly demolish the ideal periodicity and affect on the free propagation of lattice wave. For example, a substitutional point impurity, having a mass and a density greater than that of the host atom, causes scattering of the phonon wave at the impurity site that results in a shorter mean free path and hence less thermal conductivity.

Both phonon-phonon and phonon-imperfection collisions become ineffective at very low temperatures, because in the former case, there are only a few phonons available, and in the latter case, the few phonons which are roused at this temperature are associated with long wavelength. So these are not effectively scattered by impurities, which are much small in size than the wavelength. In the low temperature regime, the main scattering is

the external boundary of the specimen; which is commonly called size or geometrical effects. This mechanism becomes effective because the wavelengths of the excited phonons are very long comparable, in fact, to the size of specimen. The mean free path here is: $l \approx D$, where D is approximately equal to the diameter of the specimen; and hence independent of temperature.

The only temperature dependant term on the right of the above equation is c_v, the volumetric heat capacity, which varies as T^3 at low temperatures. We may therefore expect the thermal conductivity to vary as T^3, at low temperature [3].

2.2.2. Thermal Conductivity in Metals and Alloys

As mentioned earlier, lattice waves and electrons play a fundamental role for thermal conduction in metals and alloys. Also it has been proved experimentally that electronic conduction is dominant around the melting point although the mechanism of phonon or lattice conduction can make a contribution at lower temperatures. In many practical cases, electrical conductivity σ_e or electrical resistivity $1/\sigma_e$ measurements are much easier to measure than the determination of the thermal conductivity λ itself. Therefore a relationship is required which correlates these two quantities properly. The main advantage of expressing λ in terms of σ_e is that both quantities are directly proportional to the electron mean free path l and hence the ratio λ / σ_e is independent of the mean free path l. The mean free path l is assumed to be the same for electrical and for thermal conduction, although, this is definitely not always true, difference in these two is important mainly at low temperatures where electron scattering is inelastic and anisotropic. Interactions between phonons and electrons determine the thermal conductivity in a pure metal. In alloys additional lattice distortions by alloying elements cause similar disturbances. Both thermal and electrical conductivity rely on electron transport and behave analogously, and in the ideal case these two are related by the well known equation, Wiedemann–Franz law:

$$L = \frac{\lambda}{\sigma_e T} \tag{2.7}$$

where L is the Lorentz number, λ is thermal conductivity, σ_e is electrical conductivity and T is temperature. Table 2.2 shows the validity of the WFL for higher (> 273 K) temperatures, although the electrical conductivity values are differing in the range of 10^2. Unfortunately, values of Lorentz number for different materials and theoretical estimated values are not exact the same, which leads to an uncertainty while using the WFL because WFL does not include the lattice contribution in conduction. (which is dominant at low temperatures). Commonly used value of Lorentz number L is $2.45 \cdot 10^8$. Table 2.2 shows the failure of the WFL in the low temperature range [6].

Table 2.2. Electrical conductivities σ_e and Lorentz numbers L for different metals at different temperatures [10].

	Electrical conductivity , $\sigma_e \cdot 10^{-5}$ / $\Omega^{-1} \cdot cm^{-1}$				**Lorentz number $L \cdot 10^8$ / $V^2 \cdot K^{-2}$**			
Temperature / K	**80**	**273**	**373**	**573**	**80**	**273**	**373**	**573**
Silver	32.5	6.70	4.76	2.97	1.77	2.28	2.36	2.41
Copper	43.6	6.45	4.50	2.79	1.56	2.24	2.35	2.37
Gold	20.6	4.90	3.51	2.20	2.03	2.35	2.36	2.42
Aluminum	28,8	4.15	2.86	1.80	1.11	2.03	2.11	2.13
Zinc	9.90	2.08	1.47	0.890	1.70	1.90	1.92	1.96
Nickel	9.30	1.65	0.990	0.452	1.68	1.95	2.28	2.43
Platinum	4.95	1.02	0.733	0.476	2.00	2.55	2.60	2.75
Lead	2.02	0.532	0.375	0.224	2.33	2.31	2.40	2.62

To testify the validity of the WFL relation, ratios of the experimental to theoretical values for the Lorenz function (L/L_0), were evaluate for temperatures close to the melting point and it was found close to unity for most metals and the small deviations seen may be due to uncertainties of measurement. For some metals fairly large disagreement from the theoretical Lorenz number were found and attempts to modify the WFL relation were made at lower temperatures. Even larger discrepancies have been observed when using the WFL relation for alloys, because electron-electron interactions, electron-phonon interactions, as well as lattice contributions, need to be considered. These effects disappear at melting due to destruction of crystal structure and the WFL becomes a reasonable tool for determining thermal conductivities for liquid metals and alloys [11].

2.3. Heat Conduction Equations

In the case of an isotropic medium the heat flux, $\vec{J}$ (dQ/Adt), through an unit area is given as:

$$\vec{J} = -\lambda\left(\vec{\nabla}T\right) \tag{2.8}$$

where $\vec{\nabla}T$ is the temperature gradient. Here $\vec{J}$ and $\vec{\nabla}T$ are collinear, but in the case of an anisotropic medium $\vec{J}$ and $\vec{\nabla}T$ are not collinear. We consider an arbitrary volume V of a homogeneous isotropic solid within which no heat is being generated. If the temperature at any point (x, y, z) at the time t is T (x,y,z) then the total flux of heat, or quantity of heat leaving a surface S enclosing the volume V, per unit time is:

$$\oint d\vec{s}\cdot\left(-\lambda\left(\vec{\nabla}T\right)\right) \tag{2.9}$$

Using the divergence theorem, we can change the surface integral into a volume integral:

$$\oint_S d\vec{s}\cdot\left(-\lambda\left(\vec{\nabla}T\right)\right) = \int_v \vec{\nabla}\cdot\left(-\lambda\vec{\nabla}T\right) \tag{2.10}$$

The amount of heat entering the surface per unit time will be equal to:

$$\int_v \vec{\nabla} \cdot \lambda\left(\vec{\nabla} T\right) dv \tag{2.11}$$

If c_p is the specific heat of the solid at constant pressure and d is the mass density then heat contained in a volume V is:

$$\int_v c_p dT dv \tag{2.12}$$

and the increase in specific heat per unit time is:

$$\frac{\partial}{\partial t}\int_v c_p dT dv = \int_v c_p d \frac{\partial T}{\partial t} dv \tag{2.13}$$

Comparing equations. (2.11) and (2.13), we get:

$$\int_v c_p d \frac{\partial T}{\partial t} dv = \int_v \vec{\nabla} \cdot \lambda\left(\vec{\nabla} T\right) dv \tag{2.14}$$

$$\int_v \left[c_p d \frac{\partial T}{\partial t} dv - \vec{\nabla} \cdot \lambda\left(\vec{\nabla} T\right) \right] dv = 0 \tag{2.15}$$

Since volume V is arbitrary, the integrand in the last equation is zero; resulting in the general equation of heat conduction:

$$\vec{\nabla} \cdot \lambda\left(\vec{\nabla} T\right) = c_p d \frac{\partial T}{\partial t} \tag{2.16}$$

If temperature variations are small and λ is almost independent of temperature, then:

$$\lambda\left(\vec{\nabla}^2 T\right) = c_p d \frac{\partial T}{\partial t} \tag{2.17}$$

Which may be written as:

$$\vec{\nabla}^2 T = \frac{1}{a}\frac{\partial T}{\partial t} \tag{2.18}$$

Where a is thermal diffusivity. This is the basic equation of heat conduction for non-steady state or transient type measurements. But in steady state, $\frac{\partial T}{\partial t}$ reduces to zero and, therefore, the above equation reduces to the Laplace equation:

$$\vec{\nabla}^2 T = 0 \tag{2.19}$$

There are numerous methods for the determination of the thermal transport properties of the materials. Broadly, we can categorize them into two groups, namely steady state methods and non-steady state or transient methods. Both of these methods are based on the solutions of the equations (2.18) and (2.19), under proper boundary conditions. Steady state methods make use of equation (2.19), whereas non-steady state or transient methods use equation (2.18). The steady state methods require time-consuming procedures to set up the experiment as well as to establish the steady state temperature gradient, especially in the case of insulating materials. Also, it is not possible to determine simultaneously the two thermal properties namely thermal conductivity and thermal diffusivity of the material using the steady state methods. To overcome these difficulties non steady state methods are utilized to measure the thermal transport properties [8].

2.4. Prediction of Effective Thermal Conductivity

In general, three basic types of models for the prediction of effective thermal conductivity of multi-component systems have been used. The first type connects the application of the mixing laws for aggregates containing various fluids. These models have limited applicability because these models do not take into consideration the structural features of the fluid material. A second type is the empirical model in which more easily measureable physical quantities are related to thermal conductivity by regression analysis to laboratory data with the addition of certain adjustable parameters, exponents and coefficients. This method has its inadequacy in such a way that the resulting model may

only be applicable to a particular material being investigated. For example, in two separate papers, Sugawara and Yoshizawa have used different exponents for essentially two identical sets of experiments on similar materials [12, 13]. The third type is the theoretical model based on the mechanism of heat transfer; these models also have limited applicability and cannot be used for all types of systems, especially when the difference in the thermal conductivities of the constituent phases is very large [14]. A universal formulation to predict the effective thermal conductivity is still required.

2.5. Mixing Law Models

These laws or models combine values of the thermal conductivities of the one material of the alloy solid λ_A with the thermal conductivity λ_B of the other constituent [14]. Examples of mixing law models are given in the following sections.

2.5.1. Weighted Arithmetic Mean Model

When there are two constituents in an alloy with two different thermal conductivity values then there is an equal probability for them to be in series or in parallel. Weighted arithmetic mean is the equivalent of parallel arrangement of the components relative to the direction of heat flow, as shown in Figure 2.1.
For such an arrangement, the effective thermal conductivity of the sample is given by:

$$\lambda_e = \Phi\lambda_A + (1-\Phi)\lambda_B \tag{2.20}$$

Where Φ is the weighted percentage of one of the alloy constituent and (1- Φ) is the weighted percentage of the second constituent alloy. This form gives the highest values of thermal conductivity of the fluid system of all the mixing law models.

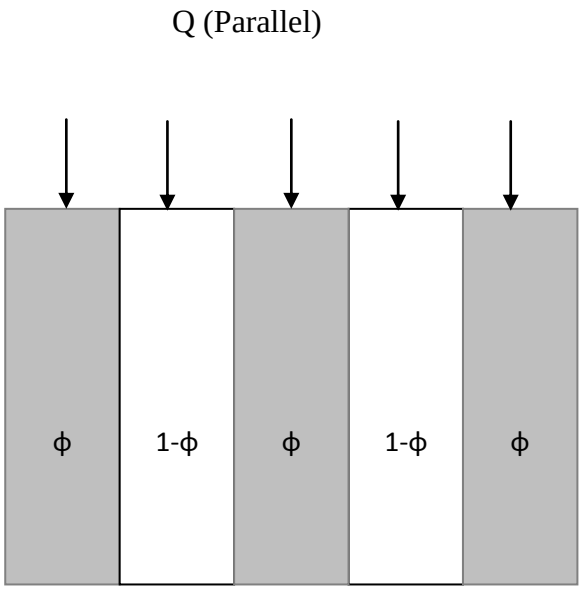

Figure 2.1. Parallel arrangement of components relative to the direction of heat flow Q.

2.5.2 Weighted Harmonic Mean Model

The harmonic mean model would imply a series arrangement of the components, as shown in Figure 2.2

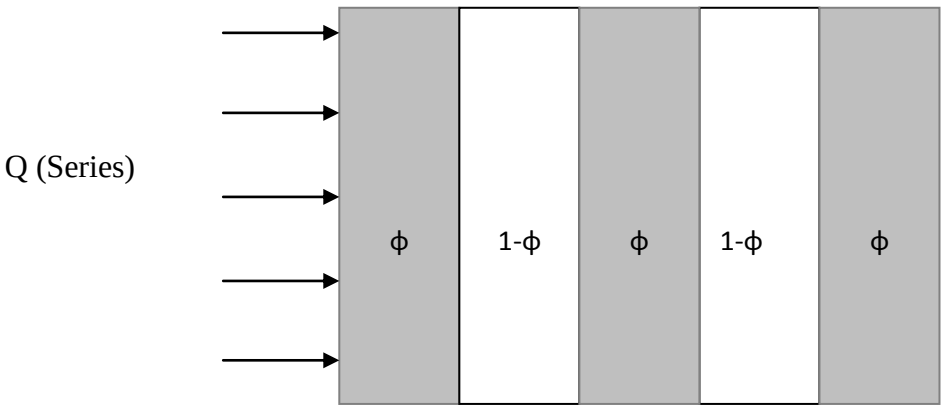

Figure 2.2. Series arrangement of components relative to the direction of heat flow Q.

For such an arrangement, the effective thermal conductivity of the sample is given by:

$$\lambda_e = \left[\frac{\Phi}{\lambda_A} + \frac{1-\Phi}{\lambda_B} \right]^{-1} \tag{2.21}$$

This equation gives the lowest value of thermal conductivity. The problem with these models is that they are physically unrealistic, because it seems unrealistic that a material has alternating portions of first and second type of material. But these model give estimate values of thermal conductivities and these values are called Wiener's upper and lower bounds, respectively [15].

2.5.3 Weighted Geometric Mean Model

One of the mixing law models is the weighted geometric mean model given as [16]:

$$\lambda_e = \lambda_B \left(\frac{\lambda_B}{\lambda_A} \right)^{\Phi} \tag{2.22}$$

Turian et al found that the weighted geometric mean model provides as good or even a better prediction of thermal conductivity than any of the theoretical models [17].

2.6.4. Extended Maxwell Model

The extended Maxwell model, which is the direct analogue of the electrical case of Maxwell's model, is the best example of mixing-law models which have firm physical basis is given by [18, 19]:

$$\lambda_e = \lambda_A \left(\frac{\left(\frac{2\lambda_A}{\lambda_B} + 1 \right) - 2\Phi \left(\frac{\lambda_A}{\lambda_B} - 1 \right)}{\left(\frac{2\lambda_A}{\lambda_B} + 1 \right) + \Phi \left(\frac{\lambda_A}{\lambda_B} - 1 \right)} \right) \tag{2.23}$$

This model is based on two important assumptions. First, based on Fourier's law, that the thermal diffusion is the main mechanism of heat flow, second, there is thermal continuity at the interface. Under these assumptions, the model predicts that the effective thermal

conductivity λ_e depends on the volume concentration of the constituent B, Φ , and the thermal conductivities of the constituent B, λ_B, and the media with thermal conductivity λ_A (Figure 2.3).

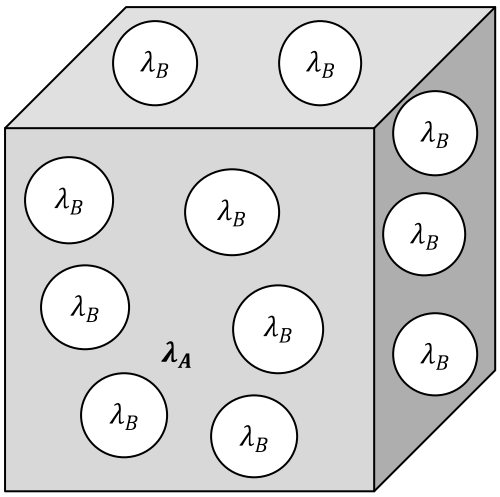

Figure 2.3. Dispersive arrangement of components relative to the direction of heat flow.

Maxwell considered a very dilute suspension of spherical particles embedded into a continuous solid phase. The separation between spheres is assumed to be sufficiently large so that their disturbance to the thermal field is not seen by the neighboring spheres. This model is based on the physically real situation where spheres of conductivity λ_B are dispersed in a medium of conductivity λ_A (Figure 2.3)

In the case of a two-component system, the distance between neighboring particles of dispersed material will require modification to equation (2.23) and will depend upon the conductivity ratio of the two materials as well as the fraction of the total volume occupied by the dispersed material. The same factors will determine the extent to which the particles can depart from a spherical shape before the equation must be modified. It is obvious from equation (2.23) that in the limit where $\lambda_A = \lambda_B$ the dispersed particles may be of any shape and may touch each other.

The weighted geometric mean model has no physical basis, but since it is easier to use than the Maxwell model and gives similar results over the limited range of conductivity ratio, some authors prefer to use it [20].

2.6. Empirical Models

In case of empirical models, some easily measured physical parameters are correlated to thermal conductivity with the addition of some empirical coefficient, exponent or adjustable parameter; whose value can be evaluated by regression analysis to laboratory data. An example is given in the following sections, whereas a comprehensive detail is coming in chapter 7.

2.6.1. Asaad's Model

Asaad's model is quite similar to the weighted geometric mean model and is given as:

$$\lambda_e = \lambda_B \left(\frac{\lambda_A}{\lambda_B} \right)^{c\Phi} \tag{2.24}$$

Where c is the empirical exponent, when c=1, this equation becomes identical to equation (2.22) [21].

References

[1] Cengel Y A and Turner R H, 2001 *Fundamentals of Thermal-Fluid Sciences* Boston Burr Ridge: McGraw-Hill pp 604-613.

[2] Nellis G, Klein S, 2009 *Heat transfer* Cambridge University Press 32 Avenue of the Americas, New York, NY 10013-2473, USA,pp 1-10.

[3] Daniel V S, 2000 An *Introduction to Thermal Physics* Addison Wesley Longman pp 1-37.

[4] Gonnet P, *Master of Science thesis* (The Florida State University College Of Engineering, 2004).

[5] Aurangzeb, *PhD Dissertation* (Queid-e- Azam University Islamabad, 2008).

[6] Cagran C, *Diploma thesis* (Technical University Graz, 2000).

[7] http://hyperphysics.phy-astr.gsu.edu/hbase/hph.html.

[8] Mehmood S, *M Phil thesis* (Queid-e- Azam University Islamabad, 2007).

[9] Peet M, Hasan H S and Bhadeshia, 2011 *Prediction of thermal conductivity of steel* International Journal of Heat and Mass Transfer **54**: pp 2602-2608.

[10] Bergmann L, Schaefer C, 1990 *Lehrbuch der Experimentalphysik Band L IO./Aluflage*, Walter de Gruyter, New York.

[11] Michael E B, 2008 *Handbook of Thermal analysis and calorimetry* **Chapter 10** Elsevier publisher Radarweg 29, PO Box 211, 1000 AE Amsterdam, The Netherlands Linacre House, Jordan Hill, Oxford OX2 8DP, UK.

[12] Sugawara A and Yoshizawa Y, 1961 *An Investigation on the Thermal Conductivity of Porous Materials and its Application to Porous Rook.* Australian Journal of Physics, **14**(4): pp 469-480.

[13] Sugawara A and Yoshizawa Y, 1962 *An Experimental Investigation on the Thermal Conductivity of Consolidated Porous Materials.* Journal of Applied Physics, **33**(10): pp 3135-3138.

[14] Somerton W H, 1992 *Thermal Properties and Temperature Related Behaviour of Rock/Fluid Systems* New York: Elsevier.

[15] Robert W Z, 1989 *Thermal conductivity of fluid-saturated rocks.* Journal of Petroleum Science and Engineering, **3**(3): pp 219-227.

[16] Woodside W and Messmer J H, 1961 *Thermal Conductivity of Porous Media. I. Unconsolidated Sands.* Journal of Applied Physics, **32**(9): pp 1688-1699.

[17] Turian R M, Sung D J and Hsu F L, 1991 *Thermal conductivity of granular coals, coal-water mixtures and multi-solid/liquid suspensions.* Fuel,. **70**(10): pp 1157-1172.

[18] Maxwell J C, 1904 *A Treatise of Electricity and Magnetism* 3rd edn. vol 1 Oxford: Clarendon pp 440.

[19] Beck A E, 1977 *A potential systematic error when measuring the thermal conductivity of porous rocks saturated with a low-conductivity fluid.* Tectonophysics, **41**(1–3): pp 9-16.

[20] Maqsood A, Kamran K and Gul I H, 2004 *Prediction of thermal conductivity of granite rocks from porosity and density data at normal temperature and pressure : in situ thermal conductivity measurements.* Journal of Physics *D* **37**: pp3396-3401.

[21] Asaad *PhD Dissertation* (University of California: Barkeley, 1955).

Chapter 3

Specific Heat

Specific heat measurements have been a helping means for studying and understanding the physical and thermodynamic properties of materials since the start of the twentieth century. In spite of the fact that specific heat and other thermodynamic properties of many compounds are well known, measurements of specific heat render a new look into the properties of matter, which helps us to take into consideration new ways about the thermodynamic properties of materials. A specific heat measurement makes no differentiation between vibrational energies and is different from some techniques like Raman or infrared spectroscopy which provide vibrational information of molecules, where this molecular vibrational information provides discrete lines in a spectrum. Hence to obtain these vibrational energies one must use some other indirect ways or methods, often with the use of other physical properties, to get full detail about them.

The specific heat originates right from the vibrational modes of a body, and it is a sum of all possible energies available in the body, whether they are vibrational, magnetic, or of any other sort. Moreover, the specific heat concedes the enthalpy and entropy of a body, which can be utilized in connection with other data to calculate the free energy scenario. At high temperature the specific heat is only weakly affected by crystal defects because it is a bulk property, except so called substitutional defects (impurities) which influence the specific heat very sensitively.

The quantum theory and thermodynamics provide ways to correlate specific heat to free electrons, phonons and a variety of other phenomena, therefore, specific heat measurements are a helping tool in characterizing the properties of a body or system on a microscopic level [1, 2]. As we are concerned here, in this research work, with theoretical and experimental investigation of specific heat so it seems logical to discuss some factors which influence or can affect values of specific heat.

In the first place we shall discuss precisely some fundamental relations of specific heat with other thermodynamic quantities and then we shall have elaborate descriptions of the various microscopic phenomena which contribute to total specific heat.

3.1. Theoretical Background of Specific Heat

Mainly, in this work, we are interested in the measurement and evaluation of both manifestations of the specific heat, normally the specific heat at constant pressure c_p and the specific heat at constant volume c_v, thermodynamically, these quantities are obtained:

$$c_p(T) = \left[\frac{\partial H(T)}{\partial (T)} \right]_p \tag{3.1}$$

$$c_v(T) = \left[\frac{\partial H(T)}{\partial (T)} \right]_v \tag{3.2}$$

where H is the enthalpy and U is the internal energy [2]. In most of the experimental investigations specific heat at constant pressure c_p is being measured, however, both values c_p and c_v are related to each other by the relation:

$$c_p = c_v + T \left(\frac{\partial p}{\partial T} \right)_v \left(\frac{\partial V}{\partial T} \right)_p \tag{3.3}$$

This above equation is specifically beneficial when the equation of state for a body is known.

In general, specific heat is described by the *molar* heat capacity C_{mol} in units $J \cdot mol^{-1} \cdot K^{-1}$, the *specific* heat capacity c_p in units $kJ \cdot kg^{-1} \cdot K^{-1}$, and the *volume-specific* heat capacity c_{vol} in units $kJ \cdot m^{-3} \cdot K^{-1}$. The connections between these quantities are as follows:

$$c_p = \frac{1}{m_a} C_{mol} \qquad \text{and} \qquad c_p = \frac{1}{d} C_{vol} \tag{3.4}$$

where m_a means the *atomic (molecular)* mass of the substance in gram, and d is the density of the substance in $kg \cdot m^{-3}$. Measurement of the specific heat yield direct information on the absolute entropy and relative changes to the enthalpy and Gibbs free

energy. The molar entropy S_m is related to the specific heat at constant pressure by the expression:

$$S_{m,T} = \int_0^T \frac{c_p}{T} dT \tag{3.5}$$

In the above expression the lower limit of the integral is set to absolute zero temperature, then by the third law of thermodynamics the lower limit of the entropy is also zero. Quite different from entropy, the enthalpy and the Gibbs free energy do not have absolute values; however, it cannot be concluded that relations derived for the specific heat from theses quantities are not helpful. The equation which shows the relation between enthalpy and specific heat at constant pressure is:

$$c_{p,m} = \left[\frac{\partial H_m}{\partial T} \right] \tag{3.6}$$

After rearranging we have:

$$H_{m,T} - H_{m,o} = \int_0^T c_{p,m} dT \tag{3.7}$$

Where $H_{m,0}$ is the enthalpy at 0 K. The Gibbs free energy can be expressed in terms of the entropy using the equation:

$$\left(\frac{\partial G_m}{\partial T} \right) = -S_m \tag{3.8}$$

By integration and taking functions at standard state where $G^0_{m,T} = H^0_{m,0}$, we get:

$$G^0_{m,T} - H^0_{m,0} = \int_0^T S_m dT \tag{3.9}$$

where, like as above, $G_{m,0}$ is the enthalpy at 0 K. Up to this point, we have established some direct or indirect relationships of the specific heat to the entropy, enthalpy and

Gibbs free energy. These expressions permit us to make calculations of thermodynamic data at any temperatures that we have, not just at the standard reference temperature (298.15 K).

3.2. Sources of the Specific Heat

Besides providing contribution to many thermodynamic properties, specific heat offers us an insight into the microscopic behavior of a body. As considered before, the specific heat originates from a combination of several different types of atomic interactions; hence it gives discrete information about each of these phenomena.

The specific heat arises from lattice displacement, the electrons in metals, splitting of electronic and nuclear energy levels (Schottky specific heat), magnetic alignment phase transitions, structural and superconducting transitions: each of these making distinct contributions to specific heat. Some of these are discussed precisely hereafter.

3.2.1 Specific Heat and Degree of Freedom

The atomic and molecular displacements (degrees of freedom) are the main source of contribution to the specific heat and from thermodynamical laws one can evaluate how these modes contribute to the heat capacity at constant volume c_v. As described earlier, c_v can easily be converted to c_p by equation (3.3). All three modes, translational, rotational, and vibrational, of motions of atoms and molecules contribute to the specific heat for gases.

According to the equipartition theorem every degree of freedom contributes $\frac{1}{2}RT$ per mole to the internal energy or $\frac{1}{2}R$ to the specific heat of the gas. Hence, the translational motion of gas particles contribution to c_v is $\frac{3}{2}RT$ because it has three degrees of freedom, one for each dimension [1]. Similarly rotations and vibrations of molecules also contribute to c_v depending on configuration and number of atoms per molecule n.

Nevertheless, the equipartition theorem is not enough to estimate specific heat contributions because it does not take into consideration the quantization of rotational and vibrational modes. Therefore, quantum mechanics, taking into account these modes, is

preferable to describe the specific heat of a body. Quantum mechanics gives vibrational contribution to the specific heat $c_{v,vib}$, as:

$$C_{v,vib} = R\left(\frac{\theta_v}{T}\right)^2 \frac{e^{\theta_v/T}}{\left(e^{\theta_v/T} - 1\right)^2} \tag{3.10}$$

where $\theta_v = hv/k$ with h being Plank's constant, k is Boltzmann's constant, and v is a fundamental vibrational frequency. The rotational specific heat can also be calculated by solving the Schrödinger equation, which is usually done numerically [1].

In general, the specific heat at constant pressure for gases is calculated by the equation: $c_p = c_v + R$ considering the gases as ideal gases. The molecules of gases are totally free to move with almost no interaction with neighboring molecules, whereas in liquids translational, vibrational, and rotational energies are more often interchanged because of the increased number of collisions with neighboring molecules, hence it is difficult to model their behavior.

On the other hand solids, which are quite well ordered and the atomic interactions are very small, are easier to model. Due to the problems described above, there is very little information about the liquid phase than the other two phases, therefore, models which describe liquids and their specific heat contributions have varying degrees of success. There is an exact relation between the heat capacity c_v at constant volume, and c_p at high temperature [3]:

$$c_v(T) = c_p(T) - VT\beta^2/B_T \tag{3.11}$$

where β is the volume expansion coefficient, V is the specimen volume and B_T is the isothermal bulk modulus [4]. In simple solids such as non-magnetic insulators, the vibrational motion of the atoms alone contributes to the specific heat which is also known as lattice specific heat. By using the classical picture, of the equipartition theorem, each atom is considered as a three dimensional oscillator having six degrees of freedom and adds 3nR or $n \cdot 24.9\ J \cdot K^{-1} \cdot mol^{-1}$ where n is the number of atoms per molecule.

This outcome is in good agreement with the experiment for most solids at room temperature, but at high temperatures there are still many materials for which specific heat just begins to approach 3nR as can be seen in Dulong-Petit law. The specific heat of all materials comparatively decreases fast in value at low temperatures and approaches zero as the temperature approaches 0 K. This phenomenon can be explained by quantum mechanics combined with Maxwell-Boltzmann statistics that only certain small numbers of permissible vibrational energy states are populated at low temperature and hence the specific heat is relatively small. Specific heat increases sharply as the thermal energy, k_bT, comes close to the energy of the vibrational modes. When the thermal energy increases more than vibrational energy, most of the energy levels begin filling completely and at that stage the specific heat approaches the Dulong-Petit limit. According to the quantum mechanical point of view, there are three significant way to model the lattice specific heat: The Einstein model, the Debye model, and direct calculation from known density of states.

3.2.2. The Einstein Model

The Einstein model describes qualitatively by the characteristics of a specific heat curve and is based on two assumptions. Firstly, each atom in the lattice is an independent three dimensional quantum harmonic oscillator and secondly, all atoms oscillate with the same frequency [1]. One can find by Maxwell-Boltzmann statistics, that the contribution of the *optic* phonons to the (molar) heat capacity of a crystal lattice can be theoretically approximated:

$$C_{mol}^{E}(T) = 3(r-1)N_A k_B \left(\frac{\Theta_E}{T}\right)^2 \frac{e^{\Theta_E/T}}{(e^{\Theta_E/T}-1)^2} \tag{3.12}$$

Where N_A = 6.02257·10^{23} is the Avogadro's number, k_B = 1.38054·10^{-23} J·K^{-1} is Boltzmann's constant, and θ_E the Einstein temperature of the material. The parameter r in equation (3.12) means the number of atoms within the unit cell of the crystal.

The Einstein function which is often expressed in terms of the Einstein temperature, $\theta_E = h\nu_E/k_B$, allows to understand the vibrational frequency in terms of the thermal energy which is necessary to populate the vibrational modes. Unfortunately, a severe drawback

of Einstein function is that it cannot be applied on simple materials like Al or Cu, because it (Einstein function) is only applicable to optical phonons which do not appear in only atomic system. But even for more atomic system the Einstein function is an oversimplification because it includes one frequency for all vibrating atoms. In fact, different atoms will vibrate with different frequencies and the vibrations are influenced by all atoms around it: However, such effects are neglected in this model.

3.2.3. The Debye Model

The Debye model is different from the Einstein model by using a frequency dispersion rather than same frequency for all oscillators. The range of these frequencies is expressed in terms of the vibrational density of phononic states *g(v)*. The number of states (modes) between any two frequencies can be evaluated by integrating *g(v)* over the range of the frequencies [5, 6].

In the Debye model it is assumed that the density of states follows a quadratic distribution up to a characteristic frequency, ν_D, (Debye frequency). Above that frequency density of states drops to zero (see Figure 3.1) [1]. The Debye frequency, similar to the Einstein frequency, can be expressed in terms of temperature called Debye temperature, $\theta_D = h\nu_D/k_B$. This relation is very useful because evaluating the Debye temperature for various materials gives an opportunity to measure and compare the strength and type of bonds between atoms of the materials.

By applying statistical mechanics, specific heat can be derived in terms of Debye temperature and given by [1]:

$$C_{mol}^{D}(T) = 9N_A k_B \left(\frac{T}{\theta_D}\right)^3 \int_{x=0}^{\Theta_D/T} dx \frac{x^4 e^x}{(e^x - 1)^2} \tag{3.13}$$

At low temperatures, when $T \ll \theta_D$, the specific heat should obey a T^3-law and the integral in equation (3.5) can be simplified into:

$$c_v = \frac{12\pi^4 N_A k_B T^3}{5\theta_D^3} \tag{3.14}$$

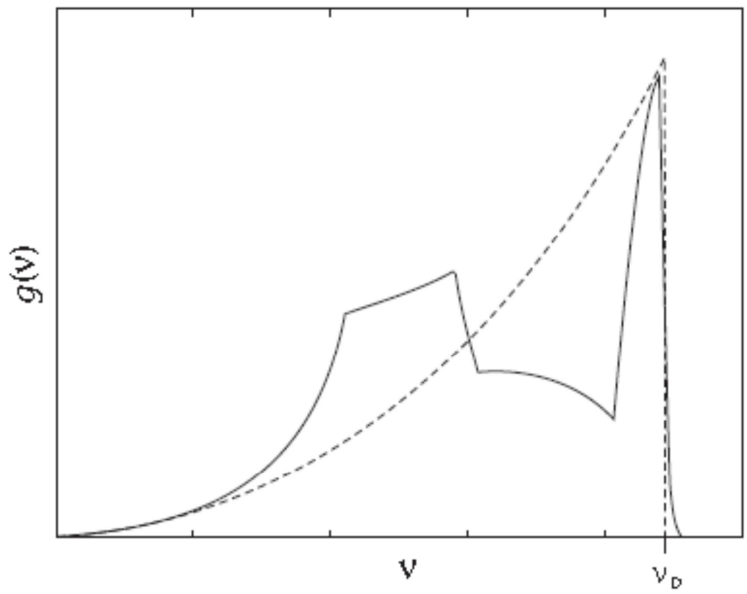

Figure 3.1. The vibrational density of states of copper as represented by the Debye model (dashed line) and from experimentally derived values (solid line) taken from [5, 6].

The Debye model is much better than the Einstein model to calculate specific heat, but it cannot be used as an exact and accurate model for real systems. This model does not work well for very small temperature ($T < \theta/50$) where the electronic part of the specific heat plays the main role and also in the high temperature ($T > \theta/2$) because it neglects completely all anharmonic effects.

3.2.4. Dulong and Petit law

Dulong and Petit in 1819 found that all metals, except the very light ones, have an average molar specific heat that is roughly equal to 25 $J \cdot mol^{-1} \cdot K^{-1}$ or 3R (where R is the universal gas constant for 1 mole). This law is an approximation but gives an important perception about the metals that the specific heat of a metal sample depends only on the number of molecules the sample has and not on the mass of an individual molecule [5].

Furthermore, experimental results conducted at various temperatures reveal that specific heat values changes with the change of temperature and depend upon the nature of the material. A graphical representation of the change of molar specific heat with the change

of temperature is shown in the Figure 3.2. From classical theory molar specific heat should have a fixed value no matter what the temperature of the system is but experimental results are different to what was predicted by classical theory. Einstein and Debye tried to explain thermal behavior of metals and non-metals by using Planck's quantum theory. It is very satisfying that, in the limit of high temperature, the sum of Einstein and Debye expression exactly leads to Dulong- Petit law:

$$\lim_{T\to\infty}\left[C_{mol}^{D}(T)+C_{mol}^{E}(T)\right]\equiv C_{mol}^{DP}=3rN_{A}k_{B} \tag{3.15}$$

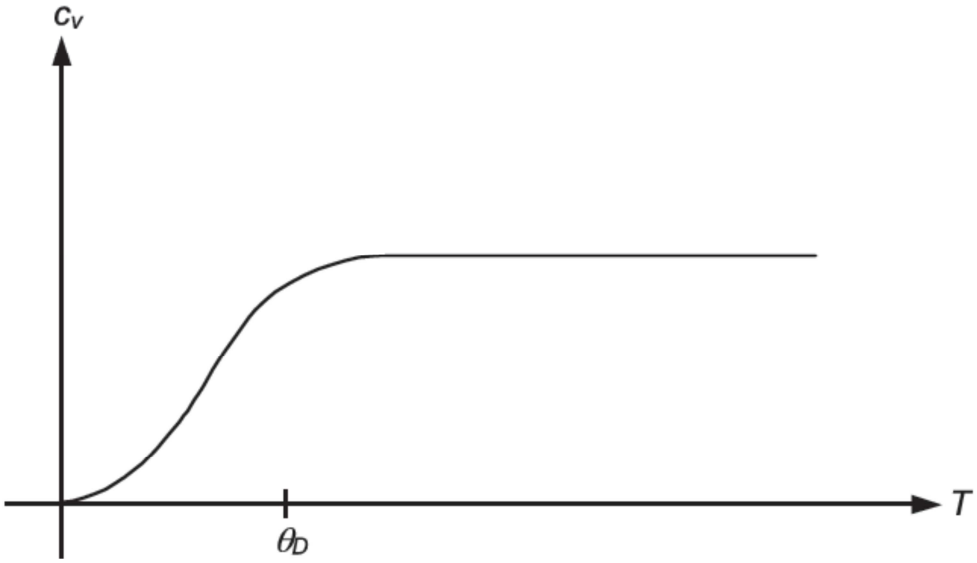

Figure 3.2. The variation of specific heat C_v, of solids with temperature, where θ_D is Debye temperature [5].

For a proper comparison of the Dulong-Petit values for the different materials, one has to transform the *molar heat capacity* (units $J\cdot mol^{-1}\cdot K^{-1}$) into the experimentally used units $kJ\cdot kg^{-1}\cdot K^{-1}$ by using the relations in (3.4).

After transforming the above equation we get the expression:

$$c_{v}^{DP}(T)=24.9432\frac{r}{M} \tag{3.16}$$

where c_v^{DP} in equation in units of kJ·kg^{-1}·K^{-1}. The above equation is used for quite a well-ordered structure of the alloy or for a strictly periodical system of unit cells with *r* is number of atoms per cell. This atomic system (throughout this work, we call it *molecule*) consists of *r* atoms and has the total molar mass *M*. It has been seen that the alloys which have been measured for the present investigation are often far away from this ideal situation. Only for that, we perform our theoretical studies for binary alloys AB for their simplest ordered structures A, A_3B, AB, AB_3 and B, generally for

$$A_\alpha B_\beta \text{ with } \alpha, \beta \in N_0$$

It is easy to calculate the relative mass contribution of the corresponding constituent B by

$$x = \frac{\beta m_B}{\beta m_B + \alpha m_A} \tag{3.17}$$

with m_A and m_B as the atomic masses of the pure metals A and B.

3.2.5. Specific Heat from the Density of States

Lattice specific heat can be calculated more accurately from already known phonon density of states for a material (see Figure 3.1). Applying the rules of statistical mechanics, the specific heat can be determined by integrating the density of states over all vibrational energies, ν, that gives the relation as:

$$c_v = \int_0^\infty g_0(r) \frac{v}{k_B T^2} \frac{e^{\frac{v}{k_B T}}}{(e^{\frac{v}{k_B T}} - 1)^2} dv \tag{3.18}$$

where $g_0(\nu)$ is the density of states of phonon at 0 K [5]. Even though this technique gives an accurate value for lattice specific heat but it is much more difficult to get exact values for the density of states. The phonon density of states in equation (3.18) can either be obtained by using high-energy inelastic neutron scattering data or from theoretical

investigations based on specially designed software programs, e.g. FP-LAPW WIEN2k or similar programs [7].

3.3.6. Lattice c_p/c_V Corrections

Experimental data for the heat capacity usually refer to c_P, i.e., the heat capacity at constant pressure, on the other hand, theoretical models are often performed under the condition of constant volume, c_v. At low temperatures, typically T < 20 K, the difference between c_p and c_V is almost insignificant and usually ignored, and more importantly c_p can be modeled with the functions used to describe c_v. Contrary to this, at high temperatures this difference becomes increasingly larger and significant. Therefore, equation (3.11) is an exact relation between c_v at and c_p at high temperature.
Anharmonic effects can make $c_p(T)$ larger than the classical result, $3k_B$/atom, at high temperature [2, 5]. Nevertheless, the actual specific heat credited to the free electrons is much smaller than what is predicted by classical mechanics; it is only by applying quantum mechanics to the system that one can accurately find the electronic specific heat.

3.2.7. Heat Capacity of the Valence Electrons

High thermal and electrical conductivity in metals is due to the conduction electrons which can move almost freely throughout the lattice. For getting specific heat capacity from these free electrons it is considered that these electrons act as ideal gas particles. From the equipartition theorem, each mole of conduction electrons contributes $\frac{3}{2}R$ to the entire specific heat of the metal which is quite higher than the actual specific heat of metals. According to quantum mechanics, Pauli Exclusion Principle, no two electrons can exist in the same energy state, so there must be a broad range of distribution of the energies up to some maximum energy state. Possibility of electrons to excite to higher states is very small at low temperatures only high energy electrons are able to move to energy states close to the Fermi energy, ε_F [6]. These are the electrons which are able to change energy states and contribute to the specific heat and, at lower energies, there is zero probability of the electron transitioning to a higher state. Probability of transitioning

to a higher state is 50 % pertained to Fermi energy. Applying Fermi-Dirac statistics one can express electronic specific heat as:

$$C_{vol}^{el}(T) \approx \frac{\pi^2}{3\Omega_0} N_0(\varepsilon_F) k_B{}^2 T \tag{3.19}$$

where N_0 means the electronic density of states with respect to Ω_0, the volume of the unit cell of crystal. At low temperatures, the electronic contribution is the major portion to specific heat and is directly proportional to the change of temperature. Conversely, in the high- temperature region, the electronic specific heat is only a small fraction of the total specific heat. The specific heat is observed as $C = \gamma T + \beta T^3$ in the low-temperature range, where γT is the electronic and βT^3 is the lattice contribution to the specific heat [6].

3.3. Mathematical Derivation

Valence electrons contribution to specific heat from the energy density of an electron gas within a crystal of volume Ω at a certain temperature T is given by:

$$u(T) = \frac{1}{\Omega} \int d\varepsilon N(\varepsilon) f(\varepsilon; T) \tag{3.20}$$

where N (ε) is the total (for both spin directions) electron density of states (DOS) and f (ε; T) is the Fermi-Dirac probability function. For practical reasons, in the following we prefer to use the quantity

$$N_0(\varepsilon) = \frac{\Omega_0}{\Omega} N(\varepsilon) \tag{3.21}$$

with Ω_0 as the volume of the unit cell of the crystal. N_0 (ε) is normalized as

$$\int^{\varepsilon_F} d\varepsilon N_0(\varepsilon) = Z_0 \tag{3.22}$$

where Z_0 is the number of valence electrons per unit cell. Then one gets for the electronic part of the *volume-specific* heat capacity

$$C_{vol}^{el}(T) \equiv \frac{d}{dT}u(T) = \frac{d}{dT}\int d\varepsilon \frac{N_0(\varepsilon)}{\Omega_0}\frac{\varepsilon}{e^{(\varepsilon-\mu(T))/k_BT+1}} \tag{3.23}$$

Including the chemical potential of the electron gas, μ (T), this is defined by

$$\lim_{T\to 0}\mu(T) = \epsilon_F$$

Where ϵ_F is the Fermi energy, and by the relation

$$Z_0 = \int d\varepsilon N_0(\varepsilon)\frac{1}{e^{(\varepsilon-\mu(T))/k_BT+1}} \tag{3.24}$$

If the chemical potential $\mu\ (T)$ is known, one can start the evaluation of Equation (3.23), namely

$$C_{vol}^{el}(T) = \int d\varepsilon \frac{N_0(\varepsilon)}{\Omega_0}\varepsilon\frac{\partial}{\partial T}\left[\frac{1}{\exp[x(T)+1]}\right] \text{ with } \quad x(T) = \frac{\varepsilon-\mu(T)}{k_BT}$$

Using the derivative of the term in brackets [· · ·]

$$\frac{\partial}{\partial T}\left[\frac{1}{\exp[x(T)+1]}\right] = \frac{\exp[x(T)]}{\{\exp[x(T)+1]\}^2}\frac{dx(T)}{dT} = -\frac{1}{2[1+\cosh(x(T))]}\frac{dx(T)}{dT}$$

one obtains the final result.

$$C_{vol}^{el}(T) = -\int d\varepsilon \frac{N_0(\varepsilon)}{\Omega_0}\varepsilon\frac{1}{2[1+\cosh(x(T))]}\frac{dx(T)}{dT} \tag{3.25}$$

With $\frac{dx(T)}{dT} = [-\mu'(T)T - \varepsilon + \mu(T)]/[k_BT^2]$ and $\mu'(T) = \frac{d\mu(T)}{dT}$

In many practical cases – (as It will be demonstrated in this work) - it is sufficient to evaluate Equation (3.23) approximately by using the so-called Sommerfeld formula [2] which gives the result

$$C_{vol}^{el}(T) \approx \frac{\pi^2}{3\Omega_0} N_0(\varepsilon_F) {k_B}^2 T \tag{3.26}$$

As we already expressed that the contribution of the valence electrons to the heat capacity requires the numerical evaluation of the Equations (3.24, 3.25) or the evaluation of the Sommerfeld approximation (3.26). The following expressions differ from the Equations. (3.23, 3.24) in two points: (i) the volume-specific heat capacities are changed into the mass-specific ones - a division by the density d (equation 3.4), and (ii) all physical constants in the formulas are reset by their numbers: By doing so, the following expressions are ready for computer.

With c^{el} given in $kJ \cdot kg^{-1} \cdot K^{-1}$, T in K, d in $kg \cdot m^{-3}$, ε and μ in eV, N_0 in 1/eV, and Ω_0

in $Bohr^3$, the exact formulas read as

$$C^{el}(T) = -1.081146.10^9 \frac{1}{d} \int d\varepsilon \frac{N_0(\varepsilon)}{\Omega_0} \frac{\varepsilon}{2\left[1+\cosh(x(T))\right]} \frac{dx(T)}{dT} \tag{3.27}$$

With $x(T) = 1.1604155.10^4 \frac{\varepsilon - \mu}{T}$

and $\frac{dx(T)}{dT} = 1.1604155.10^4 \frac{-\mu' T - \varepsilon + \mu}{T^2}$ with $\mu' T = d\mu(T)/dT$

The corresponding *Sommerfeld approximation* (in units of $kJ \cdot kg^{-1} \cdot K^{-1}$) reads as:

$$C^{el}(T) = 26.41409 \frac{1}{d} \frac{N_0(\varepsilon_F)}{\Omega_0} T \tag{3.28}$$

References

[1] Gopal E S R, 1966 *Specific Heats at Low Temperatures*, New York: Plenum Press.

[2] Barron T H K, White G K, 1999 *Heat Capacity and Thermal Expansion at Low Temperatures,* New York: Kluwer Academic/Plenum Publishers.

[3] Ott J B, Boerio G J, 2000 *Chemical Thermodynamics: Principles and Applications*, London: Academic Press.

[4] Grimvall G, 1999 *Thermophysical Properties Of Materials* Elsevier Science B.V. Sara Burgerhartstraat 25 P.O. Box 211,1000 AE Amsterdam, The Netherlands pp 208.

[5] Kittel C, 1996 *Introduction to Solid State Physics*, New York: John Wiley and Sons, 7th edn.

[6] Stokes H T, 2000 *Solid State Physics,* Provo, Utah: Brigham Young University, 3rd edn.

[7] Blaha P, Schwarz K, Madsen G K, Kvasnicka D and Luitz J in WIEN2k, 2001 *An Augmented Plane Wave + Local Orbitals Program for Calculating Crystal Properties*, edited by K. Schwarz (Technical University Wien, Wien, Austria.

Chapter 4

Experimental Method and Technique

It is well known that thermophysical properties of solids vary extensively depending on the structure, density, porosity, electrical conductivity, etc., of different materials. Frequently these properties exhibit a strong dependence on temperature and pressure. Because of these large variations a number of experimental techniques have been developed and these are [1]:

ohmic pulse heating technique	laser pulse heating technique
electromagnetic levitation	electrostatic levitation
sessile drop technique	chemical flame technique
shock wave technique	solar heating technique
fission/fusion Technique	electron/neutron heating

All others are considered to be non-calorimetric and have lack of information about the exact energy input to the test specimen except ohmic pulse heating technique.

4.1. Ohmic Pulse Heating Technique

Conventional high-temperature techniques to investigate thermophysical properties create many difficulties like chemical interaction of the liquid specimen with the container and the loss of mechanical strength, problems with heat transfer, evaporation, and electric insulation. A pulse heating technique has been developed to cope with these difficulties and enable the measurements to extremely high temperature. During the last two decades ohmic pulse heating technique have matured because of improved, fast and reliable electronic data-acquisition devices, which are commercially available. This technique uses resistive self-heating of an electrical conductor typically wire-shaped samples (the diameters ranging from a few hundred micrometers up to a few millimeters), rectangular shaped samples, foils, or tubes by passing a large current pulse over the sample. Because of its resistivity, the test specimen can be heated to its boiling point in a fraction of a second. Heating rates up to 10^8 $K \cdot s^{-1}$ are achieved and the sample is heated from room temperature up to the end of stable liquid phase in about 30 μs, where it is being

destroyed when crossing the spinodal line (‘‘exploding wire’’). Despite of high heating rates, the measured results agree well with data obtained by static and quasi-static methods. Within this short time, the geometry of the sample is neither destroyed through force of gravity, instabilities nor other effects, so short-time measurements are possible on "standing” liquid columns. The measurements are performed in an inert environment e.g., nitrogen or argon at ambient pressure and using water at high pressure. The energy storage fitted in this circuit is 500-μF capacitor bank, which could be charged up to 10 kV using a high voltage power supply [2]. Therefore, different precautions have been made to avoid electromagnetic interferences and all signal wires are constructed in a double-coaxial fashion with a coaxial cable shielded by an additional copper tube. All measurement devices (amplifiers, voltage dividers, pyrometers, etc.) are isolated so that electrically active pick-up loops can be avoided and the data acquisition equipments are kept in an electrically shielded room (Faraday room). Personal computers with A/D conversion-based data acquisition cards are used to record all transient measurement signals. Great care has been taken when it comes to the starting and terminating of an experiment because accurate knowledge of the timescale (experimental duration) during all dynamic pulse-techniques is essential. Different switches are used and operated by a common trigger signal. A schematic diagram of the discharge circuit and a picture of the setup used in our laboratory are shown in Figure 4.1 and Figure 4.2 respectively.

The major parts in pulse heating experiments are the energy storage (500 μF, max) with a charging unit (variable voltage from 0-10 kV), a main switching unit (i.e., high-voltage mercury vapour ignition tubes), the sample chamber with windows for optical diagnostics and the ability to maintain and control ambient atmosphere, the data recording equipment and a fast CCD-camera system for expansion measurements.

4.2. Sample chamber

Figure 4.2 shows the cross section of a sample chamber, in which the experiments are performed. It is a cylindrical container with the outer diameter of Ø = 18 cm and an effective internal diameter of Ø = 15 cm. The sample chamber is made of aluminum and is anodized black. This is done to prevent stray light during the experiment and acts

as insulation. In an experiment, the current runs through the sample and is then discharged through the exterior wall of vessel. The actual sample holder is designed to insert in the sample chamber. All parts in the circuit are made of brass while the rest are made from insulator to isolate the chamber from any electrical signal. The electrical terminals are designed so that there is no short circuit of electric current. For the optical measurement, three windows are made in the walls of the sample chamber. Two out of these three windows are used for expansion measurements using a fast CCD camera while flash on one side and camera on other side whereas one window is for temperature measurement using the pyrometer. These windows contain ordinary float glass with a thickness of 5 mm. All windows are sealed using an O-ring and with a bracket attached outside of the chamber window.

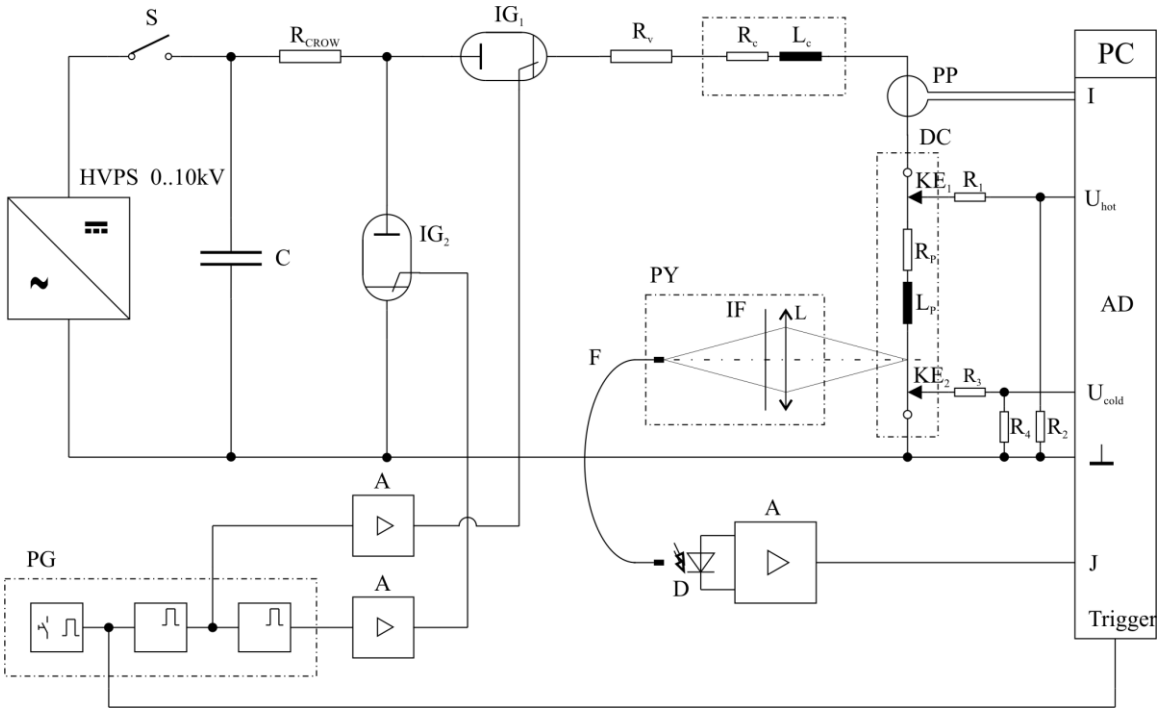

Figure. 4.1. Schematic diagram of discharge circuit

Key: HVPS; High voltage power supply, C; Capacitor bank, S; Switch, R_{crow}; Crowbar resistor; R_v; Variable resistor, $IG_{1,2}$; Ignitron, PG; Pulse generator, A; Amplifier, PP; Pearson probe, DC; Discharge chamber, $KE_{1,2}$; Knife-edges, R_1-$R_{2;}$ Ohmic voltage divider resister; PY; Pyrometer, L; Lens; IF; Interference filter, F; Light-fiber, D; Photodiode [3].

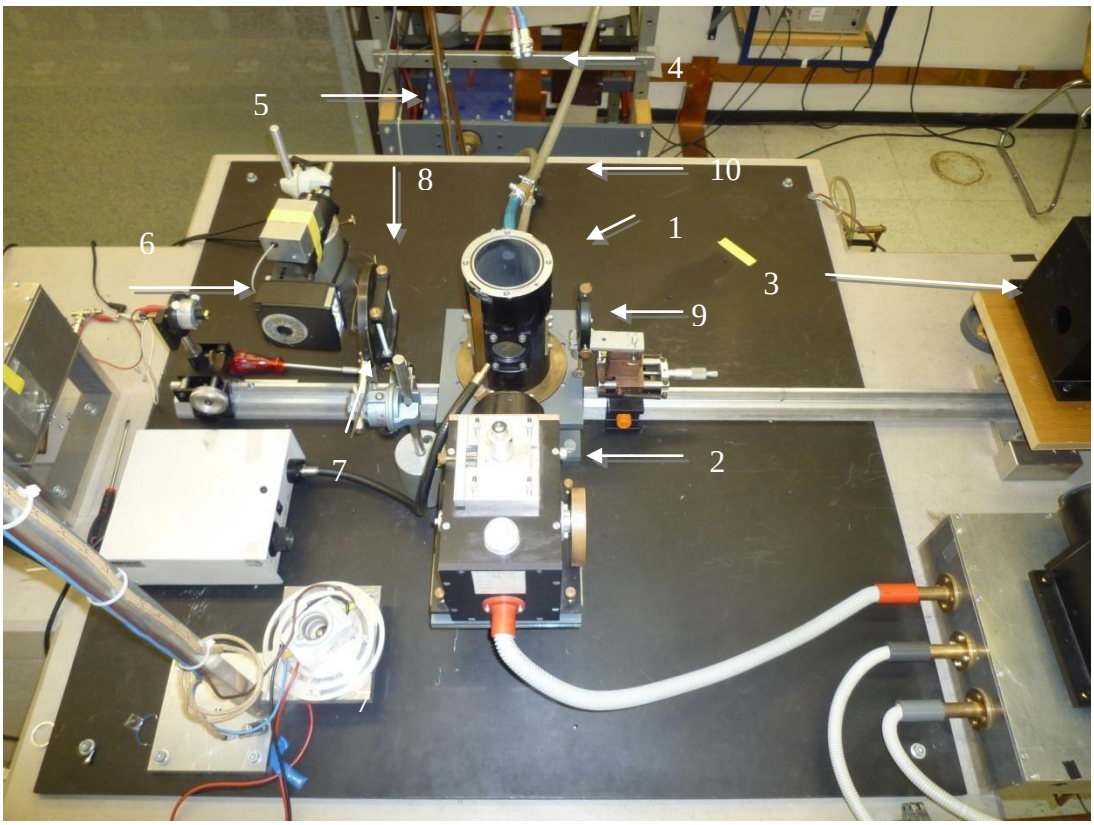

Figure 4.2. A view of the central components of the experimental set up is shown with its components. 1. Sample chamber, 2. Pyrometer, 3. CCD Camera, 4. Voltage drop Probes, 5. Pearson probe, 6. Flash, 7. Aperture, 8. Infrared filter, 9. Focusing lens, 10. Inert gas pipes.

The chamber has two gas connecting pipes for inlet and outlet of inert gas (pressure = 1.3 bar) with a mechanical lockable valve so that gas supply and removal can be controlled. Inert gas environment is necessary for some materials to suppress discharges between wire and sample and to prevent burning of the liquid metal. Inert gases like argon or nitrogen are generally used. This chamber does not need too much cleaning; only it should be rinsed well after each experiment with inert gas and organic detergent. The experiment chamber is fastened from its base using a large banded clamp with ground connection.

4.3. Pyrometer and Temperature Measurement

Temperature is an important quantity to be measured when investigating thermophysical properties of metals using pulse-heating techniques. The temperature measurement is based on the detection of the thermal radiation emitted by the sample by a fast pyrometer. A pyrometer is a non-contacting device that can be used to determine the temperature of an object's surface by its emitted thermal radiation. A pyrometer consists of a lens system for optical imaging of the sample surface, a wavelength selective element such as an interference filter, aperture for an area limitation and a photodiode detector. Furthermore, a pyrometer has an alignment system by which the surface of the sample can be selected or adjusted for the pyrometric measurement and a wave guide that lead the light signal to the photodiode detector. A schematic diagram of the pyrometer is shown in the following Figure 4.3.

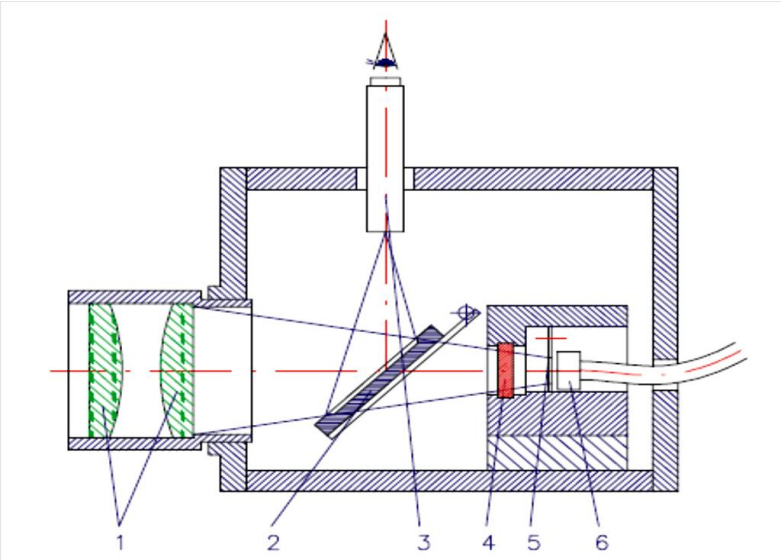

Figure 4.3. A schematic diagram of pyrometer with optical design: 1. Achromatic lens, 2. Folding mirrors, 3. Measurement microscope, 4. Interference filter, 5. Aperture, 6. Optical waveguide [4].

In the pyrometer wire intensity is focused on the rectangular area of 0.2 mm x 10 mm of the pulse-heated sample surface (sample dimensions: 50 mm length, 0.5 mm diameter) with a 1:1 magnification onto the rectangular entry slit of an optical waveguide. The interference filter is in front of the entry slit of the waveguide. The optical waveguide leads the radiation to a metal housing where it is detected by a Si-photodiode and

amplified with a fast amplifier (bandwidth 1 MHz). An amplified intensity signal (J) of the sample radiation is sent to a shielded room by means of coaxial cable inside of a copper tube and then recorded by data acquisition card of a computer.

Pyrometry measures thermal radiation, emitted from any heated body or substance and their temperature is determined using the Planck's radiation law.

$$T = \frac{c_2}{\lambda \ln\left\{1 + \frac{J_m(T_m)\,\varepsilon(\lambda,T)}{J(T)\,\varepsilon(\lambda,T_m)}\left[\exp\left(\frac{c_2}{\lambda T_m}\right) - 1\right]\right\}} \qquad (4.1)$$

Whereas c_2 is 2nd Plank's constant ($c_2 = 1.43879.10^{-2}$) λ is the wavelength selected by the interference filter (in this work λ = 1570 nm), ε is the emissivity; J is the radiance intensity detected by the pyrometer; the subscript m denotes the temperature at the melting point [5]. The output signal of pyrometer along with two voltages (hot and cold) and current and shown in Figure 4.4.

Since the emissivity $\varepsilon\,(T)$ of most liquid metals is unknown, an assumption has to be made for the ratio $\varepsilon\,(T)$ / $\varepsilon\,(T_m)$ in the liquid phase of the metal. The $\varepsilon\,(T_m)$ is the value of the emissivity of the sample at the melting temperature T_m, where temperatures are calculated by forming ratios of radiance $J(T)$ at a temperature T to the radiance $J_m(T_m)$ at T_m. The melting temperature T_m is taken from literature data [3]. Up to now a constant emissivity $\frac{\varepsilon(T)}{\varepsilon(T_m)} = 1$ was assumed for the liquid phase for pulse-heating experiments. Simulations showed that a change of emissivity during the liquid phase does not affect the temperature results too much [6].

A black body for the calibrations of the pyrometer is shown in the Figure 4.5b. The most accurate temperature can be achieved for pulse-heated liquid samples if the emittance is known in the temperature range of interest. Four different pyrometers are being used at TU Graz which operate depending on the investigated material and centre wavelength selected by interference filters. Details of the pyrometers with corresponding temperature ranges are given in the Table 4.1 below,

Table 4.1. General classification of the four pyrometers according to their interference filters (IF) and estimated temperature range. The filter data are from the supplied data sheets.

λ_0 = Central wavelength

$\Delta\lambda$ = Full width half maximum

λ_0	$\Delta\lambda$	Temperature range
649.7	37.2	$2100 < T < 5500$
902.0	18.2	$2000 < T < 5000$
1569.5	83.6	$1100 < T < 2500$
2106.7	94.0	$800 < T < 2000$

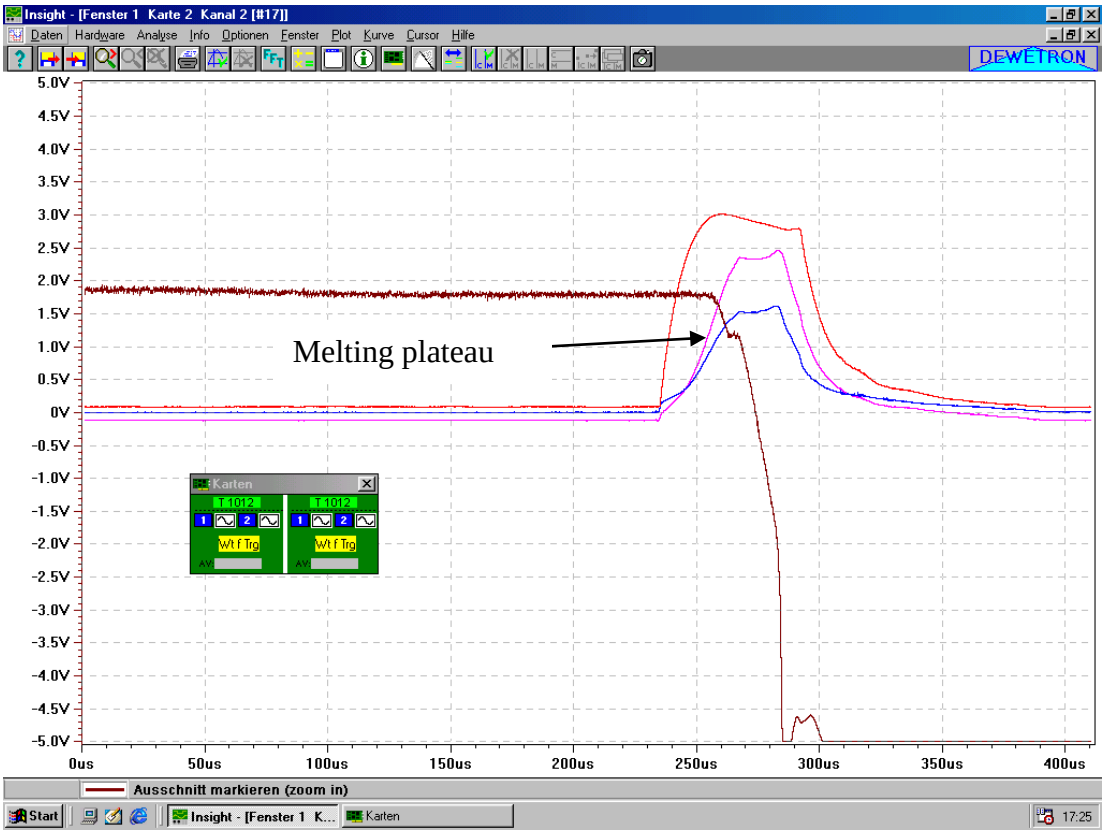

Figure 4.4. Four input signals from pulse heating set-up to ‘‘insight’’ software, red curve; current signal, purple curve; hot voltage, blue curve; cold voltage, brow curve; pyrometer signal (inverted temperature signal).

(a)

(b)

(c)

Figure 4.5. Parts of pulse heating set up. Figure (a) 1. Capacitor bank, 2. Ignitrons, 3. Krytrons, Figure (b) A black body source, Figure (c) 1. High voltage power supply, 2. Actual voltage display meter, 3. Multimeter (displays 1/276th of actual voltage).

4.4. Pearson Probe and Current Measurement

The current is measured with an annular flow probe (type 3025 made by Pearson Electronics, USA) using the induction principle. It produces a proportional voltage signal of the direct current flowing through its measurement aperture (see Figure 4.5). The calibration factor of the probe is 79.6 A/V, the accuracy is reported to $\pm$ 0.5 %. During a measurement, very high currents (about 10^4 A) can occur, depending on the specimen and the charging voltage. Therefore the probe is double shielded to protect against interference of any external unwanted signals.

4.5. The Voltage Probes and Voltage Drop Measurement

The voltage drop across the resistive sample inside the discharge chamber is measured by two knife edges placed on two places of the wire sample. The desired voltage is obtained by subtracting the two voltage signals (high voltage or hot voltage and low voltage or cold voltage). The high voltage comes from start of the sample and low voltage comes after or ends of the sample. This method of getting voltage signals helps to cancel out arbitrary resistance at the contact points of the knife-edges, which could be nearly impossible to determine otherwise. The Knife-edges collect voltages through coaxial cables inside a copper pipe. The measured voltage terminates at digital oscilloscope through voltage divider by ratio 1000:1 for high voltage and 300:1 for low voltage. The values of the resistances used in divider are 50 k Ω and 5 Ω for hot and cold signals respectively, (see Figure 4.4).

4.6. CCD Camera and Expansion Measurement

The thermal expansion of the sample during pulse-heating experiment is performed by a fast CCD-camera system. The camera system consists of a multi-channel plate (electron multiplier), a lens with a 1:1 imaging, a CCD - chip combination and a controller. The camera can be operated in two modes, one is the normal camera mode, which is used in the pulse heating experiment, and the other one is the live-screen mode. The live-screen mode provides a real-time image of the sample. In both modes, the image is transferred to the image processing program Winsis by Theta System Elektronik GmbH.

A schematic of the CCD camera is shown in Figure 4.6 and the display system is shown in Figure 4.8a. During the pulse heating experiment a magnified image of a small section of the specimen is focused onto a multichannel-plate (MCP) - CCD - chip combination by using a focusing lens. Light reaches on the MCP, which acts as a shutter and amplifier and sets the pre-defined exposure time while the CCD- chip records and stores the images. In order to obtain a high frame rate, which should enable more than one picture per experiment, only a small part of the chip is exposed to light for example 32, 16, or 8 out of total 576 lines while the rest area is masked for quick succession of pictures and memory. Figure 4.7 shows CCD- pictures after shifting of 32, 16 and 8 lines. The camera system takes images of radial expansion of the sample about every 5 µs or 2.5 µs, which depends on the preset exposure time.

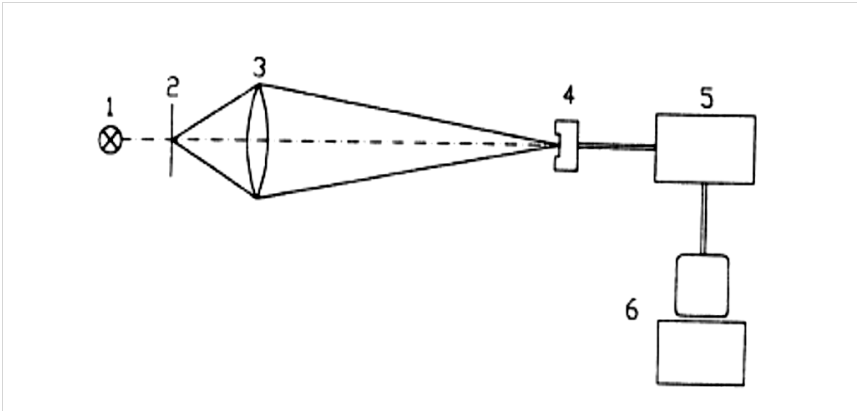

Figure 4.6. Schematic of the experimental setup for measuring expansion. l. Background light source (flashlight); 2. Sample; 3. Lens, 4. CCD- Camera, 5. Camera control; 6. Computer [7].

After a successful experiment the captured images can be saved and further used through a 12-bit analog - digital converter in a personal computer using a software package Winsis (developed by Theta - system company, Munich). These obtained CCD pictures are used for the evaluation of thermal expansion of the sample. For that purpose two sequences of pictures are taken one before the heating process as cold picture and the second sequence is taken during heating as ‘‘hot picture’’. Consequently, the pictures are converted into intensity profiles and the diameter is evaluated using a software named ‘‘Wiredia’’ which gives the wire diameter by calculating full-width-half-maximum (FWHM) from the intensity profiles of the pictures. Then, each hot picture diameter is

divided by its corresponding cold picture diameter for expansion calculation. The intensity profile of a picture is given in the Figure 4.8b. The controller of the camera system manages amplification factor, frame rate and working of multi- channel plate. The existing image acquisition system was first described, designed and built by Nussbaumer [8].

This CCD camera technique does not image the entire specimen during an experiment, but is limited to a small spatial portion of the sample radius/diameter and yielding only the time propagation of that part. This method can be used as an experimental evidence of stability of the sample during expansion. It is assumed that expansion in the solid state occurs in both radial and axial directions but only in radial direction in liquid state. It has been proofed experimentally that samples only expand radially and do not show any longitudinal expansion above a sufficiently high heating rate, which is the case of pulse heating technique. Different systems and techniques developed for expansion are briefly discussed in [9].

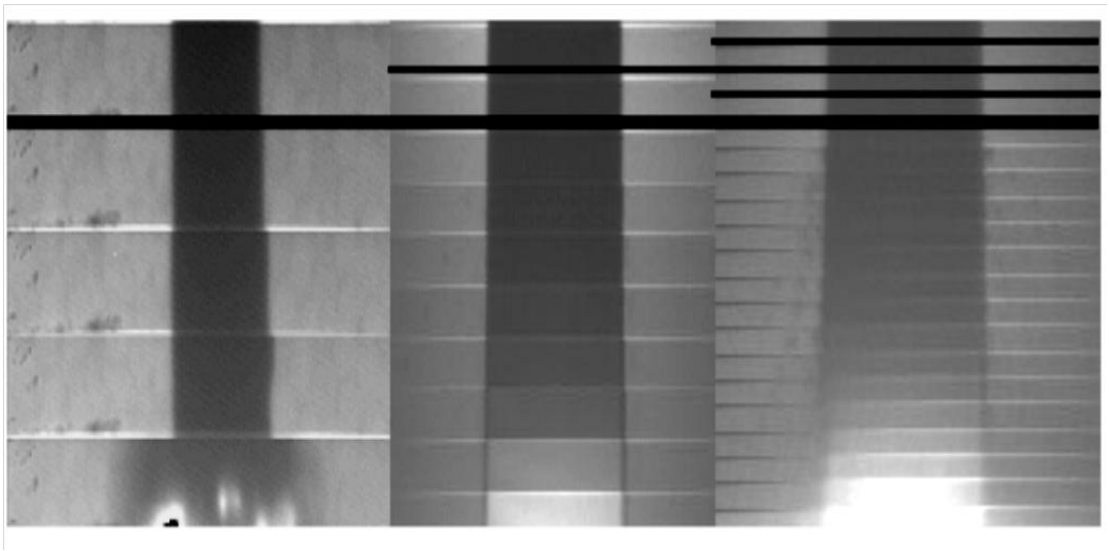

Figure 4.7. CCD-camera pictures, time axis from top to bottom, left: 32 lines shifted, middle: 16 lines shifted, right: 8 lines shifted [9].

4.7. Experimental procedure

Ohmic Pulse heating experiment include the following steps.

i) Pre-experimental settings/stages ii) Sample preparation iii) Pulse heating process

4.7.1. Pre-Experimental Settings/Stages

Procedure of an experiment starts with turning on equipments, two computers one for electrical data and other for expansion measurement along with their softwares ‘‘Insight’’ and ‘‘Winsis’’, pulse generator, infrared lamps for ignitron heating, camera control, flash lamp and opening valve of inert gas cylinder to allow gas to reach pressure gauge.

Removing lids from the camera, pyrometer and illuminating torch are also being done. Setting parameters values on the pulse generator, these values depend on the material properties. The pyrometer is being selected according to the properties of sample investigated. Appropriate range for the four measurement channels on computer in the Faraday’s room for the Insight program are adjusted with a range of 100 mV to 5 V so that final traces of output signals should be within the range of the graph of the software, see traces of graph in Figure 4.4.

4.7.2. Sample Preparation and Measurement Arrangements

To prepare the sample for experiment include cutting of required length of wire (usually 7 cm), fix it in the sample holder (Figure 4.9 b) and clean its surface by an abrasive paper (grad/grain size 1200) and subsequent defatting of the wire surface with acetone. The initial wire diameter D_0 is measured using a laser micrometer (Keyence LS-7001 see Figure 4.9a) by measuring at several wire positions and taking average of all those values this value will be use later by relative radial expansion measurements. After clamping the wire in the sample holder two molybdenum notches are attached for voltages drop measurement (U_{HOT}, U_{COLD}). The distance between these two notches is measured by a cathetometer (scales divider 2 / 100 mm, see Figure 4.9c) and it is the effective length of the heated sample. Sometimes plasticine is attached to isolate the sample holder from discharges. After doing that, non-conductive sample holder is inserted into the sample chamber and connections of U_{HOT}, U_{COLD} and inert gas pipes are attached respectively. Then inert gas is allowed to flow in the sample chamber about 8 seconds to prevent

possible chemical reactions and possible discharges between sample and sample holder during the measurement. A check valve makes sure that the chamber remains under 1.3 bar pressure.

The pyrometer is being focused by folding/tilting mirror and irradiating the wire with a torch through a glass window in the sample chamber. The optimal position is at 1.1 on the eyepiece scale when viewing through the microscope of pyrometer, this ensured best possible intensity results. By folding back of the mirror, the pyrometer is ready for measurement. If necessary, we attach another filter from the gray filters set (Figure 4.9d details are given in Table 4.2) in front of the window of the sample chamber to reduce the intensity of light. The pyrometer measurements are performed at right angle to the expansion measurement. The flash is set at optimum position on one side of the chamber. An aperture is placed in front of the flash to ensure a parallel beam through the entrance window on the wire. An I.R filter is also used to suppress unwanted portions of light from the flash to the pyrometer measurement. The image of the wire is formed through the lens on the camera. A fine image is adjusted using micrometer screws on the lens system. Each view of the sample on display system is done by activating the recording on attached computer but without the charging the capacitor bank. Extra lights are switched off to minimize stray light effect. After proper adjustment, we can save the resulting image as a cold image of the sample.

Table 4.2. Details listed grey filter;

I_T = Transmitted intensity, I_0 = Incident intensity, D = Optical density

D	I_T / I_0 in %
0.1	79.43
0.2	63.09
0.3	50.11
0.4	39.81
0.5	31.62
0.6	25.12
0.7	19.95
0.8	15.85
0.9	12.59
1.0	10.00
1.3	5.01
2.0	1.00

4.7.3. Start of Heating Process

At the beginning of an experiment the capacitor bank with a total capacity of 500 μF is charged by a high-voltage transformer by closing the switch *S* (see Figure 4.1) while the digital voltmeter continuously measures and displays $1/276^{th}$ part of the charging voltage (Figure 4.5c). The required charging voltage varies from a minimum of 3 kV up to a maximum of 10 kV and is dependent on the resistance, the thickness and of length of the wire samples.

Experiment starts by pressing the input push button (yellow coloured button see Figure 4.8c). It initiates the electronic data collection at PC in the shielded room and starts the flash (Figure 4.2). After time shift of (T 1-2) the CCD camera begins recording the images. Only after this time flash reaches its maximum brightness plateau and stays there at about 100 microseconds. After the shift of T 2-3 activation signal arrives at Krytron 1 and Krytron generates a high voltage pulse (in this case 3 kV charged capacitor with the capacitance of 0.25 μF). The generated galvanically isolated trigger pulse turns on the ignitron IG1. At this stage discharges of the capacitor bank starts over the wire sample.

The final value T 3-4 indicates how long the wire is heated and it is used to end the heating process at the activation of the second ignitron (IG2) that short-circuit the capacitor through the crow bar. At the end of experiment, residual voltage is grounded whereas T 4-5 is unused in this design. The advantage of the second ignitron is to minimize contamination of the sample chamber, prevent plasma discharges and protection of the circuit components. Furthermore, there is an option of a series resistor with adjustable values, 1/2 Ω and 1/4 Ω, to regulate the speed of heating process.

At the end of the experiment the Krytrons are switch off and the sample chamber is rinsed for about 8 seconds with fresh inert gas in order to purify and clear it from produced suspended particles. The measurement results are stored on both PCs. Sample chamber and sample holder are cleaned with organic detergent whereas metal residues are removed by using sandpaper (grain size 240). All part and pieces are dismantled in reverse order.

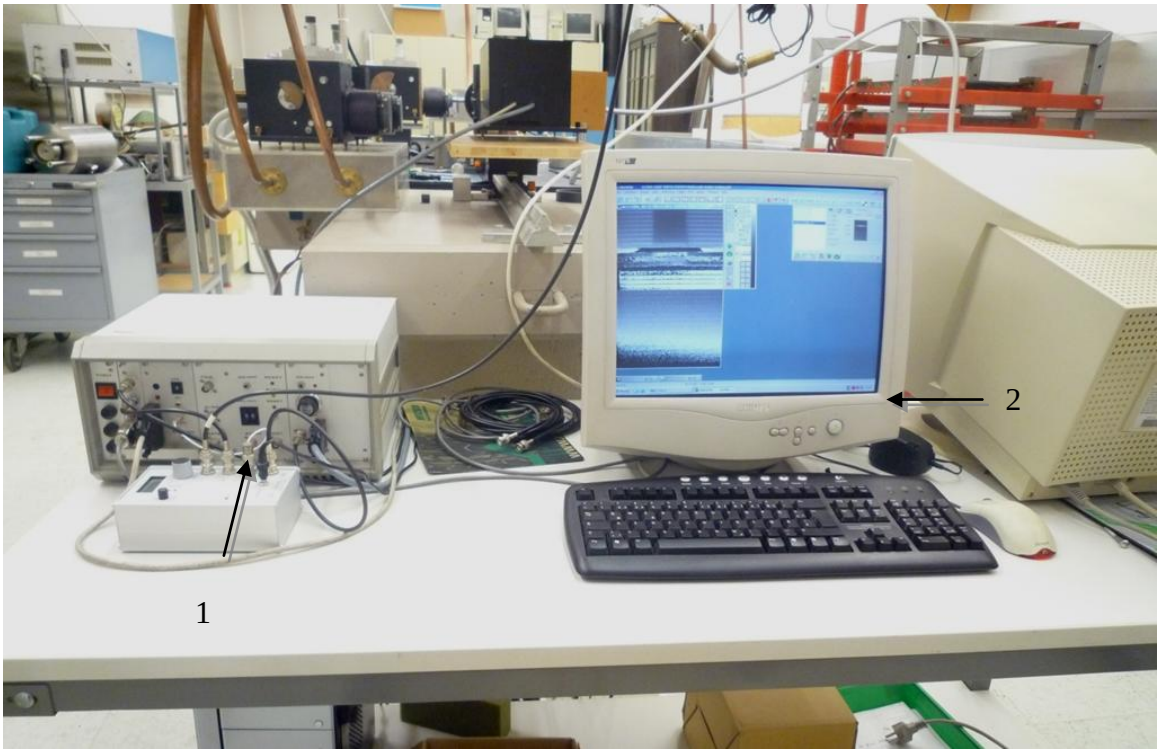

(a)

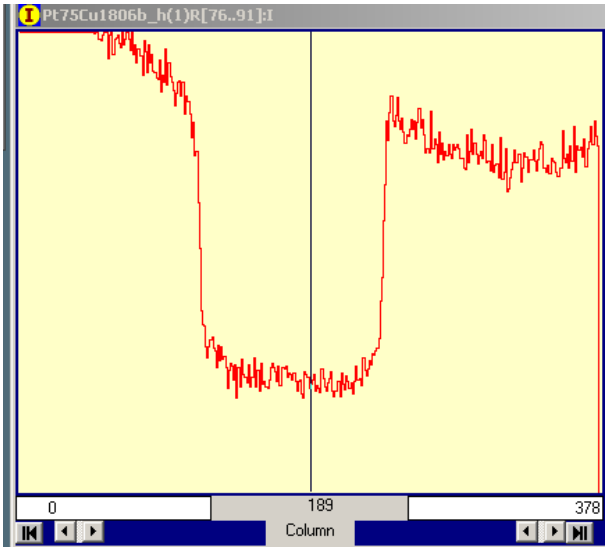

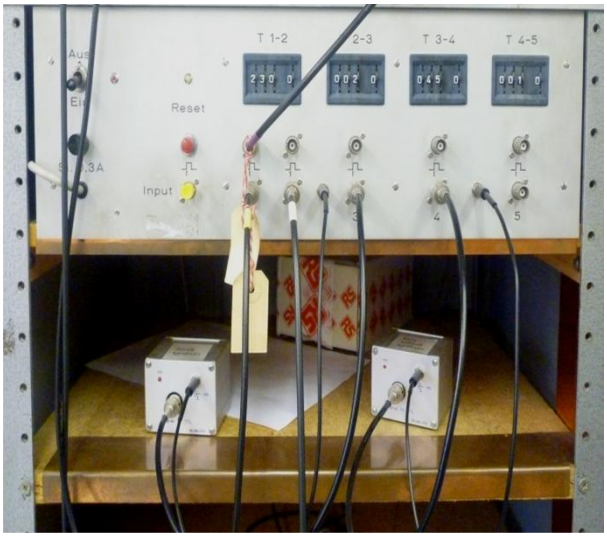

(b) (c)

Figure 4.8. Expansion system along with timing generator. In Figure (a) 1. Control system, 2. Display unit, (b) Intensity profile of expanding wire during heating process, (c) Pulse generator, where T 1-2. Flash start time, T 2-3. Time shift for image recording and the start of pulse heating experiment, T 3-4. End of the experiment, T 4-5 Unused.

(a)

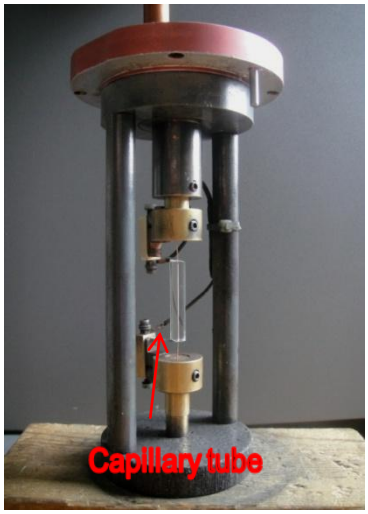

(b)

(c)

(d)

Figure 4.9. Sample holder with other measuring instruments (a) Laser micrometer (b) Sample holder (c) Cathetometer (d) Grey filters.

References

[1] Gustafsson SE, 1991 *Transient plane source techniques for thermal conductivity and thermal diffusivity measurements of solid materials.* Review of Scientific Instruments, **62**(3): pp 797-804.

[2] Mehmood S, Klotz U E and Pottlacher G, 2011 *Thermophysical Properties of Platinum-Copper System* EPD Congress pp167.

[3] Cagran C, *Diploma thesis* (Technical University Graz, 2000).

[4] Sonnberger A, *Diploma thesis* (Technical University Graz, 2004).

[5] Bergmann L and Schaefer C, 1990 *Lehrbuch der Experimentalphysik Band L IO.Auflage,* Walter de Gruyter, New York.

[6] Seifter A, *Diploma thesis (*Technical University Graz, 1996).

[7] Boboridis K, *Diploma thesis* (Technical University Graz, 1999).

[8] Nussbaumer G, *Diploma thesis* (Technical University Graz,1993).

[9] Hüpf T, *PhD thesis* (Technical University Graz, 2010).

Chapter 5

Thermophysical Properties and Data Evaluation

Thermophysical properties are material properties that vary with temperature without altering the chemical identity of the material.

According to the above definition there are many thermophysical quantities, of which some are enthalpy, resistivity, thermal conductivity, thermal diffusivity, heat capacity, thermal expansion, density, speed of sound, viscosity, surface tension, interfacial tension and thermal radiative properties etc. A few from these are described in this chapter precisely. Before going into detail about those thermophysical quantities it seems reasonable to discuss about 'Hotwire' program incisively which is used to process the data gained by the pulse heating technique into convenient data for graphical representation.

5.1. Hotwire Program

The Hotwire Software Program is designed for the evaluation of pulse heating data. Data acquisition is done by the software package INSIGHT (developed by Dewetron) which delivers raw data in ASCII-format. The data consists of two voltages (voltage hot, voltage cold) and intensity of surface radiation of sample every 0.1 µs with a capacity of 4096 data points. The imported raw data are processed within Hotwire in the following manner:

- *Offset correction*

The trigger pulse for data acquisition is typical 200 μs before the start of the experiment. This period is used to correct the offset by averaging the data during this time and subtracting the mean value from the entire signal.

- *Scaling of signals*

Two voltages (voltage hot, voltage cold) and current signal are scaled using the experimentally determined factors.

- *Smoothing of data*

An averaging filter algorithm is used to smooth the input data if necessary.

In general *Hotwire* offers two kinds of graphical representations:

- Overview of graphs

Four graphs on the screen give an overview of thematically grouped data, for instance the graphs of raw data, voltage hot, voltage cold, current and intensity are shown in Figure. 5.1.

- Single graph

A single graph for a closer view and the possibility to zoom in is also used, for an example see Figure 5.2; this shows the typical intensity signal profile during the experiment.

5.1.1. Voltage Correction

This is the main part of *HOTWIRE* program along with temperature determination, which is done by either manual voltage correction or automatic voltage correction.

Manual Voltage Correction

This task is divided into several steps as determination of beginning time and current gradient, first derivative of current, determination of voltage step and wire inductance. Finally the corrected voltage drop is evaluated which is used for determining other quantities. The value gained within the steps as well as the parameters for fitting are saved in a file and are further used for automatic voltage correction.

Automatic Voltage Correction

After performing the manual voltage correction, the inductance per unit length L_s/l and all the necessary parameters for fitting are saved in a file. Assuming L_s/l doesn't change between different experiments; the wire inductance is simply gained

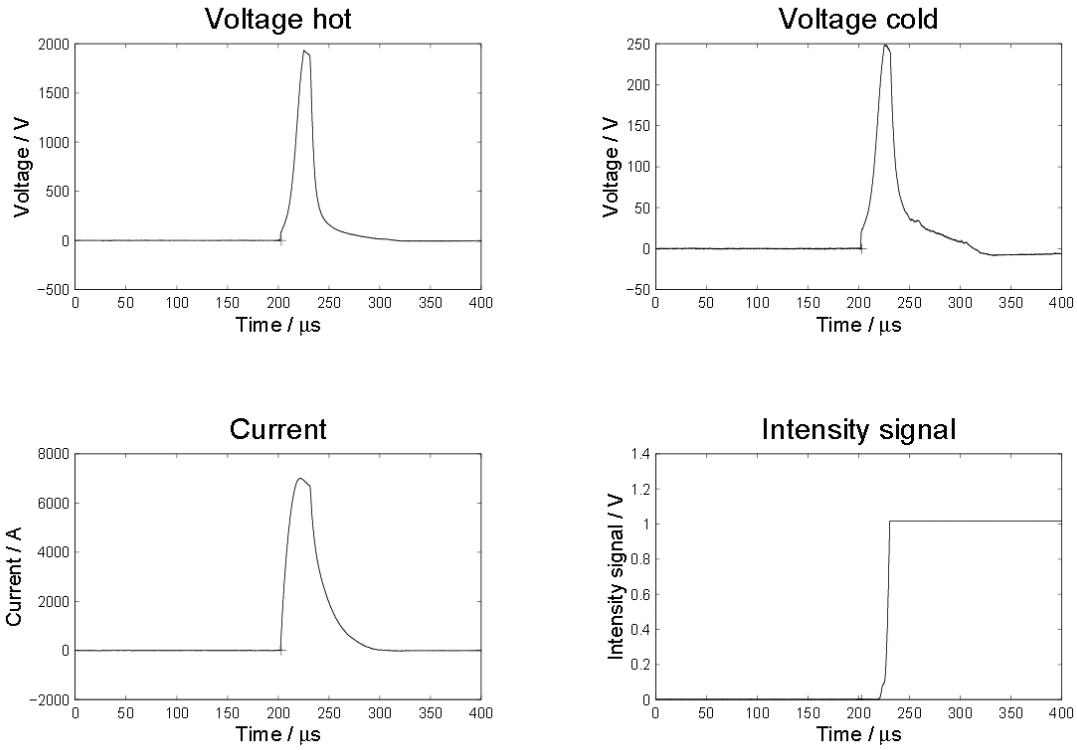

Figure 5.1. Graphical presentation of the input data: voltage hot, voltage cold, current and intensity versus time in overview-mode [1].

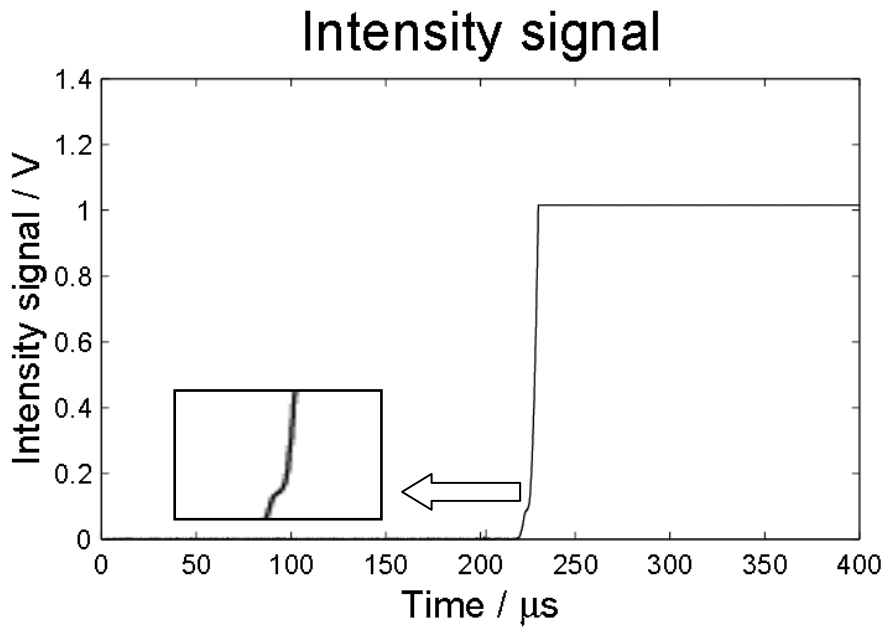

Figure 5.2. Graphical presentation of the input data: intensity versus time in single mode, magnified part shows the melting plateau [1].

by multiplication with the wire length l. This is the principle of the automatic voltage correction.

5.1.2. Temperature Determination via Melting Plateau

The theoretical part of temperature determination using the melting plateau is divided into two steps:

1. *Determination of melting plateau*

The intensity signal shows a more or less marked melting plateau as shown in Figure 5.2. In its middle a horizontal marker line must be positioned, which indicates the intensity signal at melting J_m. From this the calibration factor K is computed by

$$K = \mathrm{J_m}(T)\left(e^{\frac{c_2}{\lambda T_m}} - 1\right) \tag{5.1}$$

where c_2 is Planck's second constant, λ is the wavelength selected by the interference filter (λ = 1570 nm) and T_m is the melting temperature of the sample.

2. *Temperature*

Using the calibration factor K with J_m, temperature of the sample is calculated. The result is directly the true temperature of the wire sample. After performing voltage correction and determination of temperature, the following data are stored by HOTWIRE.

- time in μs
- current in A
- corrected voltage drop across the wire in V
- radiance temperature in K
- temperature in K
- specific enthalpy in $kJ \cdot kg^{-1} \cdot K^{-1}$
- specific resistivity in $\mu\Omega \cdot m$

Additionally, a log-file is saved which describes different parameters used during the data evaluation [1].

5.2. Data Evaluation

Data obtained by the pulse heating technique are in the form of time-resolved measured quantities which include the current through the specimen by means of a Pearson-current monitor, the voltage drop along the specimen by means of two knife-edge probes. The surface radiance is determined with a high-speed pyrometer by an interference filter. Initial radius/diameter of the specimen is measured by a high accuracy laser micrometer (KEYENCE LS-7001). The volume expansion of the wire is recorded with a fast CCD camera, which takes pictures of the diameter of the specimen during the experiment.

Measured data of voltage, current, and surface radiance were recorded by fast digital data acquisition. After processing these quantities in the "Hotwire" Program their graphical form can be shown in displaying software like Origin.

The enthalpy, electrical resistivity, and density as a function of temperature are obtained from the parameters directly measured by pulse heating setup. From these quantities we can drive some more quantities like, thermal conductivity, thermal diffusivity, thermal coefficient of resistance and thermal coefficient of expansion. The mathematical form of these relations with description is given in coming sections and their derivations are shown in Figure 5.3 [2]:

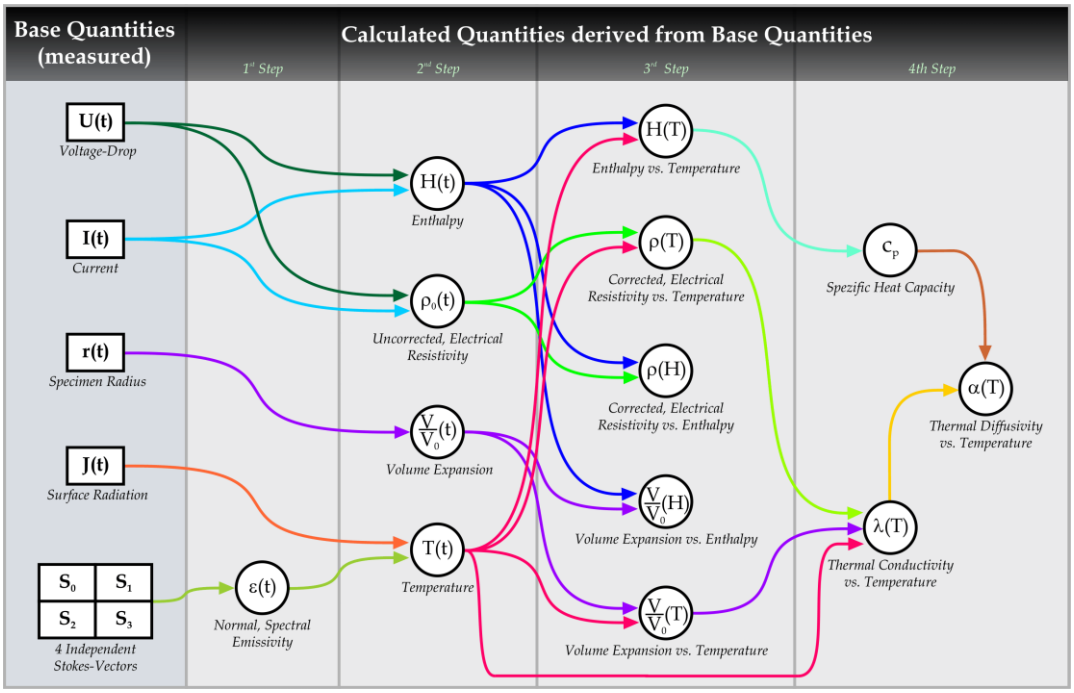

Figure 5.3. Illustration of the measured and the derived thermophysical parameters [3].

5.2.1 Specific Enthalpy

The total internal and external energy content of a system is called enthalpy [4]. Its SI based unit is J·kg^{-1} or J·mol^{-1}. The enthalpy is a measure for the energy of a system. It is symbolized by the letter H. It is the sum of two terms, the internal energy U and the quantity of work.

$$H = U_{int} + pV \tag{5.2}$$

Where, U_{int} is the internal energy, p the pressure, and V the volume. Like the internal energy, the enthalpy only depends on the state and not on the previous history of the system. Therefore, we have the exact differential

$$dH = dU_{int} + p\,dV + V\,dp \tag{5.3}$$

At constant pressure (dp = 0) we have,

$$dH = dU_{int} + p\,dV \tag{5.4}$$

Similarly we can write from the first law of thermodynamics

$$dU = dQ - p\,dV \tag{5.5}$$

where Q is an infinitesimal quantity of heat then we can write the above equation as

$$dH = Q_p \tag{5.6}$$

where Q_p is the heat change at constant pressure. Subsequently the heat delivered to the sample by the electric energy leads entirely to an increase of enthalpy. With the detected electrical signals, voltage drop U and current I, it is possible to determine the enthalpy induced into the wire by Joulean heating. The specific energy absorbed by the specimen during heating, as a function of time, was obtained from the integral of imparted electrical power over time, divided by mass (m) of the 'effective' specimen: The enthalpy is calculated with:

$$H(t) = \frac{1}{m}\int_0^t I(t')\,U(t')\,\mathrm{dt}' \tag{5.7}$$

Enthalpy is calculated by time-integration of the voltage and current assuming that the experiment is almost isobaric also fixing a reference point where the enthalpy of an element is set to zero. This is called the standard state of the material and is defined at room temperature (298 *K*) and normal pressure (1 *atm*). In equation (5.8) *m* is mass of the sample which does not change during the experiment and it can be calculated using density values d_0 at room temperature, taken from literature, its diameter *D* and its length *l* between the knife-edge probes. Therefore the mass is given by:

$$m = d_0 \frac{D^2\pi}{4} \cdot l \tag{5.8}$$

In the present work, the only significant heat loss from the specimen can be that due to thermal radiation. Using the Stefan-Boltzmann law, this heat loss can be estimated. But at

high temperatures, the heat losses due to thermal radiation are very low compared to the imparted power so it can be neglected without significant effect [5].

The enthalpy determination is one of the biggest advantage of the pulse-heating method, because the enthalpy in pulse-heating experiments equal to the energy absorbed by the wire. Therefore, we can calculate directly the total absorbed energy of the wire at any given time [6].

5.2.2. Heat of Fusion/ Latent Heat of Fusion

The latent heat of fusion or heat of solidification, from the opposite side, describes the amount of energy necessary for melting a material or is the amount of energy deposited into a coolant during solidification [7].

To obtain the heat of fusion/latent heat of fusion, the temperature was plotted as a function of enthalpy or time. A plateau in that plot indicates melting of the specimen. In solid-phase linear or a quadratic function is fitted to the data and linear functions to the melting plateau as well as to the data in the liquid phase. The intersections of these three fits were used to define the beginning and the end of melting. The heat of fusion ΔH was then computed as the increase in specific enthalpy between the beginning and the end of the melting plateau. Whereas it is obtained as the difference of H between T_{sol} and T_{liq} (subscript sol refers solidus, liq to liquidus temperature) for alloys. During phase change, the heat capacity is technically infinite [8].

5.2.3 Specific Heat Capacity

The amount of heat required to raise the temperature by one degree per unit mass of a system is the specific heat, if pressure of the system is kept constant then it is called isobaric heat capacity, c_p, and if volume of body is kept constant then it is isochoric heat capacity c_v [9]. SI based unit: $J \cdot kg^{-1} \cdot K^{-1}$ or $J \cdot mol^{-1} \cdot K^{-1}$. Both of these heat capacities can mathematically be evaluated by the following equations:

$$c_p(T) = \left[\frac{\partial H(T)}{\partial T} \right]_p \tag{5.9}$$

$$c_v(T) = \left[\frac{\partial H(T)}{\partial T} \right]_v \tag{5.10}$$

The Isobaric heat capacity values measured by pulse heating technique differ somewhat with the values measured by other techniques such as differential-scanning-calorimetry (DSC), but have been proved to be correct for the liquid state. As a result, pulse-heating data for c_p in the solid may only be considered as an estimate which is taken at the very end of the solid state before the melting transition.

Isochoric heat capacity is somewhat more complicated to calculate than c_p by pulse-heating experiments; c_v may be obtained if c_p, the isobaric expansion coefficient and the speed of sound of the test material are known. Isobaric heat capacity, c_p, is higher than isochoric heat capacity, c_v because objects often expand as they are heated and lose some energy on their surroundings if the pressure is kept constant. So there is a need to add additional heat to compensate for the energy lost plus the energy for further temperature rise. While there is no such loss of energy in isochoric heat capacity, c_v [8, 10-12].

5.2.4. Density

Density is the mass of a unit volume of the material [4]. Its SI based unit is $kg \cdot m^{-3}$. Density is an important parameter in material science. For instance, it is used as input parameter for numerical simulations of casting processes. Classical measurement methods like Archimede's principle or measurement of geometry and weighing are not applicable for hot samples. Pulse-heating technique inherently creates a big advantage regarding density measurement, as the mass of the sample usually does not change during the heating process. Therefore, only the geometric expansion has to be recorded. The mass can be measured prior to the experiment. Moreover, only the thermal expansion is stated as a function of temperature and density can be calculated on the basis of known room temperature densities, which can be obtained with higher precision by other techniques [13]. With the known room temperature density d_0 of the material under investigation and the volume expansion we obtain density as a function of temperature by the following relation [14].

$$d(T) = d_o \frac{D_0^{\,2}}{\mathrm{D}(T)^2} \tag{5.11}$$

5.2.5. Expansion/Temperature Coefficient of Expansion

The characteristic of most metals to increase their dimensions while heating is called thermal expansion, generally it is described by a parameter called temperature coefficient of expansion [4]. Its SI based unit is K^{-1}. If we consider expansion only along one dimension then it is linear and if expansion is taken along three dimensions then it is volume expansion. Whereas second is three times more than the first one. For liquids, volume expansion is the only meaningful expansion parameter [15].

The temperature coefficient of expansion depends on the material. Although it varies somewhat with temperature but for most practical purposes it can be taken as constant for a particular material.

During the pulse heating experiment expansion occurs, which is considered only in radial direction because of fixation of the sample along the longitudinal direction. Mathematically temperature co-efficient of expansion can be calculated from density by the following relation,

$$\beta = -\frac{1}{d(T)}\left(\frac{\partial d(T)}{\partial T}\right)_P \tag{5.12}$$

The expansion of the sample is an important component in the measurement of thermophysical properties. Besides being an important property itself, it is also needed for calculating compensated electrical resistivity, thermal conductivity and thermal diffusivity [8].

5.2.6. Electrical Resistivity

Definition: Resistance to the passage of electricity by a material [4]. It's SI based unit is Ω m. The specimen resistance at each instant is determined using the Ohm's law from the measured voltage drop *U* across the effective specimen length ''*l*'' and the measured current *I* through the specimen. Electrical resistivity comes in two different outcomes:

resistivity at initial geometry ρ_{IG} (subscript IG,), and ρ_{com} resistivity including thermal volume compensation (subscript com,). The former can be directly determined from the electric signals by taking the ratio of the voltage and the current, whereas information about the volume expansion is needed to obtain the latter, by multiplying D^2/D^2_0 and ρ_{IG}. Physically, electrical resistivity with volume expansion is considered of greater interest because it can be directly compared with data from other measurement techniques, e.g., 4-point measurements [8].

For each experiment the thermodynamic temperature was plotted against resistivity. A plateau indicated melting of the specimen. Linear functions were fitted to the data in the solid phase and in the liquid phase. The intersections of the melting-plateau fit with the solid-phase fit and with the liquid-phase fit provided the resistivity values at the start and at the end of melting, respectively. Electrical resistivity corresponding to the initial geometry at room temperature ρ_{IG} and resistivity including volume expansion are calculated using following equations

$$\rho_{\mathrm{IG}}(t) = \frac{U(t)\,\pi\,\mathrm{r}_0^2}{I(t)\,l} \tag{5.13}$$

$$\rho_{com}(T) = \rho_{\mathrm{IG}}(T)\ \frac{D(T)^2}{\mathrm{D}_0^2} \tag{5.14}$$

5.2.7. Temperature Coefficient of Resistance

Temperature coefficient of resistivity can be defined as the fractional change in the original resistance of the material per degree rise in temperature. Its unit is K^{-1}[16]. The value of resistivity like most physical properties varies with temperature. The relation between temperature and resistivity for most metals in general is fairly linear over a broad temperature range. For such linear relations we can write an empirical approximation that is good enough for most engineering purposes [15].

$$\alpha_R = \frac{\rho_T - \rho_0}{\rho_0 \Delta T} \tag{5.15}$$

where ρ_T, is the resistivity at the higher limit of temperature and ρ_0, resistivity at the lower limit of temperature range and ΔT. is the temperature range.

5.2.8. Thermal Conductivity

The thermal conductivity λ of a material is the quantity of heat transmitted due to unit temperature gradient in unit time, under steady state conditions in a direction normal to the surface of unit area of cross-section. It is the coefficient λ in Fourier law of heat conduction:

$$J = -\lambda(\nabla T) \tag{5.16}$$

Where J is the heat flux, λ the thermal conductivity ΔT. is the temperature gradient across the sample material. The standard unit of thermal conductivity is $W \cdot m^{-1} \cdot K^{-1}$[16].
The principal mechanism for thermal conduction in pure metals is through electrons. Although lattice conduction can make a significant contribution at lower temperatures, electronic conduction is dominant at temperatures around the melting point [17]. Under these conditions, thermal conductivity, λ, can be derived from electrical resistivity using the Wiedemann-Franz-Lorenz law:

$$\lambda(T) = \frac{L\,T}{\rho_{com}\,(T)} \tag{5.17}$$

Where T is the thermodynamic temperature, $\rho_{el,com}$ is the 'compensated' electrical resistivity, and L is Lorenz number. The published values for the Lorenz number at the melting temperature differ in the range between ($2.25 - 2.60 \cdot 10^{-8}$ as shown in Table 2.2) $W \cdot \Omega \cdot K^{-2}$ for different metals. The commonly used value of Lorenz number is $2.45 \cdot 10^{-8}$ $W \cdot \Omega \cdot K^{-2}$, see Table 2.2 [18]. However, data computed using equation (5.17) should be regarded as estimated values because the Lorenz number used in equation (5.17) varies with temperature and have different values for different material.

5.2.9 Thermal diffusivity

Another material property that appears in the heat conduction analysis is the thermal diffusivity, which represents how fast heat diffuses through a material and mathematically written as [19]:

$$a(T) = \frac{\lambda(T)}{c_p(T) \cdot d_d(T)} \tag{5.18}$$

Where $a(T)$ is thermal diffusivity $\lambda(T)$ is the thermal conductivity, $c_p(T)$ is the specific heat and $d(T)$ the density of the sample wire. Thermal diffusivity is expressed in $m^2 \cdot s^{-1}$.

Note that the thermal conductivity λ represents how well a material conducts heat and the heat capacity of unit volume $d_0 c_\rho$ determines how much energy a material stores per unit volume. Therefore, the thermal diffusivity, $a(T)$ of a material can be viewed as the ratio of the heat conducted through the material to the heat stored per unit volume. The above equation shows that thermal diffusivity varies in a manner similar to that of thermal conductivity. Thermal diffusivity is generally a strong function of temperature and it decreases with the increase in temperature.

References

[1] Franz S, *Diploma thesis* (Technical University Graz, 2000).

[2] Mehmood S, Klotz U, and Pottlacher G, 2011 *Thermophysical Properties of Platinum-Copper System* EPD Congress 2011 pp-167.

[3] Cagran C, *PhD thesis* (Technical University Graz, 2004).

[4] Brown C D, 1998 *Dictionary of Metallurgy*, John Wiley & Sons, Cichester.

[5] Boboridis K, *PhD thesis* (Technical University Graz, 2001).

[6] Cagran C, *Diploma thesis* (Technical University Graz, 2000).

[7] Michael E B, 2008 *Handbook of Thermal analysis and calorimetry* Chapter 10 Elsevier publisher Radarweg 29, PO Box 211, 1000 AE Amsterdam, The Netherlands Linacre House, Jordan Hill, Oxford OX2 8DP, UK.

[8] Schroeder D V, 2000 *An Introduction to Thermal Physics* Addison Wesley Longman.

[9] Thewlis J, 1973 *Concise Dictionary of Physics and Related Subjects*, Pergamon Press, Oxford.

[10] Hess H, Kaschnitz E and Pottlacher G, 1994 *Thermophysical Properties of Liquid Cobalt, High Pressure Research* **12**: pp 29-42.

[11] Hixson R S, Winkler M A and Hodgdon M L, 1990 *Sound speed and thermophysical properties of liquid iron and nickel.* Physical Review B, **42**(10): pp. 6485-6491.

[12] Hixson R S and Winkler M A, 1990 *Thermophysical properties of solid and liquid tungsten*, International Journal of Thermophysics. **11**: pp 709-718.

[13] Gathers G R, 1986 *Dynamic methods for investigating thermophysical properties of matter at very high temperatures and pressures,* Reports on Progress in Physics. **49**: pp 341-396.

[14] Hüpf T, *PhD thesis* (Technical University Graz, 2010).

[15] Halliday D, Resnick R and Walker J 1992, *Fundamentals of Physics*, 9th Edition, John Wiley & Sons, Inc.

[16] Aurangzeb, *PhD Dissertation* (Queid-e- Azam University Islamabad, 2008).

[17] Korobenko V N and Rakhel A D, 1999 *Technique for Measuring Thermophysical Properties of Refractory Metals at Supercritical Temperatures*, International Journal of Thermophysics. **20(4)**: pp 1257-1266.

[18] Weißmantel C and Hamann C,1990 *Grundlagen der Festkorperphysilg 7. Auflage,* Springer Verlag, Berlin.

[19] Cengel Y A and Turner R H 2001 *Fundamentals of Thermal-Fluid Sciences* (Boston Burr Ridge: McGraw-Hill) pp 609.

Chapter 6

Experimental Results and Discussions

Experimental results of platinum, copper and six platinum alloys namely, Pt95Co05, Pt95Ru05, Pt96Cu04, Pt68Cu32, Pt50Cu50 and Pt25Cu75 have been compared and discussed with different techniques and literature here. The phase diagram with corresponding solidus and liquidus lines of platinum-copper alloys are shown in Figure 6.1. The experimental data of fem DTA measurement are shown by solid black lines and compared with the data from Doetrinkel and Thermocalc SNOB1 database which are shown by dotted and dashed lines respectively [1, 2]. The data taken from SNOB1 is an extrapolation by unary data assuming ideal mixing behaviour. By comparing experimental data with other data sets, it can be confirmed that all alloys show ideal mixing behavior. In the case of PtCu alloys our presented data are approximately 50–100 K lower to older data sets in this intermediate temperature range. For the two Pt rich technical alloys, Pt95Ru05 and Pt95Co05, Pt95Ru05 has an increase of the melting range while Pt95Co05 has a decrease of the melting range about 100 Kelvin as compared to pure platinum.

6.1. Enthalpy, Isobaric Heat Capacity and Heat of Fusion

Figure 6.2 and Figure 6.3 compare enthalpies H given in $kJ \cdot kg^{-1}$ of the four PtCu alloys and Pt rich alloys with pure copper and pure platinum as a function of temperature in solid and liquid regions using Equation (5.8) [3, 4]. For all six alloys and the pure elements, we determined isobaric heat capacity c_p from the slopes of the curves closest to melting and in the liquid state; values are shown in the Table 6.1 and Table 6.2. Isobaric heat capacity c_p values of pure platinum and pure copper are compared with literature, which give quite a good agreement. For the alloys no literature data are available. Heat of fusion ΔH was obtained as the difference of H between T_{sol} and T_{liq} (subscript sol refers solidus, liq to liquidus temperature). The least square fits for all enthalpies in both solid and liquid phases along with heat of fusion are given in Table 6.1 for PtCu alloy and in Table 6.2 for Pt rich alloys with pure elements.

6.2. Electrical Resistivity and Temperature Coefficient of Resistance

Figure 6.4 and Figure 6.5 show the results of the electrical resistivity with volume compensation as a function of temperature for the range of platinum-copper binary alloy system and Pt rich alloys. The resistivity of pure copper is significantly lower than the alloyed materials. Resistivity increases rapidly with the amount of alloyed platinum and reaches a maximum at approximately 68 mass % platinum in the solid and 96 mass % platinum in the liquid region for PtCu alloys. In case of Pt rich alloys, Pt95Co05 has shown higher resistivity both in solid and liquid regions. There are no data available in literature to compare with data of the investigated alloys. Resistivity measured by the pulse heating technique of pure platinum is compared with literature data and shows a good match [3-5]. By applying Equation (5.15) we can determine temperature coefficient of resistances α_R for all measured alloys along with the pure metals. The least square fits for resistivities and temperature coefficients of resistance values are summarized in Table 6.1-6.4.

6.3. Density and Coefficient of Thermal Expansion

In Figure 6.6, density is plotted as function of composition at three different temperatures: at room temperature, in the solid and liquid range for the alloys. There is a very good correlation between experimental data and literature data for higher copper contents [5]. For high platinum contents, there is a discrepancy which is attributed to the difference in the data for pure platinum, therefore further measurements in this composition range are required. The temperature coefficient of expansion β is calculated according to Equation (5.12), plotted in Figures 6.7 and 6.8 and relevant polynomials are given in Table 6.3 and Table 6.4. It is interesting to note that β is strongly increasing with platinum contents, reaches a maximum at 50 % Pt and then decreases again for PtCu alloys, whereas Pt95Co05 has higher values both in solid and liquid regions than all other Pt rich alloys.

In Figure 6.9, the density of pure platinum determined by both techniques, namely pulse heating technique and dilatometry, is compared with literature values. Within the solid region all data match very well, but volume change during melting differs by a factor of

two. The slopes given by two sets of literature data show some discrepancies in the liquid range. The values of Savistkii match good to the platinum values obtained by the pulse heating technique, while the values of CRC handbook report significant lower values for the melting range [6, 7]. In the liquid phase, the match of the two literature values to the pulse heating values is not satisfactory. An explanation of that behaviour is not yet found.
Normalized densities of PtCu alloys and Platinum rich alloys are compared with both techniques and with pure platinum in Figure 6.10a and Figure 6.11a, whereas parts of Figure 6.10a and Figure 6.11a are magnified in 6.10b and in 6.11b for better resolution. Solid lines are pulse heating results with solid symbols, the dashed lines are dilatometric with open symbols and the thick solid line is for pure platinum. In the solid region one finds that the values of Pt95Ru05, Pt96Cu04 and Pt95Co05 lie close to that of pure platinum. The values of Pt95Ru05 alloy and pure Pt have practically the same temperature dependence of density whereas Pt96Cu04 and Pt95Co05 have somewhat higher dependence of density on temperature but all are in the same temperature range. The rest of series of the PtCu alloys with higher copper contents show a significant difference to the pure platinum values. Some order/disorder transitions can be seen in Pt68Cu32 and Pt50Cu50, which are shown in the phase diagram for this temperature range [8]. In the case of Pt96Cu04 alloy and Pt25Cu75 slopes of data set in the solid range have a very good matching to the dilatometric results but have some offsets. Pt68Cu32 has comparatively less offset and a relatively similar slope. An offset with different slope for Pt50Cu50 in the solid range is observed. The Pt25Cu75 alloy, where data are available by both techniques, show that the pulse-heating data deliver a smaller volume change during melting and a different slope in the liquid range compared to dilatometric results. Up to now there is no explanation found for this behaviour.
Now in the solid region, the comparison of densities of high platinum containing alloys with pulse heating data show that there are offsets in the values of Pt96Cu04 and Pt95Ru05 but the slope of the curve of Pt96Cu04 a quite similar. Whereas, in case of Pt95Ru05 and Pt95Co05 we observe much larger slopes. If we observe the volume changes during melting, Pt96Cu04 and Pt95Ru05 are quite similar but Pt95Co05 has a much smaller volume change. In the liquid region Pt95Ru05 has almost the same slope as the pure platinum curve, while other two platinum rich alloys show somewhat large

slopes. Some polynomial of density and temperature coefficient of expansion are given in Table 6.5 along with temperature range which starts from room temperature to the upper accessible temperature.

6.4. Thermal Conductivity and Thermal Diffusivity

In Figures 6.12 to 6.15 thermal conductivities and thermal diffusivities as a function of temperature are shown both for PtCu and Pt rich alloy in sequence. These are estimated by using Equations (5.17) and (5.18) assuming that these two quantities can be determined by using the Wiedman-Franz law. In the liquid phase, where direct measurements of thermal conductivity are almost impossible, calculation from electrical resistivity is one of the rare methods of an indirect approximation. In Table 6.3 and Table 6.4 least square fits are given for thermal conductivity and thermal diffusivity for all alloys.

6.5. Specific Heat at Constant Volume

An accurate knowledge of isochoric heat capacity at sufficient high temperature and related thermodynamical properties of metals has largely been lacking. However, the situation in regard to experiment has improved considerably during the past few decades. Taking into account the experimental advantages and limitations, specific heat at constant volume is measured by electric pulse heating technique of wire sample inside a capillary tube. Copper wires with diameter ≈ 0.5 mm are placed inside the glass capillary tubes with inner diameter 0.500 ± 0.010 mm and outer diameter 8 mm ± 1 mm. The diameter of sample wire was preselected to a value, using already known values of expansion of copper sample, so that it fills the gap between wall of capillary tube and copper sample completely, while reaching a desired temperature. The sample with glass capillary tube has been shown in the Figure 4.9 (b). Copper samples, with a purity of 99.99 %, are used because of their low melting point (1357 K). Under fast heating, the wire expands and fills the inner cavity of the capillary, after which there is no further increase of volume. It is assumed that expansion of glass tube is negligible during this fast heating process, the values of isochoric heat capacity c_v are determined by the slope of enthalpy vs. temperature curves. A graph in Figure 6.16 is plotted between enthalpy vs. temperature

and the slope of that plot gives us the c_v value which is 464.76 $J \cdot kg^{-1} \cdot K^{-1}$ and found to be close to literature value 412.62 $J \cdot kg^{-1} \cdot K^{-1}$ which is at 1250 K [9]. The experimental values shown in this research are based on an average of six independent measurements. It has been noticed that melting and explosion of the samples occurs much earlier in isochoric process as compared to the isobaric process, but values of melting point remains same as that of constant pressure. This is because the heating process is much quicker during constant volume than it is at constant pressure and most of the heat given to the system is being utilized to increase the temperature of the sample wire. It is assumed in the procedure of determining specific heat that there is no loss of mass and volume in the internal space of the capillary tube until destruction. There is also no electric discharge inside the space of the capillary tube. The later assumption is important; if it is not valid, non uniform heating of expanded metal is possible [10, 11].

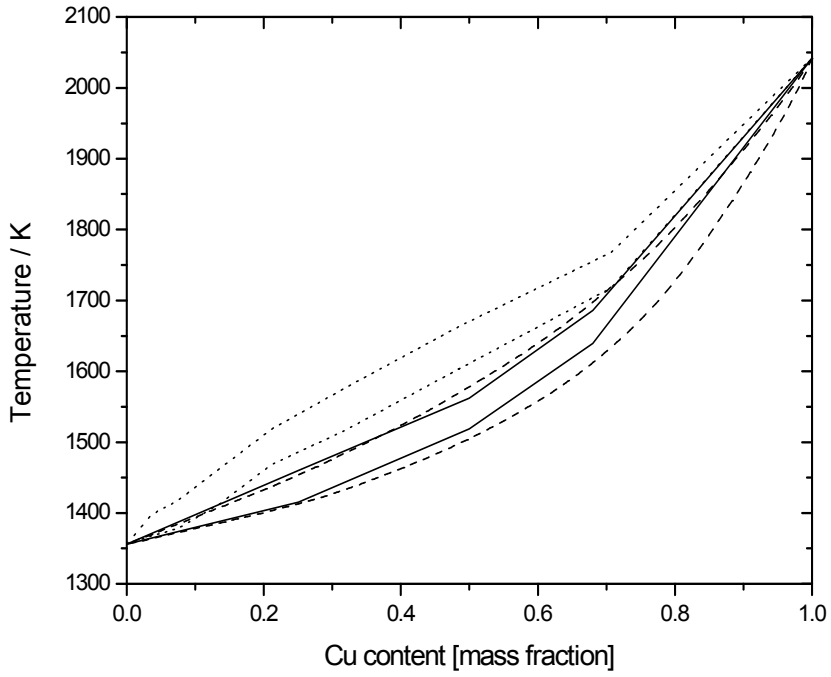

Figure 6.1. Solidus and liquidus temperatures versus copper composition of platinum alloy. Solid lines: values from the present work, dotted lines and dashed lines: values from [1, 2].

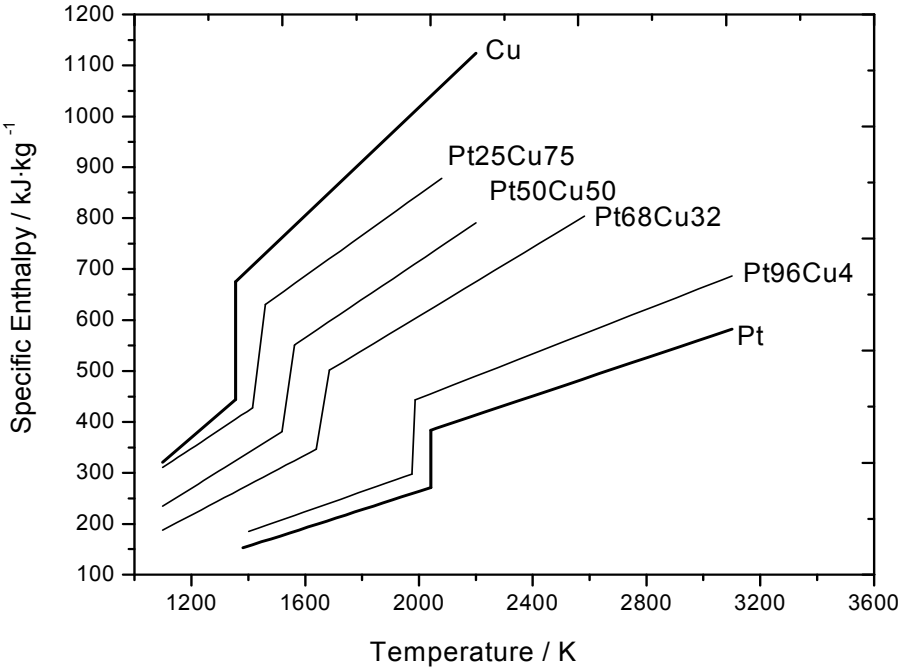

Figure 6.2. Specific enthalpy of PtCu alloys, pure platinum and pure copper versus temperature. Pt96Cu04, Pt68Cu32, Pt50Cu50 and Pt25Cu75: values from present work. Pt and Cu: values from [3, 4].

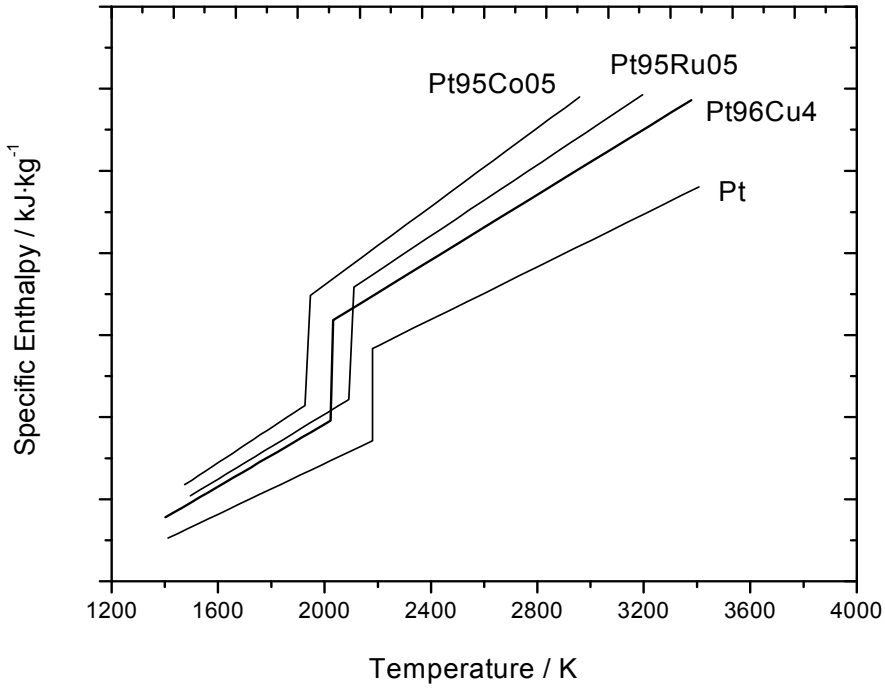

Figure 6.3. Specific enthalpies of Pt rich alloys. Pure Pt, Pt96Cu04, Pt95Co05 and Pt95Ru05 versus temperature [3].

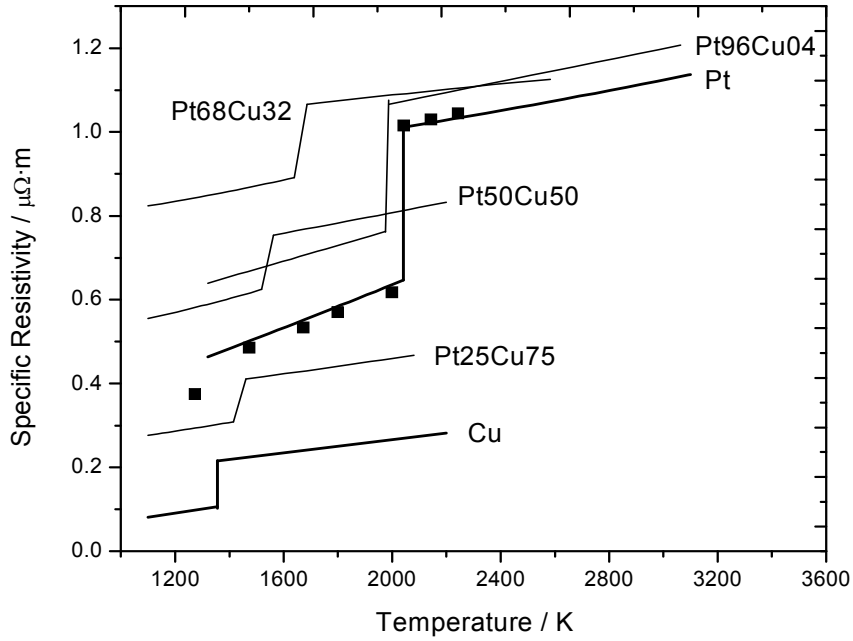

Figure 6.4. Electrical resistivity of four PtCu alloys, pure platinum and pure copper as a function of temperature. Pt96Cu04, Pt68Cu32, Pt50Cu50 and Pt25Cu75: values from present work. Cu, Pt and filled rectangles: values from [3-5].

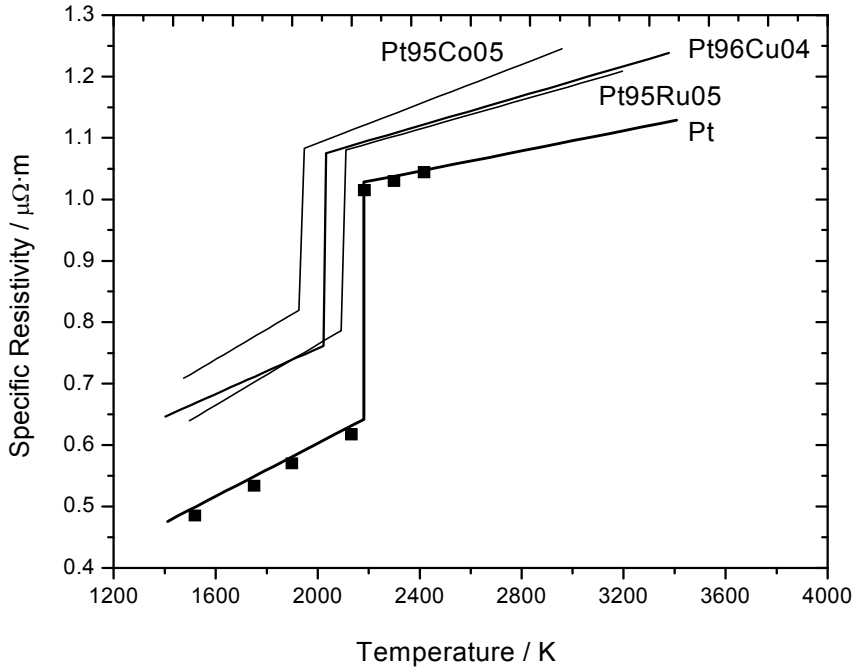

Figure 6.5. Electrical resistivities of Pt rich alloys. Pt96Cu04, Pt95Co05 and Pt95Ru05 versus temperature Pt and filled rectangles: values from [3].

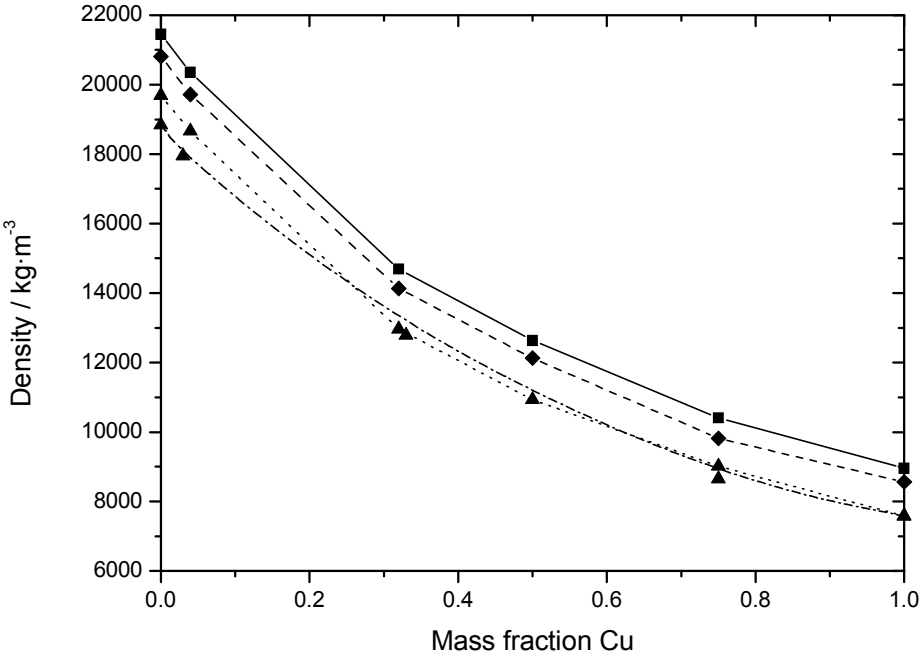

Figure 6.6. Density is plotted as function of composition at three different temperatures. Solid line: at 293 K, dashed line: at 1273 K, dotted line: at 2073 K, dashed-dotted line: literature values at 2073 K [5].

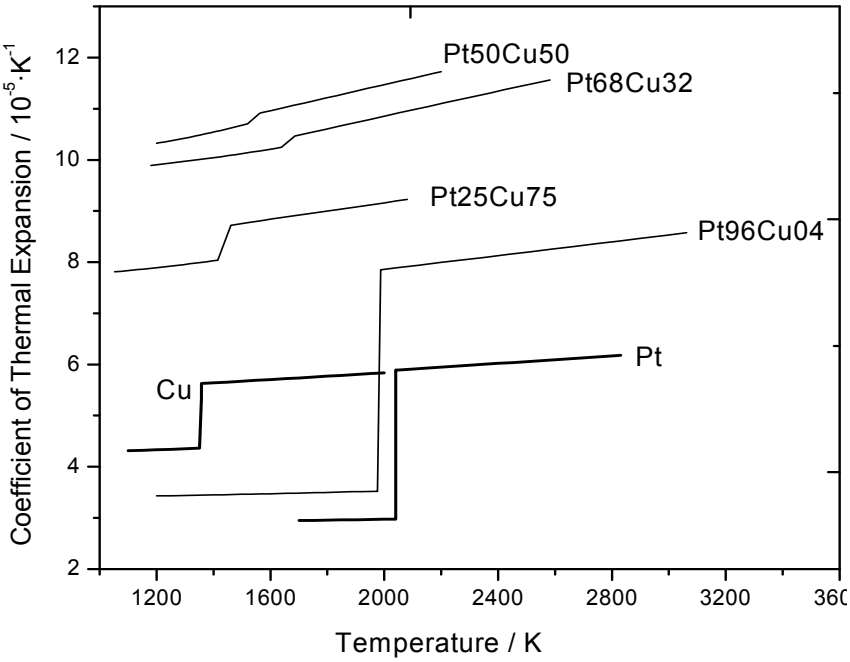

Figure 6.7. Coefficient of thermal expansion of PtCu alloys, pure platinum and pure copper versus temperature. Pt96Cu04, Pt68Cu32, Pt50Cu50 and Pt25Cu75: values from present work. Pt and Cu: values from [3, 4].

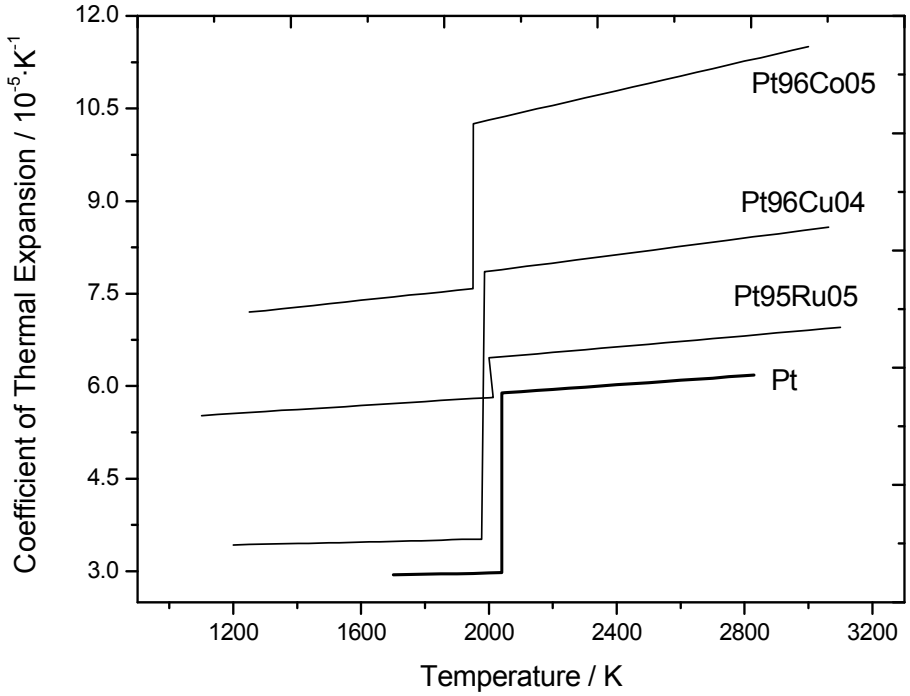

Figure 6.8. Coefficient of thermal expansion of Pt rich alloys, pure platinum, Pt96Cu04, Pt95Co05 and Pt95Ru05 versus temperature [3].

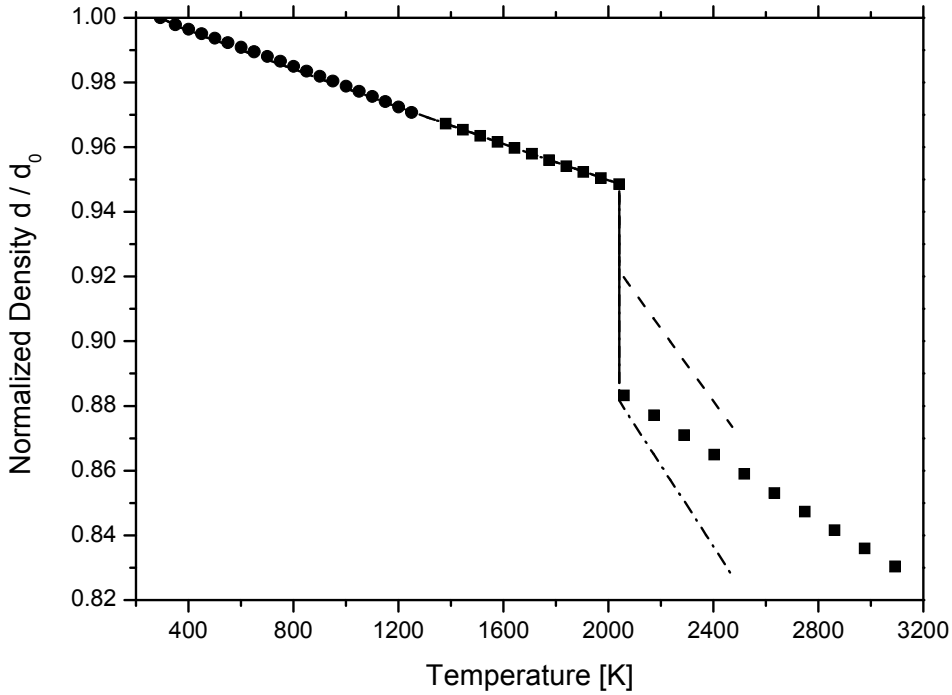

Figure 6.9. Normalized density comparison of pure platinum values. Filled circles line: Dilatometry values, filled rectangle line: Pulse heating values, dashed line and Dash-dotted lines: from [7, 8].

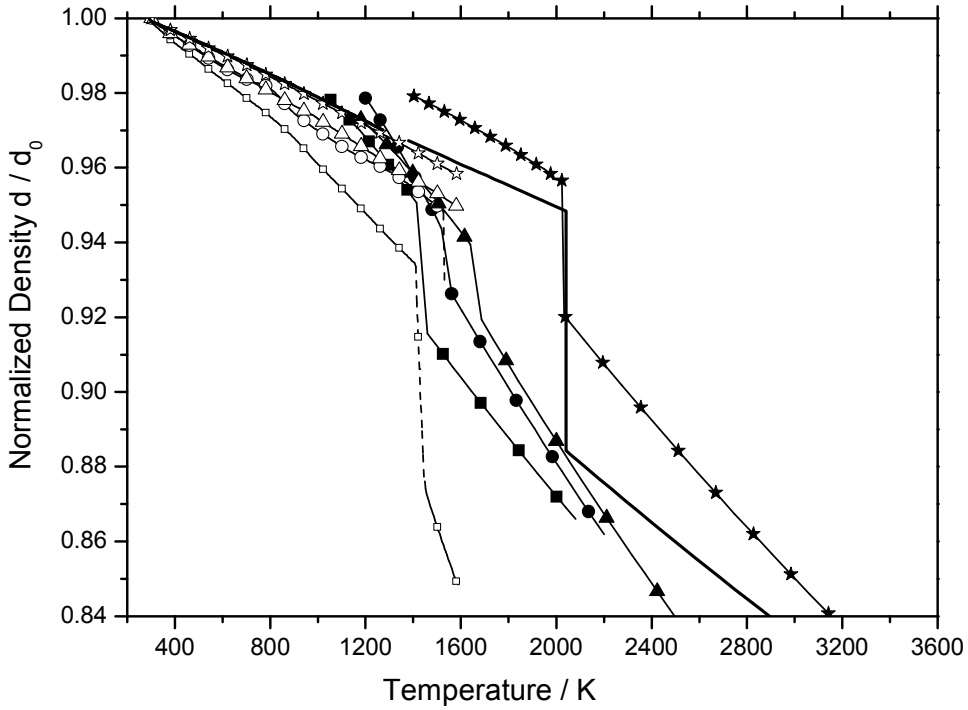

Figure 6.10(a). Comparison of normalized density values of platinum-copper alloys. Open symbols represent dilatometric results, solid symbols pulse heating results. Solid line: pure platinum, stared line: Pt96Cu04, up-triangled line: Pt68Cu32, filled-circled line: Pt50Cu50 and filled rectangled line: Pt25Cu75.

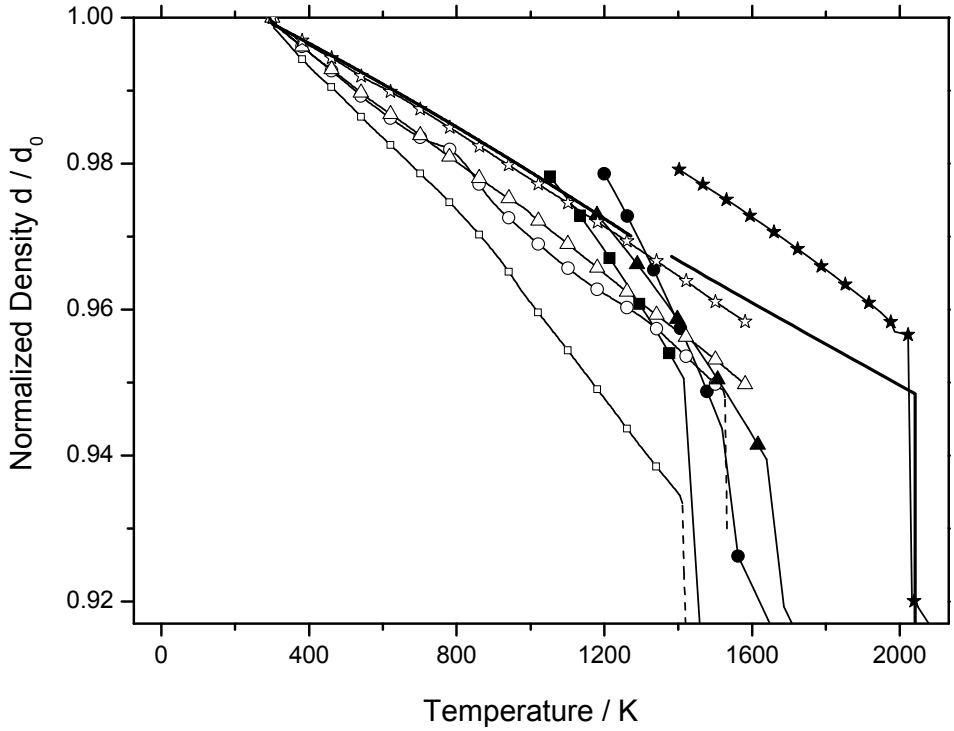

Figure 6.10(b). Magnified diagram of Figure 6.10(a), ‘‘Comparison of normalized density values of platinum-copper alloys’’.

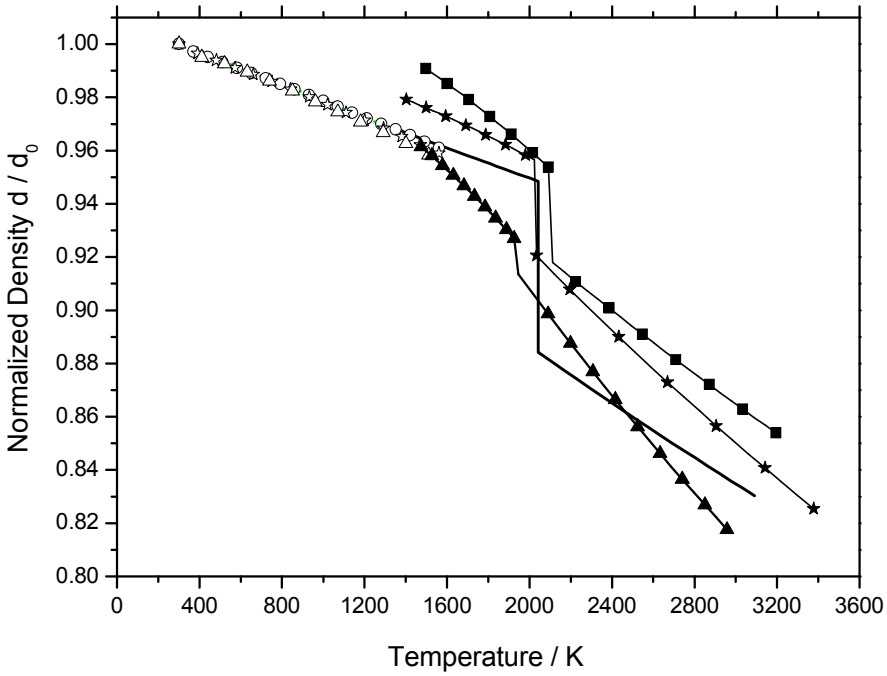

Figure 6.11(a). Comparison of normalized density values of platinum rich alloys. Open symbols represent dilatometric results, solid symbols pulse heating results. Solid line: pure platinum, stared line: Pt96Cu04, up-triangled line: Pt95Co05, filled-circled line: Pt95Ru05.

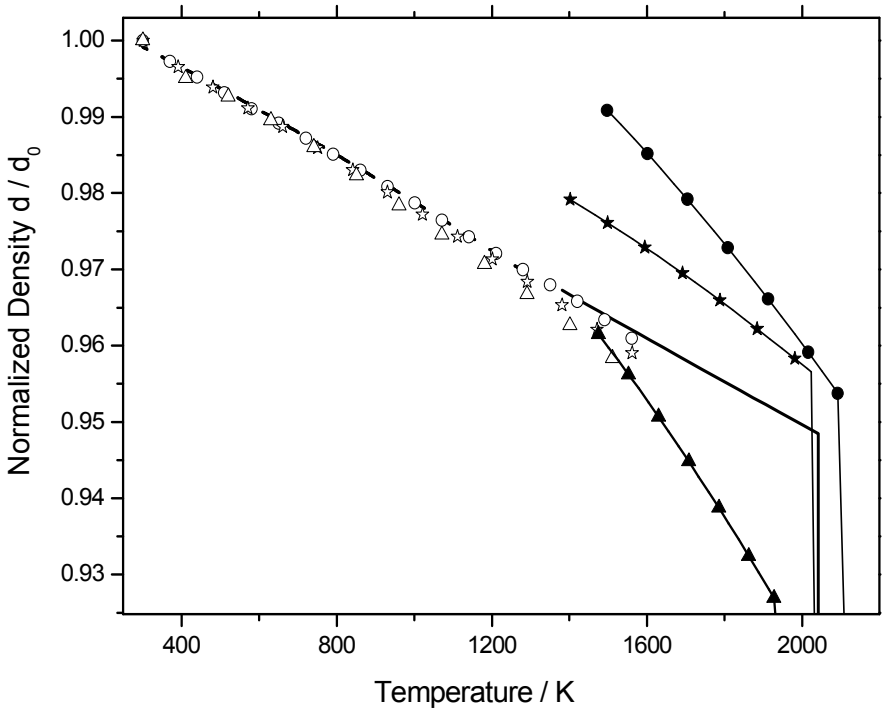

Figure 6.11(b). Magnified diagram of Figure 6.11(a), ‘‘Comparison of normalized density values of platinum rich alloys’’.

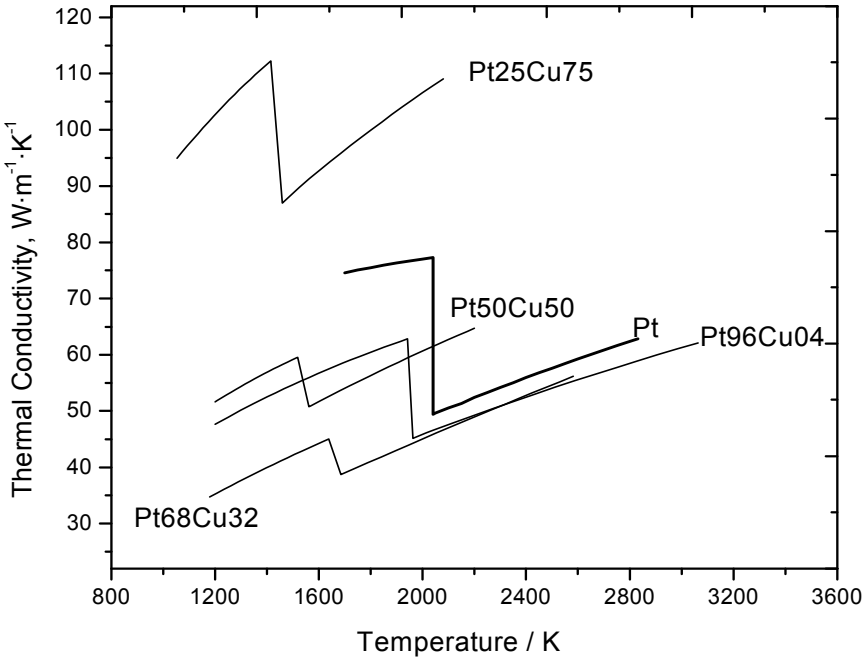

Figure 6.12. Thermal conductivity of four PtCu alloys and pure platinum versus temperature. Pt96Cu04, Pt68Cu32, Pt50Cu50 and Pt25Cu75: values from present work. Pt: literature value, Cu has values from 154 to 331 [3].

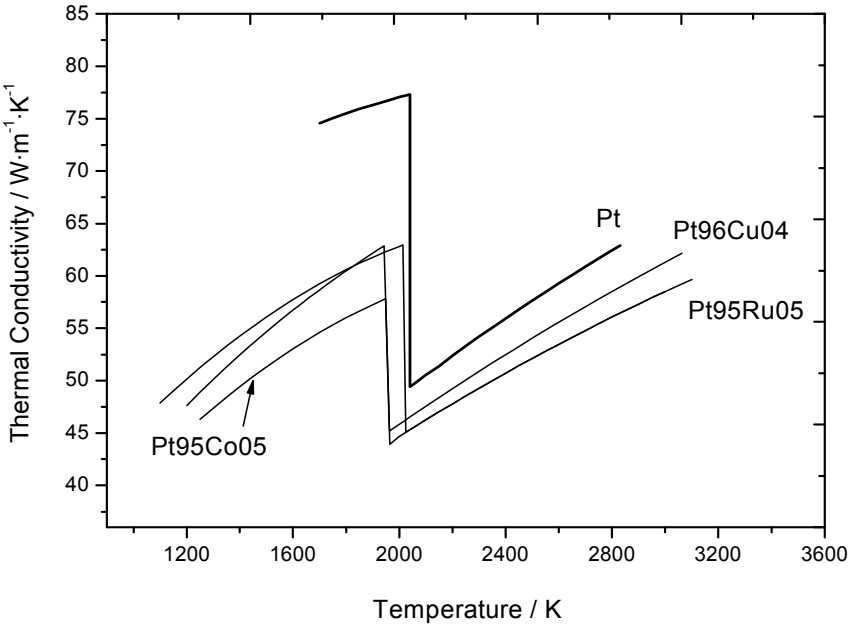

Figure 6.13. Thermal conductivity of Pt rich alloys, Pure Pt, Pt96Cu04, Pt95Co05 and Pt95Ru05 versus temperature [3].

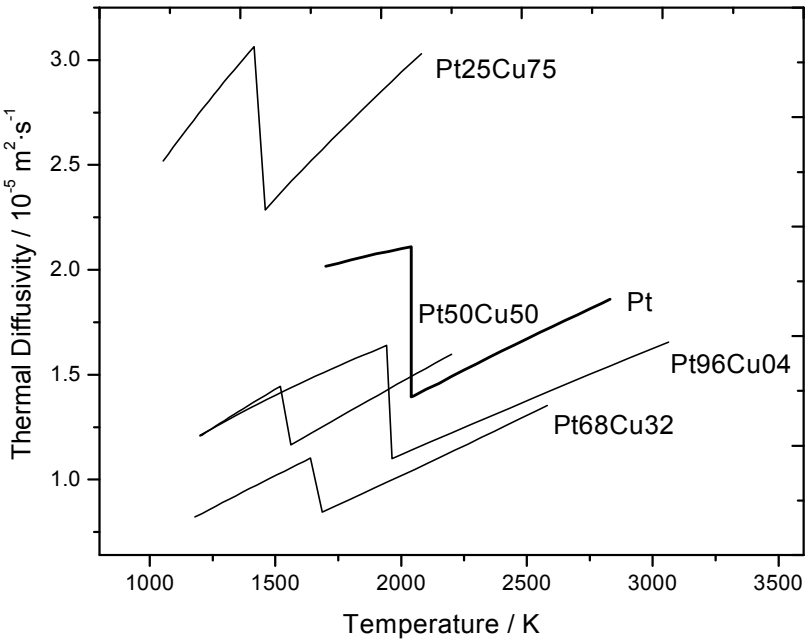

Figure 6.14. Thermal diffusivity of PtCu alloys and platinum versus temperature. Pt96Cu04, Pt68Cu32, Pt50Cu50 and Pt25Cu75: values from present work. Pt: literature value, Cu has values from 7 x 10 $^{-5}$ to 23 x 10 $^{-5}$ [3].

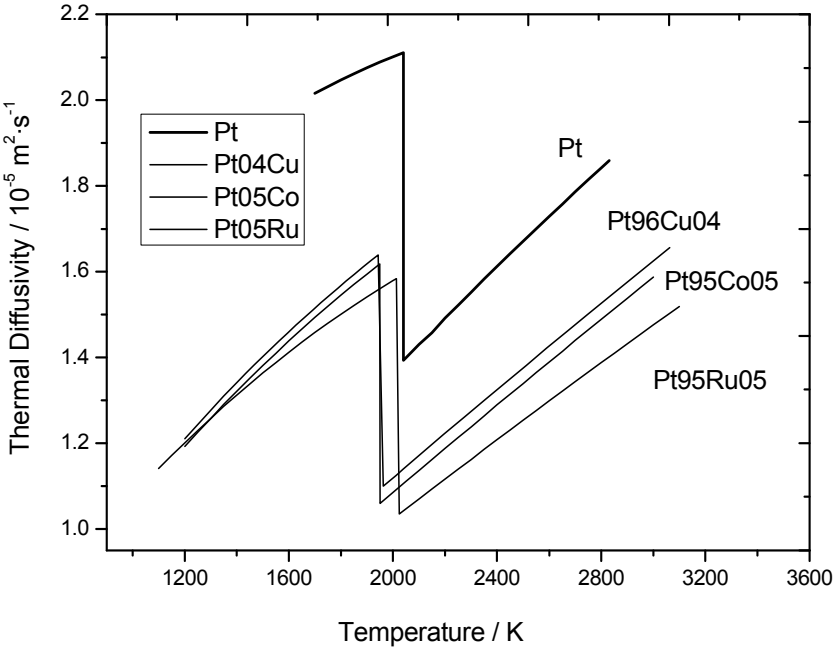

Figure 6.15. Thermal diffusivity of Pt rich alloys, pure Pt, Pt96Cu04, Pt95Co05 and Pt95Ru05 versus temperature [3].

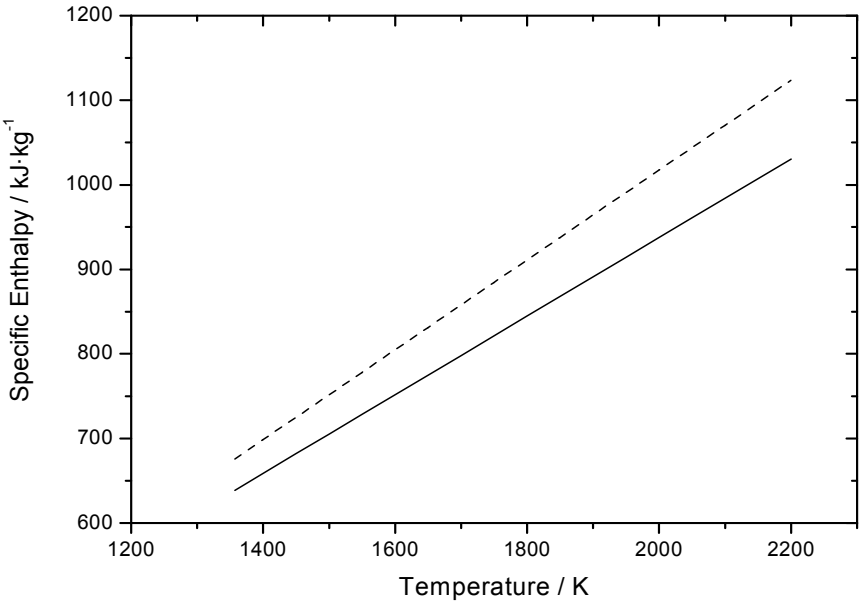

Figure 6.16. Specific enthalpies of pure copper, solid line: at constant volume and dashed line: at constant pressure [9].

Table 6.1. Electrical resistivity ρ_{com}, change of resistivity $\Delta\rho$ at melting, specific enthalpies H, heat of fusion ΔH, isobaric heat capacity c_p of four PtCu alloys; subindex IG: with initial geometry and comp: compensated.

Alloy/ element	**Temperature Range**	**ρ_{IG} / µΩ·m**	**ρ_{com} / µΩ·m)**	**$\Delta\rho$ / µΩ·m)**	**H / kJ·kg^{-1}**	**ΔH / kJ·kg^{-1}**	**c_p / J·kg^{-1}·K**
Pt94Cu04	1200 K < T < 1976 K	0.416 + 1.599 x 10^{-4}· T	0.391 + 1.881 x 10^{-4}· T	0.304	- 89.357 + 0.196 · T	145.5	196
	1986 K < T < 3100 K	0.922 + 3.270 x 10^{-5}· T	0.807 + 1.306 x 10^{-4}· T		10.500 + 0.218 · T		218
Pt68Cu32	1180 K < T < 1639 K	0.738 + 6.045 x 10^{-5}· T	0.679 + 1.291 x 10^{-4}· T	0.175	-135.982 + 0.295 · T	154.9	295
	1686 K < T < 2581 K	1.061 – 4.773 x 10^{-5}· T	0.954 + 6.678 x 10^{-5}· T		-67.457 + 0.338 · T		338
Pt50Cu50	1200 K < T < 1519 K	0.437 + 1.003 x 10^{-4}· T	0.362 + 1.723 x 10^{-4}· T	0.129	-149.243 + 0.349· T	169.9	349
	1562 K < T < 2200 K	0.652 + 3.006 x 10^{-5} · T	0.562 + 1.231 x 10^{-4}· T		-35.595 + 0.376 · T		376
Pt25Cu75	1053 K < T < 1415 K	0.185 + 7.673 x 10^{-5}· T	0.163 + 1.025 x 10^{-4}· T	0.103	-96.4951 + 0.370 · T	202.8	370
	1460 K < T < 2080 K	0.307 + 4.684 x 10^{-5} · T	0.277 + 9.149 x 10^{-5}· T		47.681 + 0.399 · T		399

Table 6.2. Electrical resistivity ρ_{com}, change of resistivity $\Delta\rho$ at melting, specific enthalpies H, heat of fusion ΔH, isobaric heat capacity c_p of four Pt rich alloys as well as pure platinum and copper; sub index IG: with initial geometry and comp: compensated.

Alloy/ element	**Temperature Range**	ρ_{IG} / **µΩ·m**	ρ_{comp} / **µΩ·m**	$\Delta\rho$ / **µΩ·m**	H / **kJ·kg^{-1}**	ΔH / **kJ·kg^{-1}**	c_p / **J·kg^{-1}·K**
Pt	1700 K < T < 2042 K	$0.155 + 2.229 \times 10^{-4} \cdot T$	$0.161 + 2.132 \times 10^{-4} \cdot T + 1.219 \times 10^{-8} \cdot T^2$	0.365	$-96.075 + 0.180 \cdot T$	112.4	180, 177 [5, 9]
	2042 K < T < 2830 K	$0.854 + 2.271 \times 10^{-5} \cdot T$	$0.842 + 5.926 \times 10^{-5} \cdot T + 1.154 \times 10^{-8} \cdot T^2$		$1.636 + 0.187 \cdot T$		187 , 178 [5, 9]
Pt95Co05	1200 K < T < 1949 K	$0.432 + 1.656 \times 10^{-4} \cdot T$	$0.368 + 2.864 \times 10^{-4} \cdot T$	0.2642	$-73.783 + 0.1967 \cdot T$	137.341	196.7
	1964 K < T < 3000 K	$0.935 + 2.539 \times 10^{-5} \cdot T$	$0.773 + 1.565 \times 10^{-4} \cdot T$		$-5.658 + 0.230 \cdot T$		230
Pt95Ru05	1100 K < T < 2013K	$0.344 + 1.903 \times 10^{-4} \cdot T$	$0.296 + 2.362 \times 10^{-4} \cdot T$	0.233	$-95.766 + 0.207 \cdot T$	136.968	206.7
	2025 K < T < 3100 K	$0.888 + 3.845 \times 10^{-5} \cdot T$	$0.825 + 1.203 \times 10^{-4} \cdot T$		$-27.941 + 0.239 \cdot T$		239.6
Cu	1100 K < T < 1356 K	$-0.021 + 9.154 \times 10^{-5} \cdot T$	$-0.029 + 9.989 \times 10^{-5} \cdot T$	0.110	$-207.894 + 0.481 \cdot T$	231	481, 509.182 [4, 9]
	1356 K < T < 2000 K	$0.109 + 6.501 \times 10^{-5} \cdot T$	$0.110 + 7.831 \times 10^{-5} \cdot T$		$-45.463 + 0.532 \cdot T$		532, 519.685 [4, 12]

Table 6.3. Polynomials and other parameters of thermal conductivity λ, thermal diffusivity a, density d, temperature coefficient of expansion β and resistance α_R.

Alloy/ element	Temperature Range	λ / W·m^{-1}·K^{-1}	a / 10^{-5} m^2·s^{-1}	d / kg·m^{-3}	β / K^{-1}	α_R / K^{-1}
Pt96Cu04	1200 K < T < 1976 K	$7.445 + 0.042 \cdot T - 6.719 \times 10^{-6} \cdot T^2$	$1.983 \times 10^{-6} + 1.009 \times 10^{-8} \cdot T - 1.378 \times 10^{-12} \cdot T^2$	$20890.597 - 0.688 \cdot T$	$3.281 \times 10^{-5} + 1.205 \times 10^{-9} \cdot T$	3.050×10^{-4}
	1986 K < T < 3100 K	$3.700 + 0.025 \cdot T - 1.882 \times 10^{-6} \cdot T^2$	$9.274 \times 10^{-8} + 5.871 \times 10^{-9} \cdot T - 1.640 \times 10^{-13} \cdot T^2$	$21706.992 - 1.470 \cdot T$	$6.510 \times 10^{-5} + 6.750 \times 10^{-9} \cdot T$	1.225×10^{-4}
Pt68Cu32	1180 K < T < 1639 K	$-1.616 + 0.037 \cdot T - 5.093 \times 10^{-6} \cdot T^2$	$9.873 \times 10^{-8} + 7.408 \times 10^{-9} \cdot T - 4.517 \times 10^{-13} \cdot T^2$	$15632.241 - 1.079 \cdot T$	$6.750 \times 10^{-5} + 5.792 \times 10^{-9} \cdot T$	1.553×10^{-4}
	1686 K < T < 2581 K	$1.938 + 0.023 \cdot T - 9.229 \times 10^{-7} \cdot T^2$	$1.200 \times 10^{-7} + 4.469 \times 10^{-9} \cdot T + 2.826 \times 10^{-13} \cdot T^2$	$15920.120 - 1.419 \cdot T$	$8.417 \times 10^{-5} + 1.219 \times 10^{-8} \cdot T$	6.261×10^{-5}
Pt50Cu50	1200 K < T < 1519 K	$-1.287 + 0.059 \cdot T - 1.258 \times 10^{-5} \cdot T^2$	$7.268 \times 10^{-7} + 1.103 \times 10^{-8} \cdot T - 1.315 \times 10^{-12} \cdot T^2$	$13909.237 - 1.372 \cdot T$	$9.627 \times 10^{-5} + 1.300 \times 10^{-8} \cdot T$	3.029×10^{-4}
	1562 K < T < 2200 K	$3.921 + 0.036 \cdot T - 3.673 \times 10^{-6} \cdot T^2$	$8.756 \times 10^{-8} + 7.855 \times 10^{-9} \cdot T - 2.874 \times 10^{-13} \cdot T^2$	$13562.302 - 1.264 \cdot T$	$8.917 \times 10^{-5} + 1.277 \times 10^{-8} \cdot T$	1.632×10^{-4}
Pt25Cu75	1053 K < T < 1415 K	$9.259 + 0.106 \cdot T - 2.375 \times 10^{-5} \cdot T^2$	$3.098 \times 10^{-6} + 2.537 \times 10^{-8} \cdot T - 4.180 \times 10^{-12} \cdot T^2$	$11024.582 - 0.795 \cdot T$	$7.153 \times 10^{-5} + 6.207 \times 10^{-9} \cdot T$	3.784×10^{-4}
	1460 K < T < 2080 K	$7.157 + 0.068 \cdot T - 9.320 \times 10^{-6} \cdot T^2$	$4.069 \times 10^{-7} + 1.782 \times 10^{-8} \cdot T - 1.659 \times 10^{-12} \cdot T^2$	$10736.545 - 0.831 \cdot T$	$7.547 \times 10^{-5} + 8.059 \times 10^{-9} \cdot T$	2.228×10^{-4}

Table 6.4. Polynomials and other parameters of thermal conductivity λ, thermal diffusivity a, density d, temperature coefficient of expansion β and resistance α_R.

Alloy/ element	**Temperature Range**	λ / **W·m^{-1}·K^{-1}**	a / **10^{-5} m^2·s^{-1}**	***d*** / **kg·m^{-3}**	β / **K^{-1}**	α_R / **K^{-1}**
Pt	1740 K < T < 2042 K	$44.054 + 2.624 \times 10^{-2} \cdot T - 4.872 \times 10^{-6} \cdot T^2$	$1.112 \times 10^{-5} + 7.305 \times 10^{-9} \cdot T - 1.148\ 10^{-12} \cdot T^2$	$21580.145 - 0.605 \cdot T$	$2.797 \times 10^{-5} + 8.755 \times 10^{-10} \cdot T$	4.558×10^{-4}
	2042 K < T < 2830 K	$0.344 + 2.912 \times 10^{-2} \cdot T - 2.480 \times 10^{-6} \cdot T^2$	$8.291 \times 10^{-8} + 7.041 \times 10^{-9} \cdot T - 1.814 \times 10^{-13} \cdot T^2$	$21242.245 - 1.117 \cdot T$	$5.147 \times 10^{-5} + 3.645 \times 10^{-9} \cdot T$	1.157×10^{-4}
Pt95Co05	1200 K < T < 1949 K	$6.251 + 0.042 \cdot T - 7.977 \times 10^{-6} \cdot T^2$	$1.922 \times 10^{-6} + 9.979 \times 10^{-9} \cdot T - 1.368 \times 10^{-12} \cdot T^2$	$21275.79 - 1.483 \cdot T$	$6.519 \times 10^{-5} + 5.45 \times 10^{-9} \cdot T$	3.534×10^{-4}
	1964 K < T < 3000 K	$4.853 + 0.024 \cdot T - 2.039 \times 10^{-6} \cdot T^2$	$5.204 \times 10^{-8} + 5.656 \times 10^{-9} \cdot T - 1.277 \times 10^{-13} \cdot T^2$	$21807 - 1.87719 \cdot T$	$7.935 \times 10^{-5} + 1.189 \times 10^{-8} \cdot T$	1.46×10^{-4}
Pt95Ru05	1100 K < T < 2013K	$12.277 + 0.041 \cdot T - 7.864 \times 10^{-6} \cdot T^2$	$2.990 \times 10^{-6} + 9.193 \times 10^{-9} \cdot T - 1.397 \times 10^{-12} \cdot T^2$	$21767.379 - 1.134 \cdot T$	$5.168 \times 10^{-5} + 3.237 \times 10^{-9} \cdot T$	4.07×10^{-4}
	2025 K < T < 3100 K	$3.078 + 0.025 \cdot T - 1.814 \times 10^{-6} \cdot T^2$	$1\text{-}252 \times 10^{-7} + 5.403 \times 10^{-9} \cdot T - 1.753 \times 10^{-13} \cdot T^2$	$21154.875 - 1.211 \cdot T$	$5.555 \times 10^{-5} + 4.505 \times 10^{-9} \cdot T$	1.124×10^{-4}
Cu	1100 K < T <1356 K	$418.778 - 0.075 \cdot T$	$9.740 \times 10^{-5} - 1.554 \times 10^{-8} \cdot T$	$9133.864 - 0.376 \cdot T$	$4.109 \times 10^{-5} + 1.884 \times 10^{-9} \cdot T$	1.23×10^{-3}
	1356 K < T < 2000 K	$89.407 + 0.050 \cdot T$	$1.731 \times 10^{-5} + 1.390 \times 10^{-8} \cdot T$	$8803.735 - 0.460 \cdot T$	$5.180 \times 10^{-5} + 3.284 \times 10^{-9} \cdot T$	3.622×10^{-4}

Table 6.5. Polynomials and other parameters of density *d*, and temperature coefficient of expansion γ .

Alloys/ element	**Temperature Range**	***d* / kg·m^{-3}**	**β / K^{-1}**
Pt	293 K < T < 1586 K	21637.146 - 0.643 · T	2.970 x 10^{-5} + 9.262 x 10^{-10} · T
Pt96Cu04	293 K < T < 1586 K	20543.752 - 0.649 · T	3.157 x 10^{-5} + 1.063 x 10^{-9} · T
Pt68Cu32	293 K < T < 1586 K	14900.619 – 0.564 · T	3.778 x 10^{-5} + 1.583 x 10^{-9} · T
Pt50Cu50	293 K < T < 1519 K	12673.059 – 0.521 · T	4.107 x 10^{-5} + 1.808 x 10^{-9} · T
Pt25Cu75	293 K < T < 1415 K	10594 - 0.602 · T	5.667 x 10^{-5} + 3.603 x 10^{-9} · T
	1460 K < T < 1586 K	11923.398 – 1.953 · T	1.466 x 10^{-4} + 4.709 x 10^{-9} · T
Pt95Co05	293 K < T < 1586 K	20073.891 - 0.672 · T	3.343 x 10^{-5} + 1.195 x 10^{-9} · T
Pt95Ru05	293 K < T < 1519 K	20901.631 – 0.627 · T	3 x 10^{-5} + 9.549 x 10^{-10} · T

References

[1] *Thermo-Calc Software AB*, Stockholm, Sweden, SGTE Nobel Metal Alloys Database (SNOB), Version 1.1.

[2] Doerinckel F, 1907 *Z. anorg. Chem*., **54**: pp 335-338.

[3] Wilthan B, Cagran C, Brunner C and Pottlacher G 2004 *Thermophysical Properties of Solid and Liquid Platinum,* Thermochimica Acta ***415***: pp 47-54.

[4] Cagran C, Seifter A and Pottlacher G, 2000 Schriften des Forschungszentrums Jülich, Science Energy Technology **1**: pp 763-766.

[5] Beck G, 1995 *Edelmetall-Taschenbuch*. 2nd edition ed.: Degussa AG, Frankfurt und Hüthig GmbH, Heidelberg.

[6] Savitskii E M, 1989 *Handbook of precious metal* New York, USA: Hemisphere publishing cooperation.

[7] Lide D R, 2007 CRC *Handbook of Chemistry and Physics* 88th edn Boca Raton, FL: CRC Press, pp 4-138.

[8] Savitskii E M, 1989 *Handbook of precious metal* New York, USA : Hemisphere publishing cooperation.

[9] White G K and Minges M L, 1997 International Journal of Thermophysics **18**: pp 1269-1327.

[10] Lebedev S V and Savvatimski, 1984 A I Uspekhi Fiz. Nauk. pp 144:215.

[11] Savvatimski A I, 1996 International Journal of Thermophysics, pp 17:495.

[12] Chaudhuri A K, Bonnel D W, Ford L A and Margrave J L, 1970 High Temperature Science **2**: pp 203 - 212.

Chapter 7

Prediction of Effective Thermal Conductivity λ_e as a Function of Temperature

In this chapter thermophysical properties of binary alloys as a function of temperature will be discussed in the temperature range from the liquidus points of the alloys up to several hundreds of Kelvin in the liquid region. The measurement of thermal properties for such a wide range of temperatures is very difficult and time consuming. Therefore, to predict these values, some model calculations have been done in terms of easily measurable parameters.

7.1. Proposed Models

Three different empirical models called the T_0-model, the *q-model*, and the η-model are proposed in this research work for the prediction of effective thermal conductivities of series of binary alloys as a function of temperature, while taking into account the thermal conductivities of the constituents and one fit parameter. For such calculations, it is of special importance to choose model functions that are both physically relevant and numerically robust. The models presented here are developed using the previously developed model by the author and a colleague that was used for non conducting materials, but here it is modified for conducting materials like metals and alloys [1]. The proposed T_0- model and the *q-model* are given as:

$$\frac{1}{\lambda_{(e)}(T)} = \frac{1}{\lambda_A(T)} + \frac{q}{\lambda_B(T)}\left(\frac{T}{T_0}\right) \qquad (T_0\text{-model}) \qquad (7.1)$$

$$q = T_0\lambda_B\left[\frac{\sum\left(1/\lambda_{\exp} - 1/\lambda_A\right)}{\sum T}\right] \qquad (7.2)$$

$$\frac{1}{\lambda_{(e)}(T)} = \frac{1}{\lambda_A(T)} + \frac{q}{\lambda_B(T)} \qquad (\text{q-model}) \qquad (7.3)$$

In Equations (7.1-7.3) λ_e and λ_{exp} mean the effective and experimental thermal conductivities whereas λ_A and λ_B represent the thermal conductivities of the constituents A and B of alloy respectively. T_0 means the reference temperature (room temperature), and T is the varying temperature in K. The value of q in T_0 - model is determined using equation (7.2), whereas in the q-model, the factors T/T_0 and q value of T_0-model are combined into a single, temperature-independent value of q, which makes it more simple and efficient than the earlier one. This new value of m in Equation (7.3) is a fit parameter, which can be found either by a least-squares process or by a simple iteration.

In models 7.1-7.3 the second term B are originally due to small addition to dominating first term A, for example in reference 1 term B meant an amount of air in the solid phase. For the system investigated in this work, the two constituents of the alloys are completely comparable; consequently the constituent B may have percentage of 0 – 100 %. Under such circumstances the parameter q may get unphysical negative values, in such cases the order of the two constitutes of alloys has to be switched.

The third model, called η-model, has the following physical background: based on the fact that, for a binary alloy AB, the heat capacity of constant volume in units $kJ \cdot kg^{-1} \cdot K^{-1}$ approximately fulfills the Neumann-Kopp relation

$$c_v = (1-x)c_v(A) + xc_v(B) \tag{7.4}$$

Where x means the mass fraction of the constituent B. Unlike this situation, transport properties like the electrical or thermal conductivity (or the correspondent inverse quantities, the specific electrical or thermal resistivity), are bounded as [2].

$$\left(\frac{1-f}{\lambda_A} + \frac{f}{\lambda_B}\right)^{-1} \leq \lambda_{AB} \leq (1-f)\lambda_A + f\lambda_B \tag{7.5}$$

Where f means the *volume fraction* of the constituent B. Surprisingly, for all examples of binary alloy AB discussed in this thesis, the above relation was in many cases not fulfilled. For this reason, it has been decided to use for a transport property like the thermal resistivity also a model of Neumann-Kopp style, but including a parameter η which describes the dominance of the constituent A over B with respect to the transport mechanism. This η-model reads as

$$\frac{1}{\lambda_{(e)}(T)} = \frac{x'}{\lambda_A(T)} + \frac{(1-x')}{\lambda_B(T)} \qquad (\eta \text{ - model}) \qquad (7.6)$$

$$x' = \frac{\eta . x}{1 - x(\eta - 1)} \qquad (7.7)$$

The parameter x is the mass contribution of B and x' is called the *effective mass contribution.* It is to be noted that in equations (7.1), (7.3), and (7.6), all the parameters affecting thermal conductivity such as material phases, material structure, convection and density, etc. play a vital role in predicting thermal conductivity. So, while discussing the dependence of thermal conductivity upon temperature, these factors should not be ignored. In fact, it is very difficult to take into account the variations of these parameters with temperature. For this reason, some adjustable parameters are introduced in developing such empirical formulae which compensate for all those effects. In other words, we can say that all these variations are dumped into the adjustable parameters, q and η, which may vary from material to material. In T_0 model, λ_A has been selected as the constituent alloy whose thermal conductivity is higher than other and in *q-model* both alloy constituents are consider as λ_A and λ_B, whereas in η- model either can be selected as λ_A, in either situation we reach the same results after simple modification.

From equation (7.1), it is obvious that when $T = T_o$, this formula resembles with proposal at room temperature [3]. The thermal conductivities of all the samples are predicted by the proposed models are plotted in Figures 7.1 to 7.37.

These proposed models are applied on the alloy series, shown in Table 7.1, it can be seen that the samples of alloys have been arranged / named on the basis of increasing alloying of copper, iron and nickel in the three modeling series namely: PtCu, FeNi and CuNi respectively. The predicted thermal conductivities of all the investigated materials, plotted in the Figures, have deviations which are shown in Table 7.2. Our predict effective thermal conductivities as a function of temperatures are in close agreement with the experimental values. The two values of q in q-model are because of the change of order in alloy constituent, some values of η are not given in Table 7.2 because in those alloy system experimental values are out of range of either of the two alloy constituent value which is logically not suitable for η- model.

It has been noticed that in most of the cases all predicted thermal conductivity values lie in the uncertainty region of experimentally determined values (8.5 % for PtCu, 8 % for CuNi and 15 % for FeNi system) which is quite promising. Also it can be seen very clearly in all alloys systems that one of the alloy constituent is more dominantly playing its role in thermal conductivity than the other one. This phenomenon can easily be observed in all graphical representation of thermal conductivity curves, especially when the mass percentage is equal or nearly equal (50Pt50Cu, 50Fe50Ni and Ni45Fe65 Pt) of the two constituent of alloy. Platinum, iron and Ni are dominant constituent in PtCu, FeNi and CuNi system respectively. For example in Fe30Ni70 alloy, the results are significantly closer to the pure iron despite the high concentration of nickel.

Two models T_0 - model and q - model are applicable in all available data sets but η – model is only applicable if experimentally determined thermal conductivity lies within the thermal conductivity values of pure constituent of binary alloy. Nevertheless, it gives much better results than the other two models from the perspective of percentage deviation with the experimental values.

Table 7.1. Three alloy series PtCu, CuNi and FeNi applied for modeling, whereas PtCu are investigated experimentally in the present work while other are taken from Hüpf and Seifter respectively [4, 5].

Pt-Cu	Cu-Ni	Fe-Ni
Pt96Cu04	Cu85Ni15	Fe20Ni80
Pt68 Cu32	Cu70Ni30	Fe40Ni60
Pt50 Cu50	Cu55Ni45	Fe50Ni50
Pt25 Cu75	Cu35Ni65	Fe64Ni36
	Cu20Ni80	Fe80Ni20
		Fe90Ni10

Table 7.2: Parameters used in three models with percentage errors from experimental values.

Alloy	% deviation in T_0 model	*q*- values	% deviation in q-model	(η- values)	% deviation η-model
Pt96Cu04	1.5	0.77	1, 2		
Pt68Cu32	15	0.79	3, 5		
Pt50Cu50	7.5	0.53	3, 1	2.4	1
Pt25Cu75	8	0.19	10, 1	1	1
Cu85Ni15	5	0.28	1, 5	3.7	2
Cu70Ni30	10	0.55	1, 1	8	1
Cu55Ni45	10	0.6	1, 1	7	1
Cu35Ni65	1	0.72	1, 1		
Cu20Ni80	2	0.75	2, 1	10	2
Fe20Ni80	7	0.28	3, 2		
Fe40Ni60	6	0.38	3, 1	18	1
Fe50Ni50	5	0.42	2, 1		
Fe64Ni36	3	0.465	2, 2		
Fe80Ni20	1	044	2, 2		
Fe90Ni10	1	0.415	1, 1		

T_o - model

Pt-Cu System

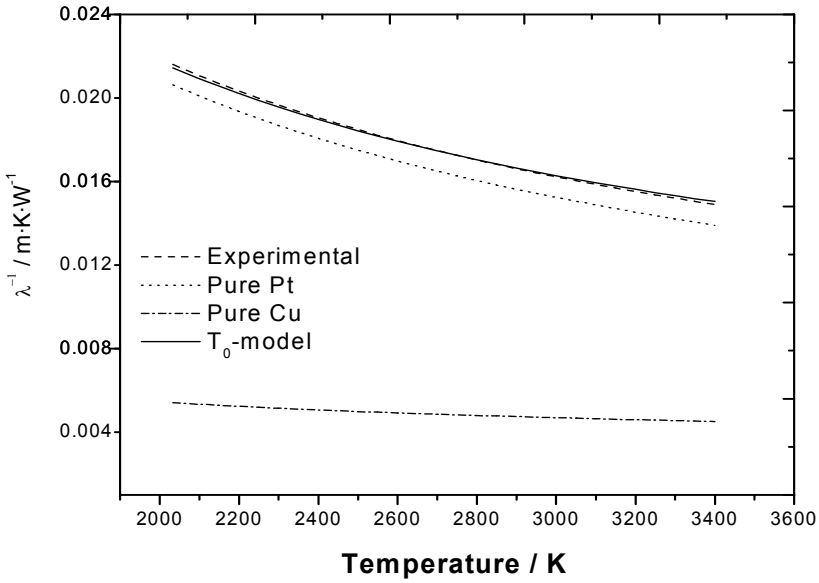

Figure 7.1. Comparison of measured and predicted thermal conductivity values of Pt96Cu04 as a function of temperature along with pure Pt and pure Cu [6, 7].

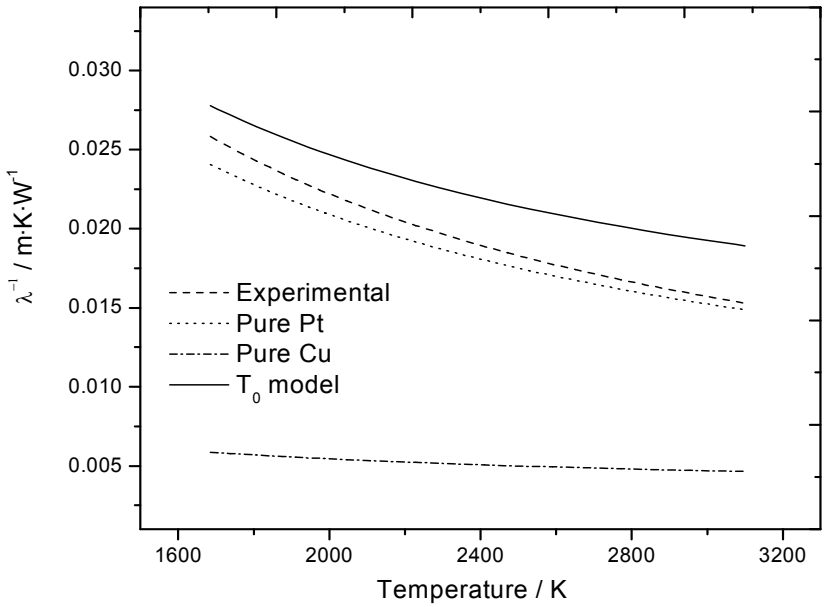

Figure 7.2. Comparison of measured and predicted thermal conductivity values of Pt68Cu32 as a function of temperature along with pure Pt and pure Cu [6, 7].

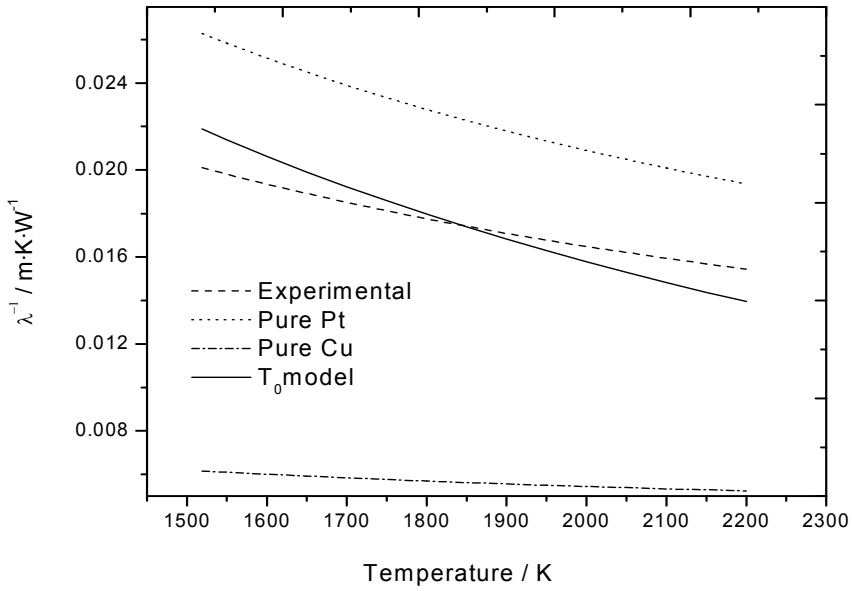

Figure 7.3. Comparison of measured and predicted thermal conductivity values of Pt50Cu50 as a function of temperature along with pure Pt and pure Cu [6, 7].

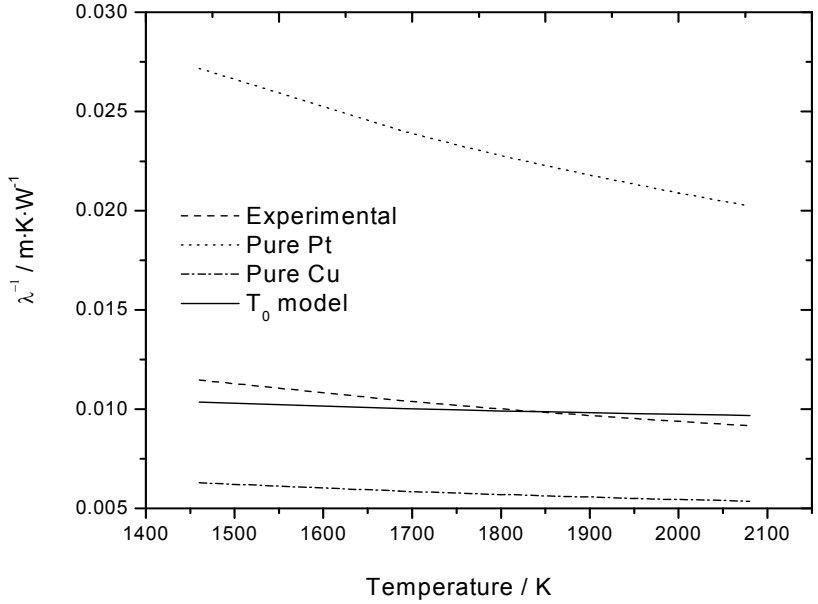

Figure 7.4. Comparison of measured and predicted thermal conductivity values of Pt25Cu75 as a function of temperature along with pure Pt and pure Cu [6, 7].

Cu-Ni System

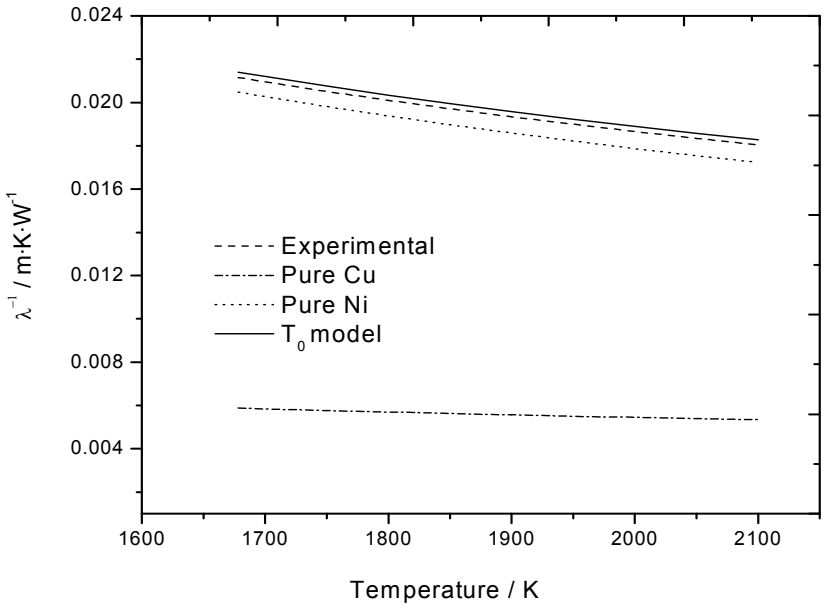

Figure 7.5. Comparison of measured and predicted thermal conductivity values of Cu20Ni80 as a function of temperature along with pure Cu and pure Ni [5-7].

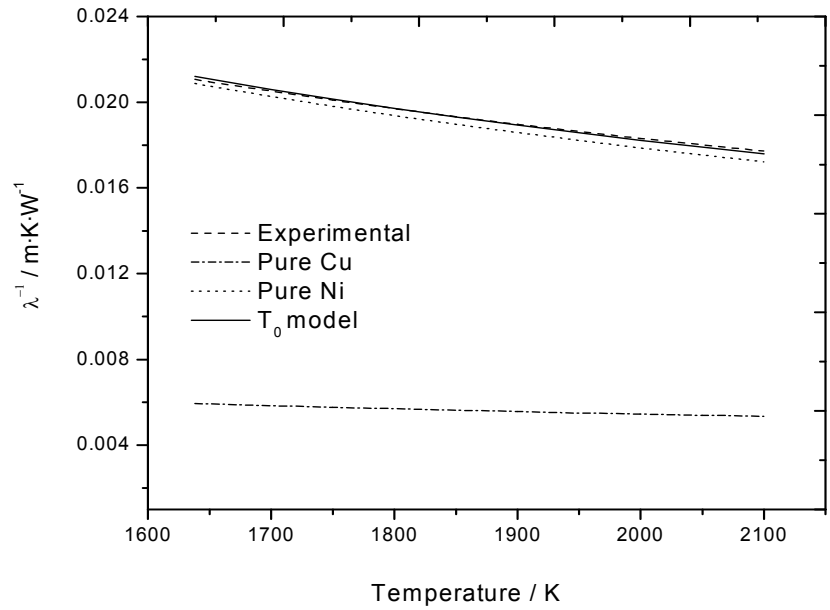

Figure 7.6. Comparison of measured and predicted thermal conductivity values of Cu35Ni65 as a function of temperature along with pure Cu and pure Ni [5-7].

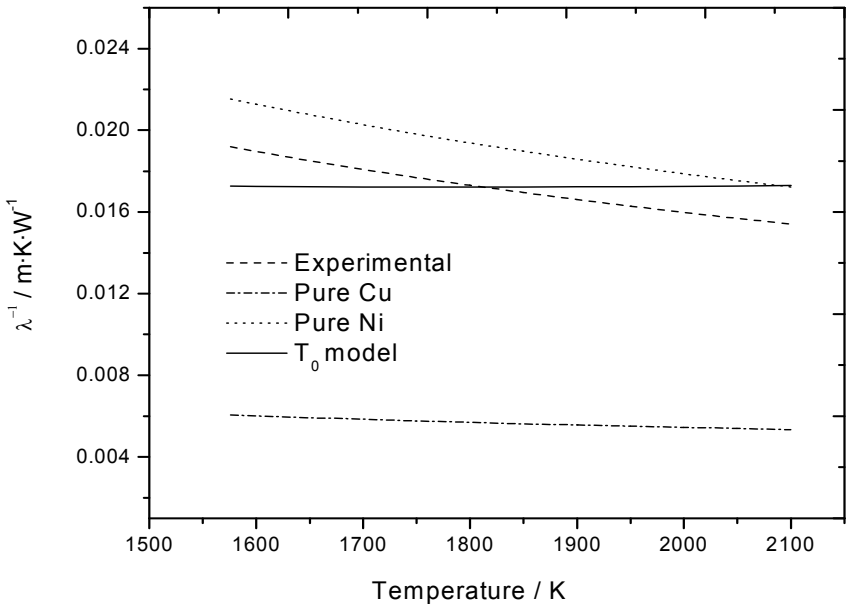

Figure 7.7. Comparison of measured and predicted thermal conductivity values of Cu55Ni45 as a function of temperature along with pure Cu and pure Ni [5-7].

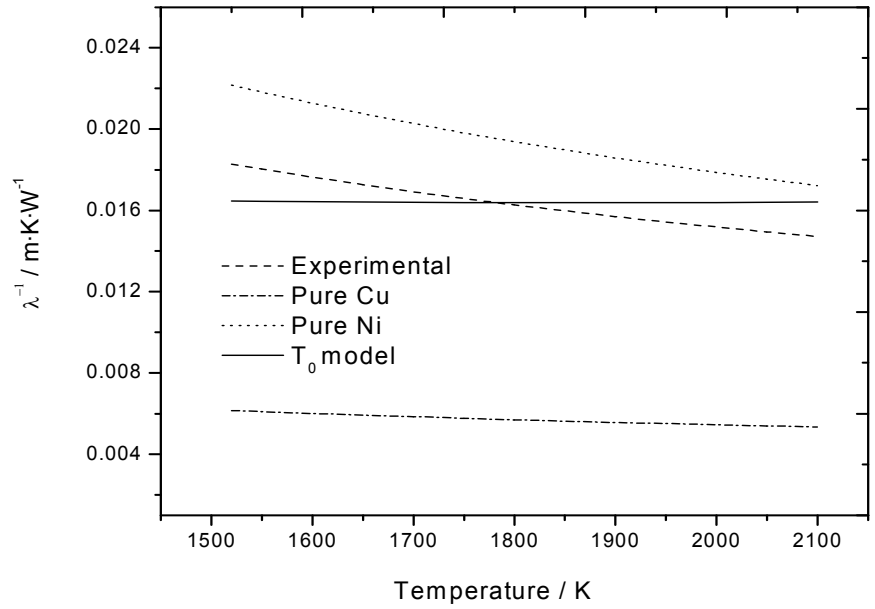

Figure 7.8. Comparison of measured and predicted thermal conductivity values of Cu70Ni30 as a function of temperature along with pure Cu and pure Ni [5-7].

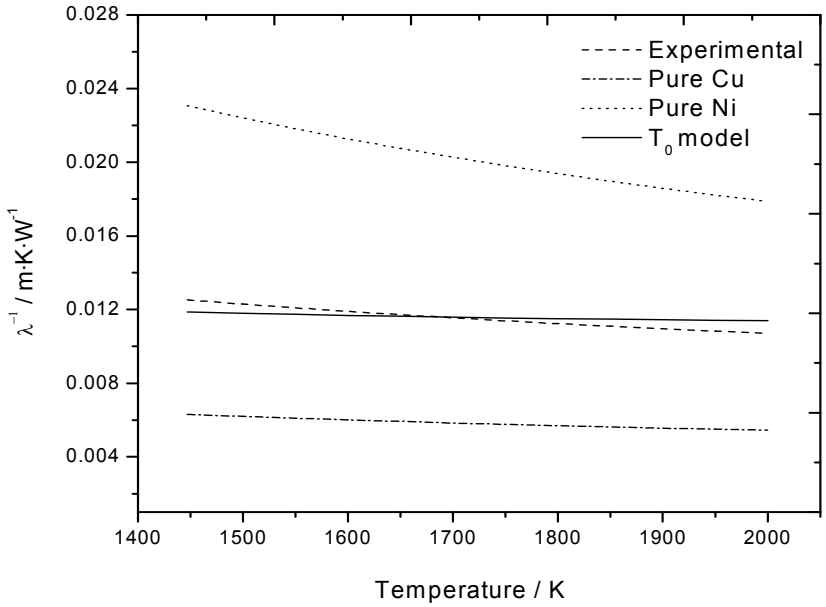

Figure 7.9. Comparison of measured and predicted thermal conductivity values of Cu85Ni15 as a function of temperature along with pure Cu and pure Ni [5-7].

Fe-Ni System

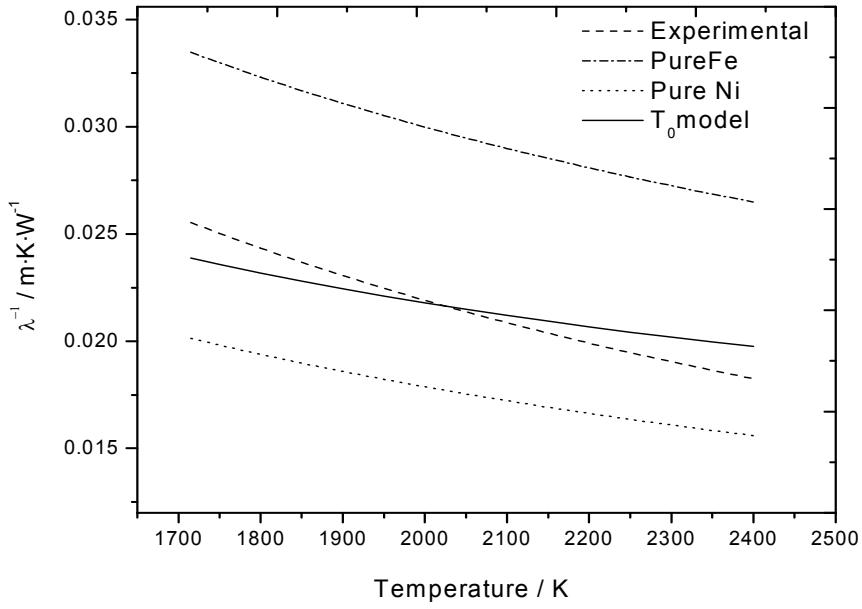

Figure 7.10. Comparison of measured and predicted thermal conductivity values of Fe20Ni80 as a function of temperature along with pure Fe and pure Ni [4, 6].

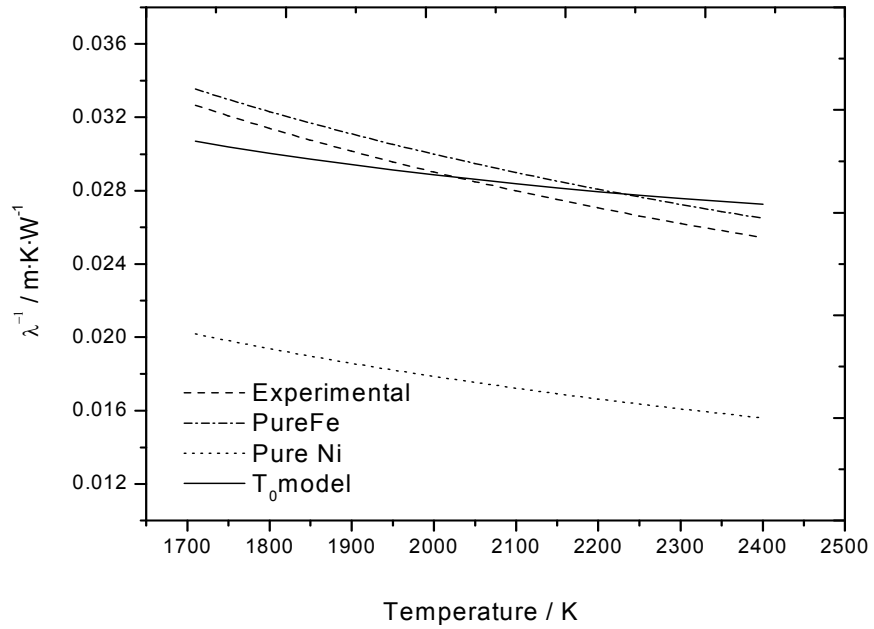

Figure 7.11. Comparison of measured and predicted thermal conductivity values of Fe40Ni60 as a function of temperature along with pure Fe and pure Ni [4, 6].

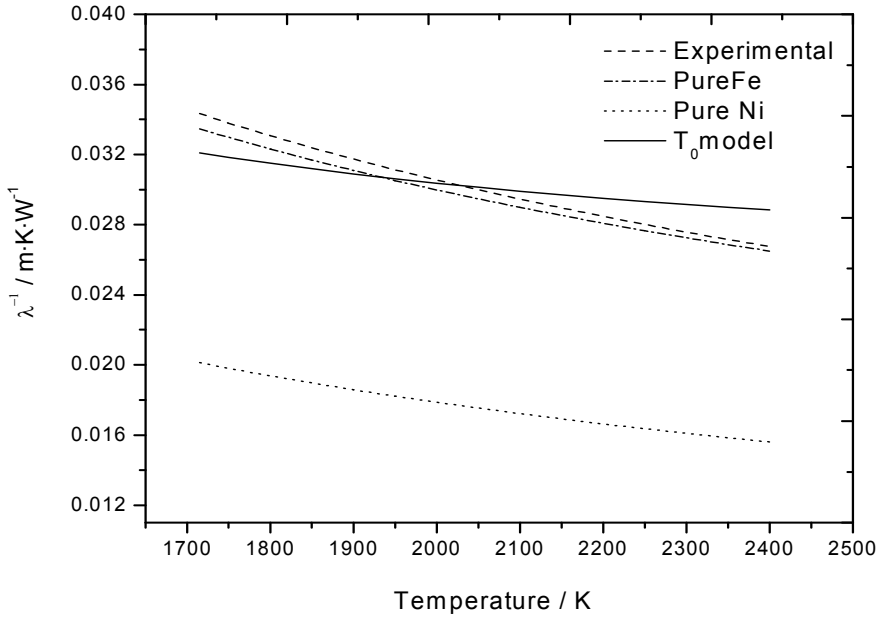

Figure 7.12. Comparison of measured and predicted thermal conductivity values of Fe50Ni50 as a function of temperature along with pure Fe and pure Ni [4, 6].

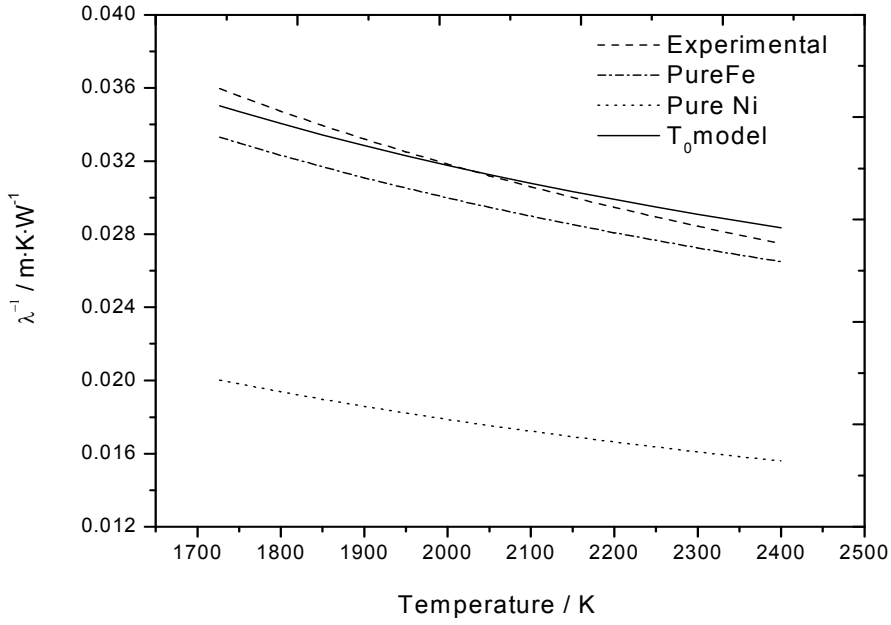

Figure 7.13. Comparison of measured and predicted thermal conductivity values of Fe64Ni36 as a function of temperature along with pure Fe and pure Ni [4, 6].

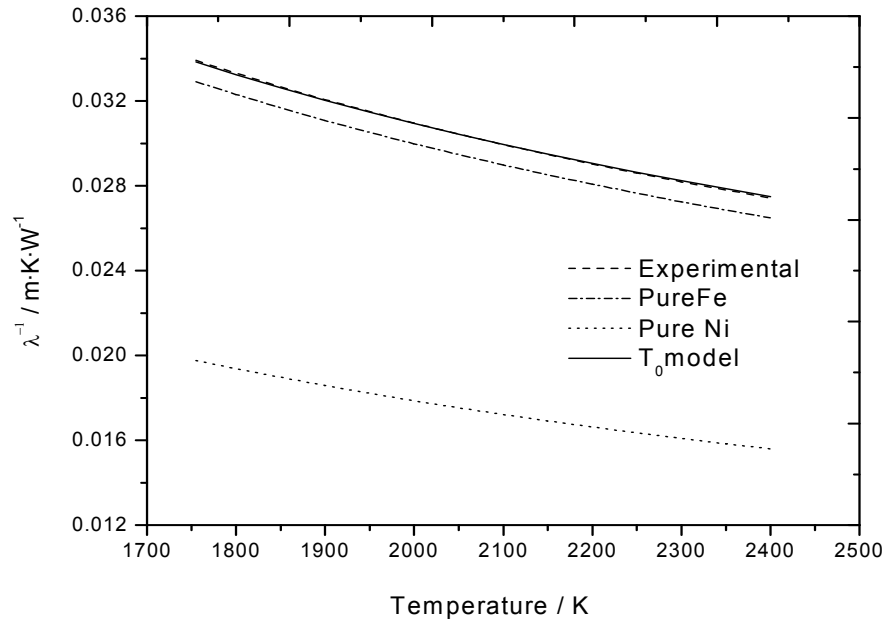

Figure 7.14. Comparison of measured and predicted thermal conductivity values of Fe80Ni20 as a function of temperature along with pure Fe and pure Ni [4, 6].

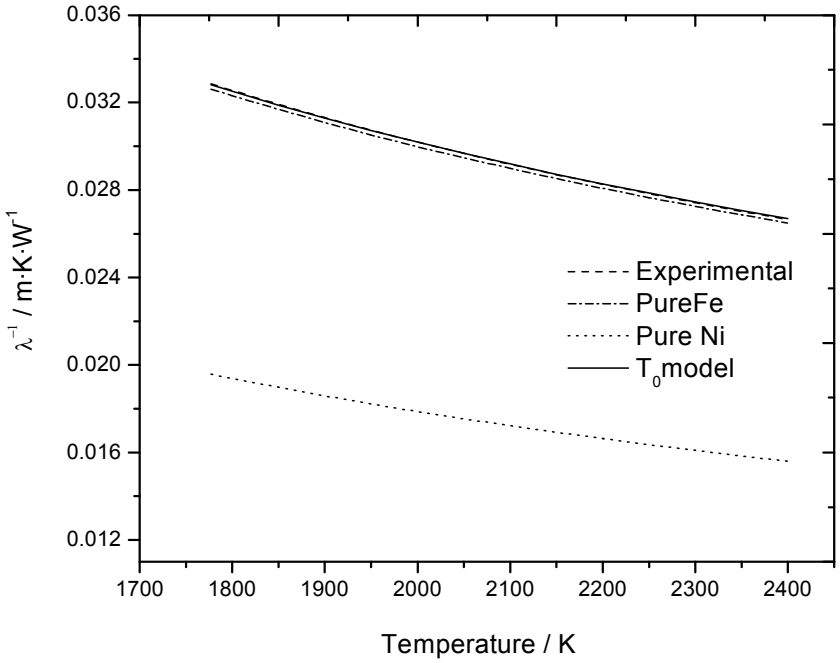

Figure 7.15. Comparison of measured and predicted thermal conductivity values of Fe90Ni10 as a function of temperature along with pure Fe and pure Ni [4, 6].

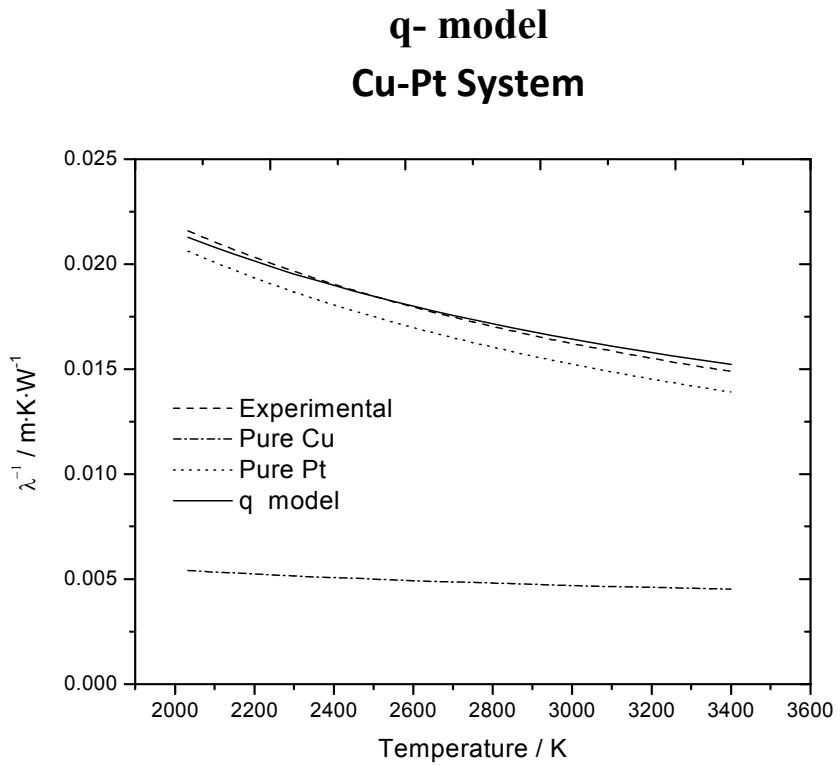

Figure 7.16. Comparison of measured and predicted thermal conductivity values of Cu04Pt96 as a function of temperature along with pure Cu and pure Pt [6, 7].

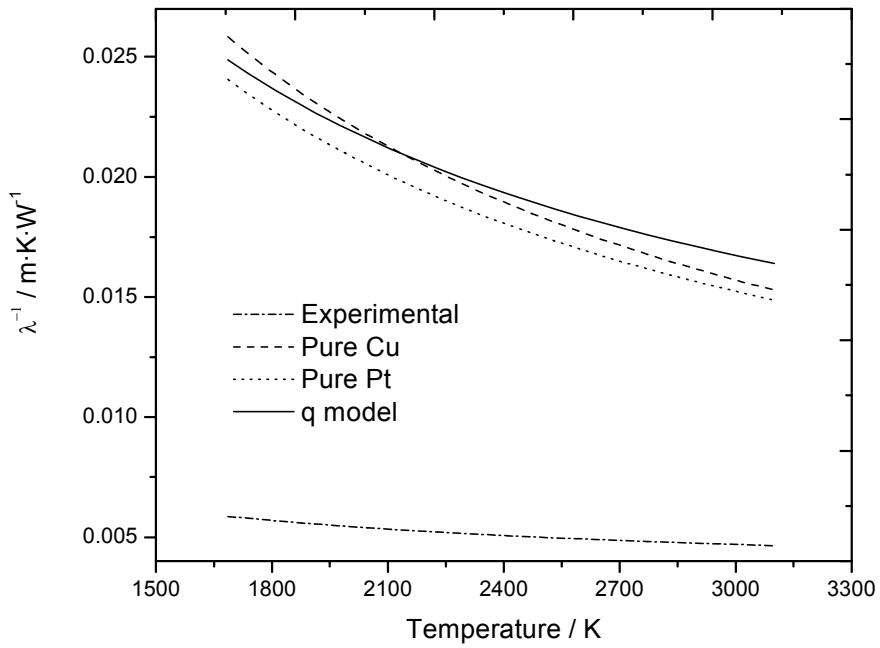

Figure 7.17. Comparison of measured and predicted thermal conductivity values of Cu32Pt68 as a function of temperature along with pure Cu and pure Pt [6, 7].

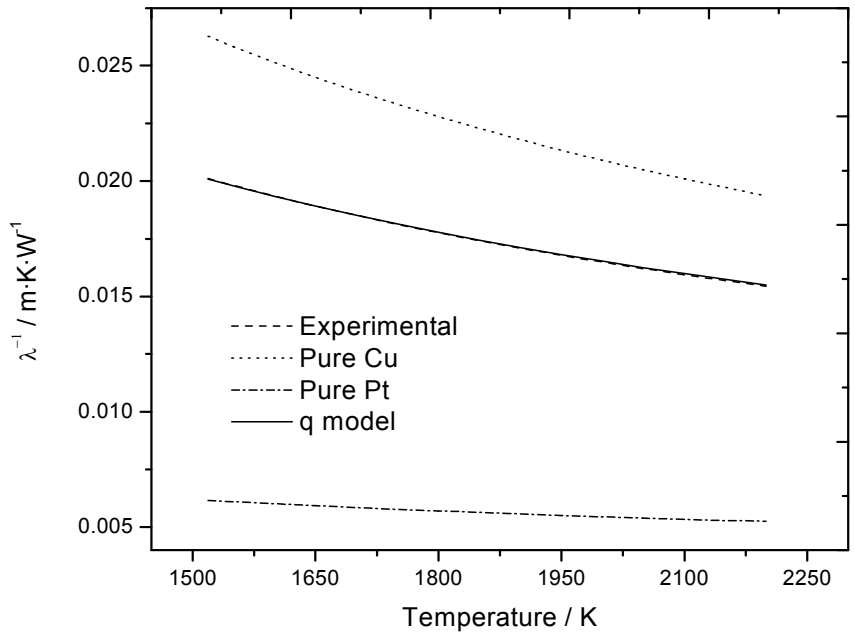

Figure 7.18. Comparison of measured and predicted thermal conductivity values of Cu50Pt50 as a function of temperature along with pure Cu and pure Pt [6, 7].

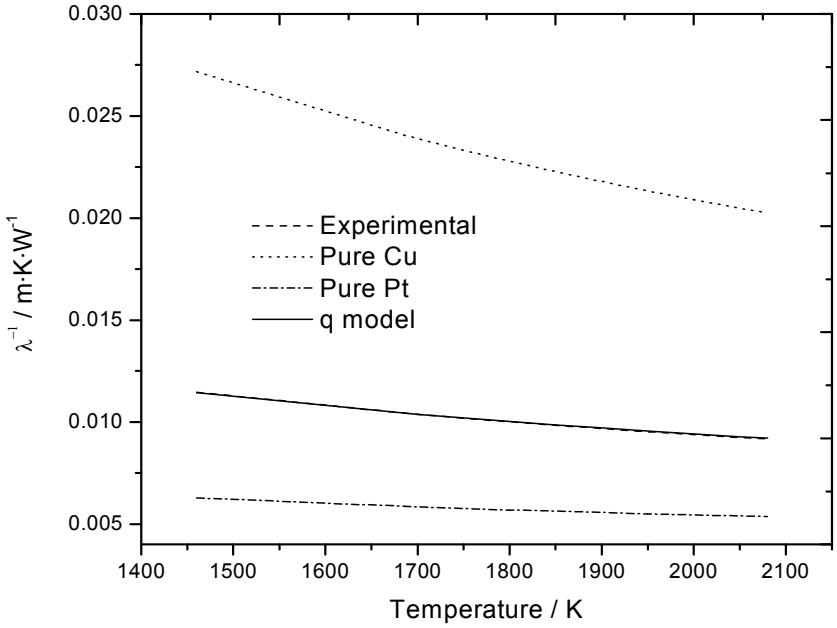

Figure 7.19. Comparison of measured and predicted thermal conductivity values of Cu75Pt25 as a function of temperature along with pure Cu and pure Pt [6, 7].

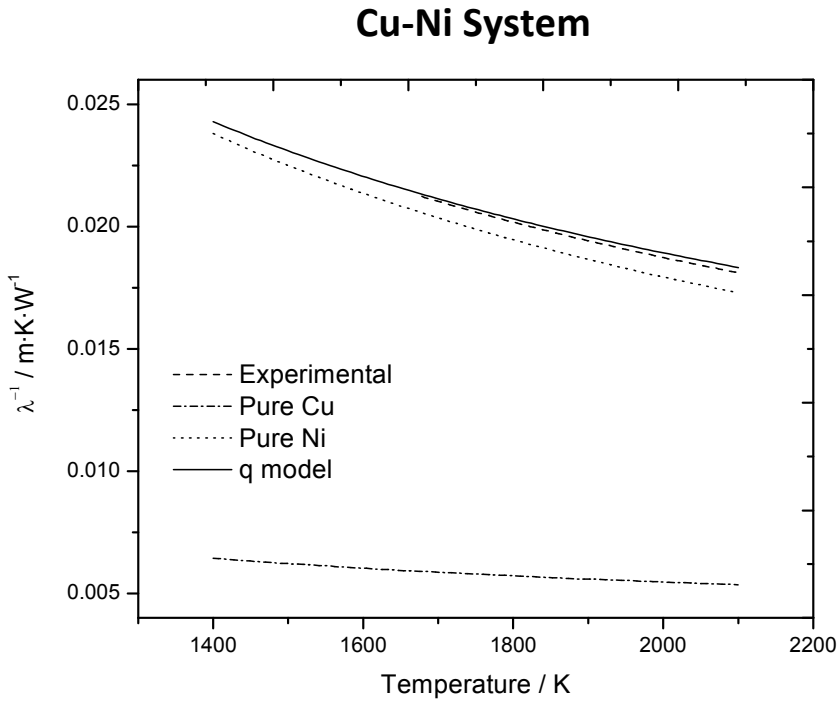

Figure 7.20. Comparison of measured and predicted thermal conductivity values of Cu20Ni80 as a function of temperature along with pure Cu and pure Ni [5-7].

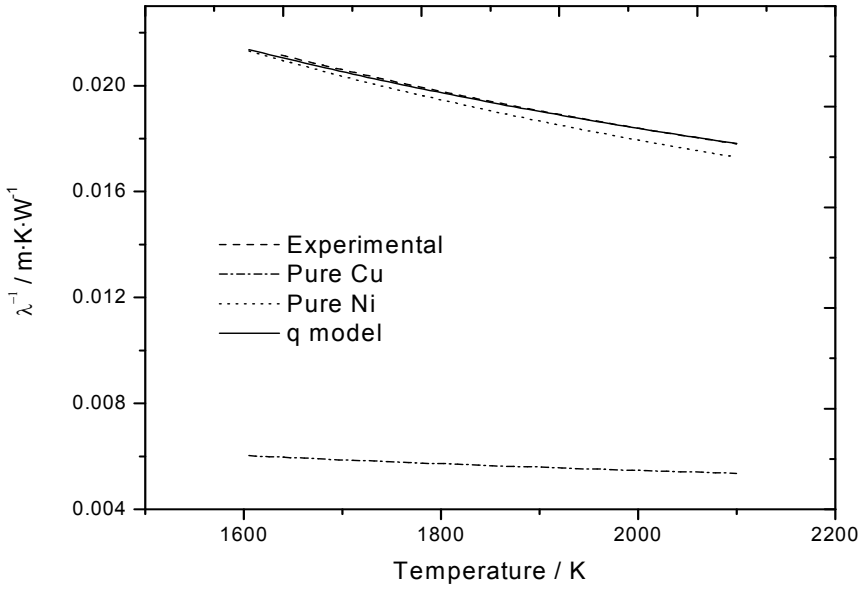

Figure 7.21. Comparison of measured and predicted thermal conductivity values of Cu35Ni65 as a function of temperature along with pure Cu and pure Ni [5-7].

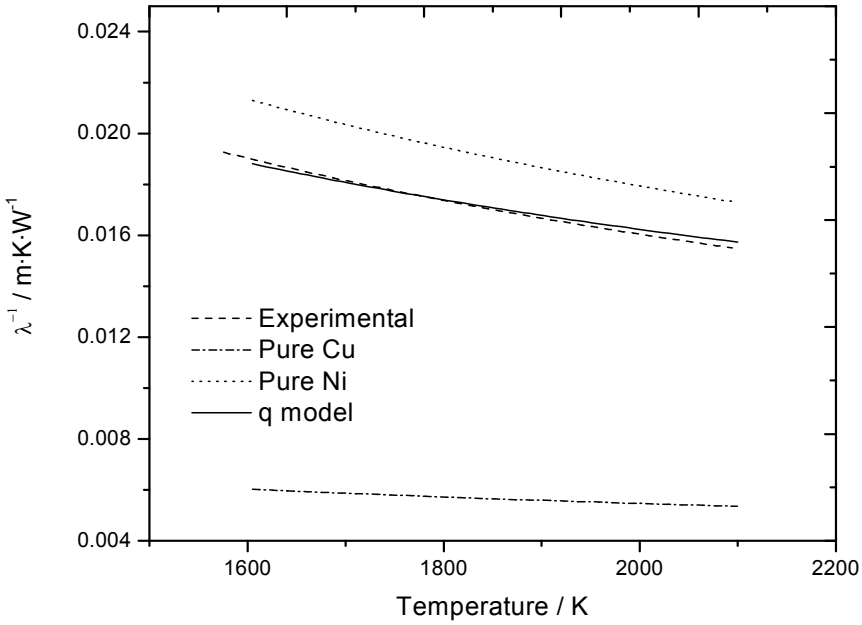

Figure 7.22. Comparison of measured and predicted thermal conductivity values of Cu55Ni45 as a function of temperature along with pure Cu and pure Ni [5-7].

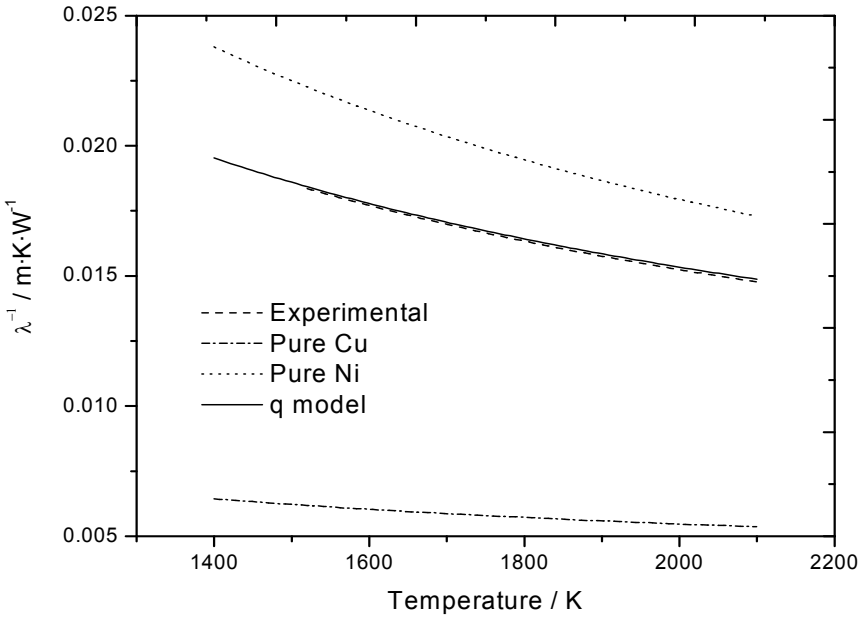

Figure 7.23. Comparison of measured and predicted thermal conductivity values of Cu70Ni30 as a function of temperature along with pure Cu and pure Ni [5-7].

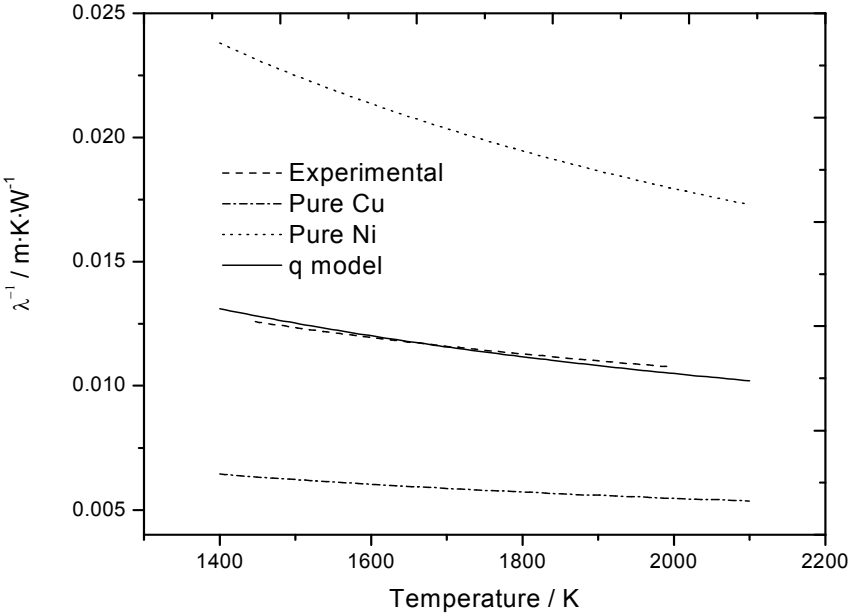

Figure 7.24. Comparison of measured and predicted thermal conductivity values of Cu85Ni15 as a function of temperature along with pure Cu and pure Ni [5-7].

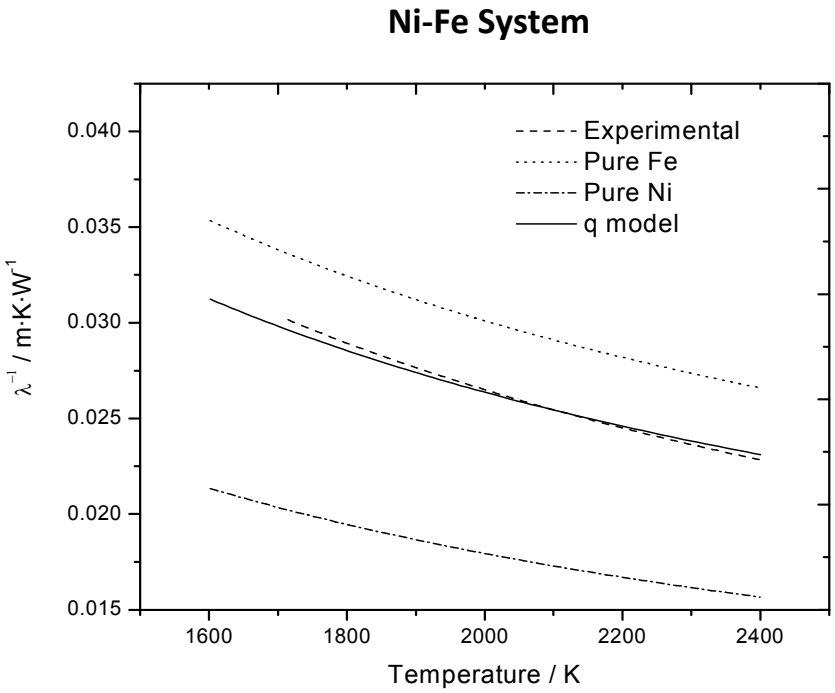

Figure 7.25. Comparison of measured and predicted thermal conductivity values of Ni80Fe20 as a function of temperature along with pure Ni and pure Fe [4, 6].

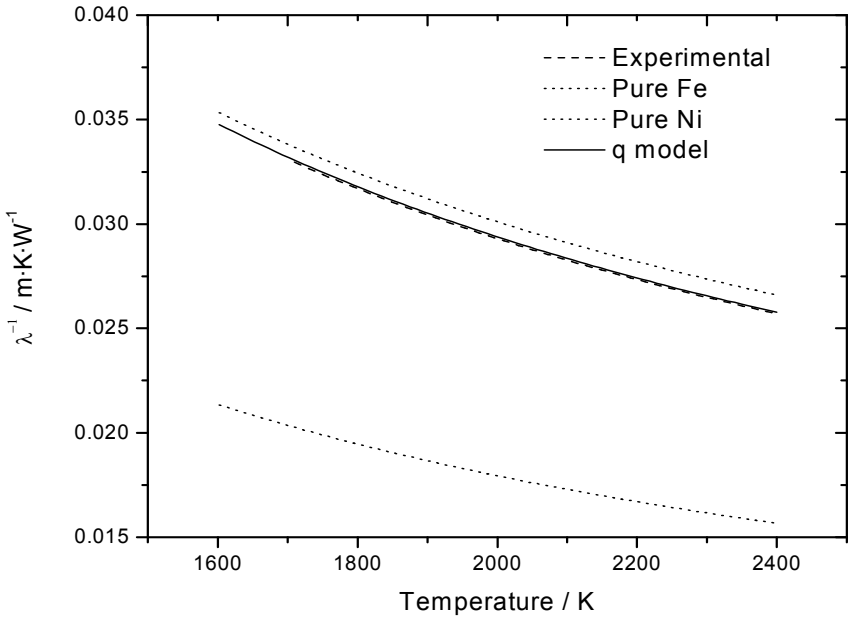

Figure 7.26. Comparison of measured and predicted thermal conductivity values of Ni40Fe60 as a function of temperature along with pure Ni and pure Fe [4, 6].

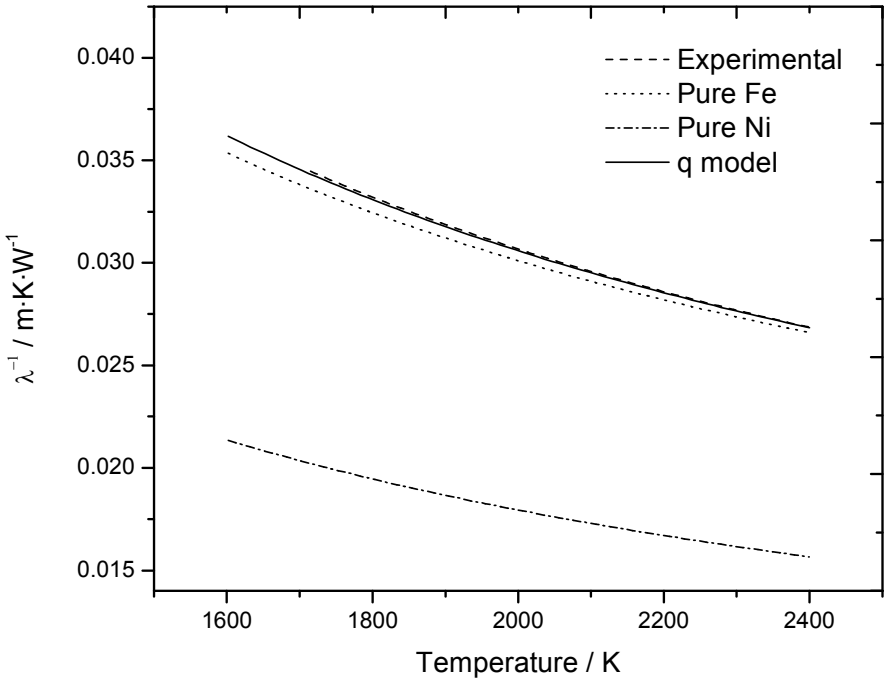

Figure 7.27. Comparison of measured and predicted thermal conductivity values of Ni50Fe50 as a function of temperature along with pure Ni and pure Fe [4, 6].

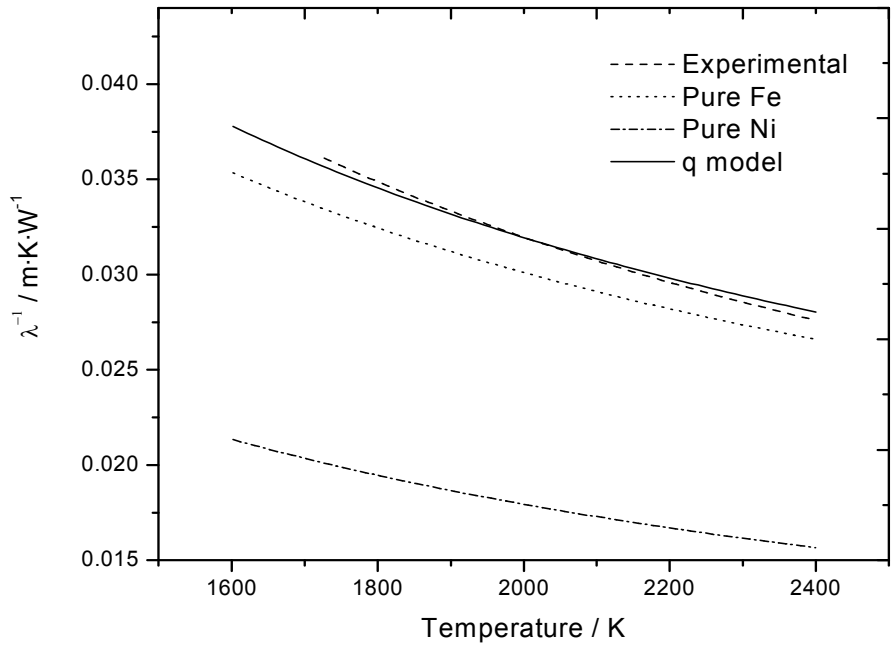

Figure 7.28. Comparison of measured and predicted thermal conductivity values of Ni36Fe64 as a function of temperature along with pure Ni and pure Fe [4, 6].

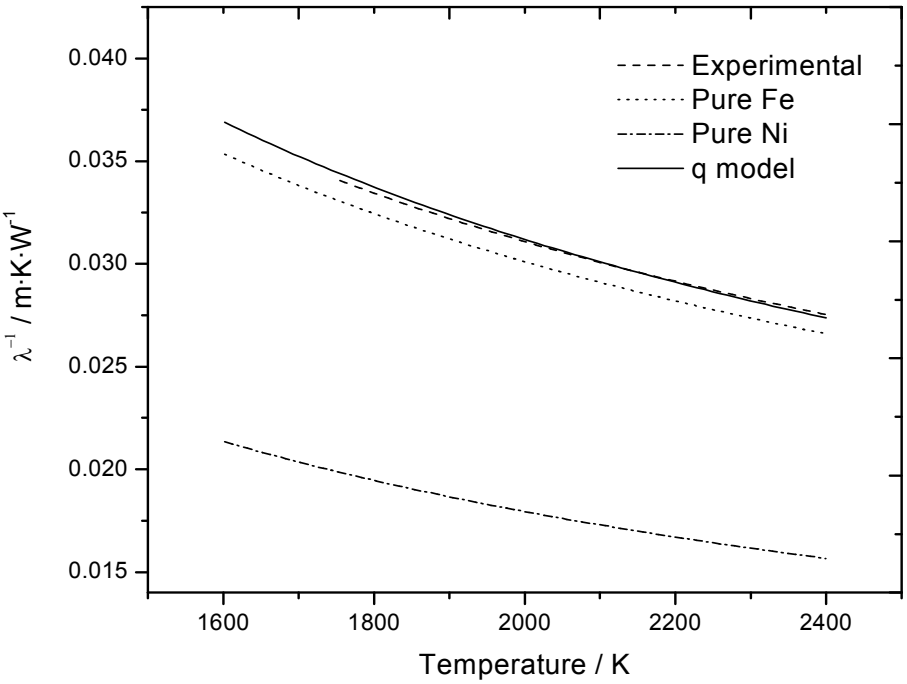

Figure 7.29. Comparison of measured and predicted thermal conductivity values of Ni20Fe80 as a function of temperature along with pure Ni and pure Fe [4, 6].

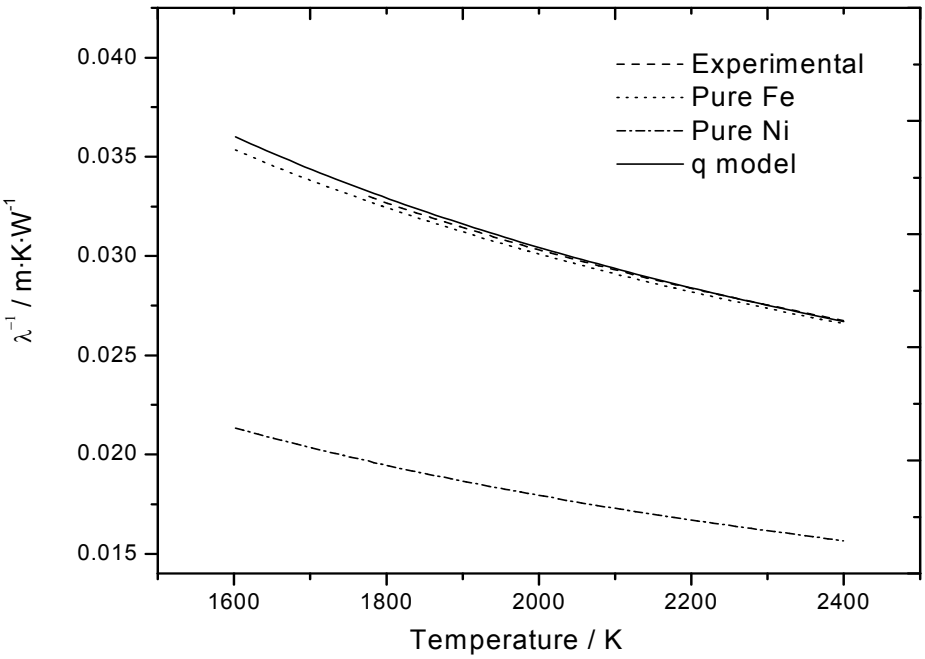

Figure 7.30. Comparison of measured and predicted thermal conductivity values of Ni11Fe89 as a function of temperature along with pure Ni and pure Fe [4, 6].

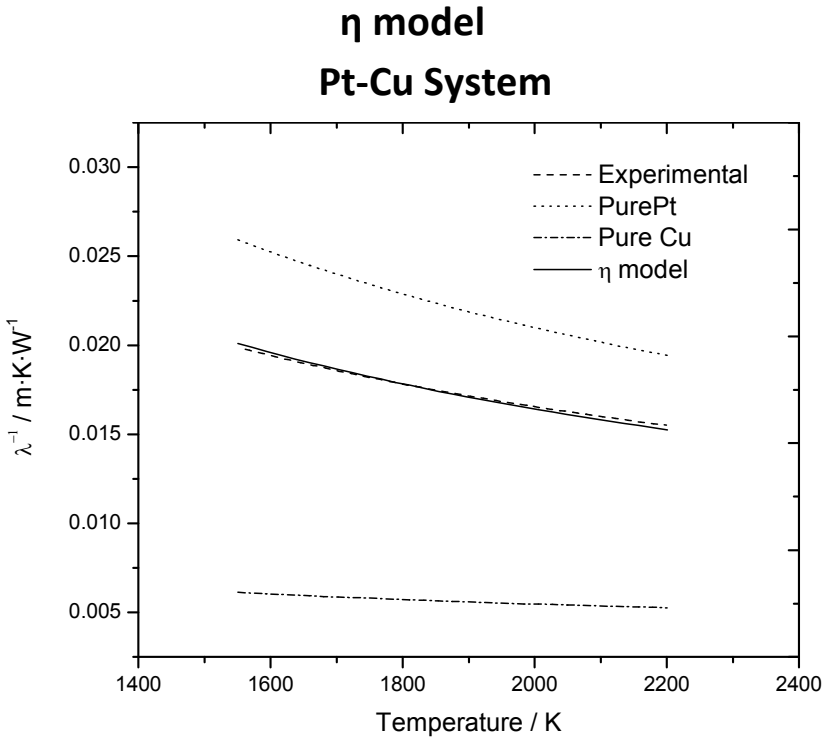

Figure 7.31. Comparison of measured and predicted thermal conductivity values of Pt50Cu50 as a function of temperature along with pure Pt and pure Cu [6, 7].

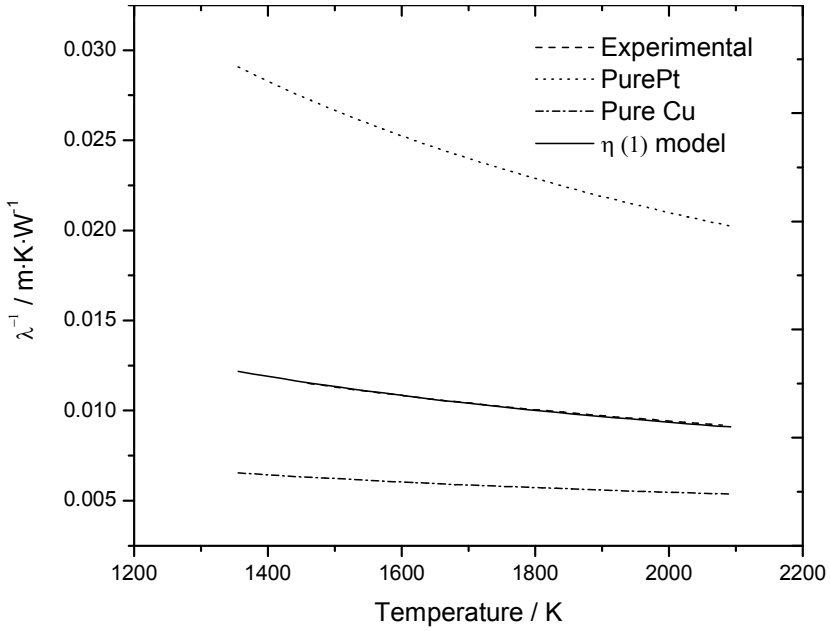

Figure 7.32. Comparison of measured and predicted thermal conductivity values of Pt25Cu75 as a function of temperature along with pure Pt and pure Cu [6, 7].

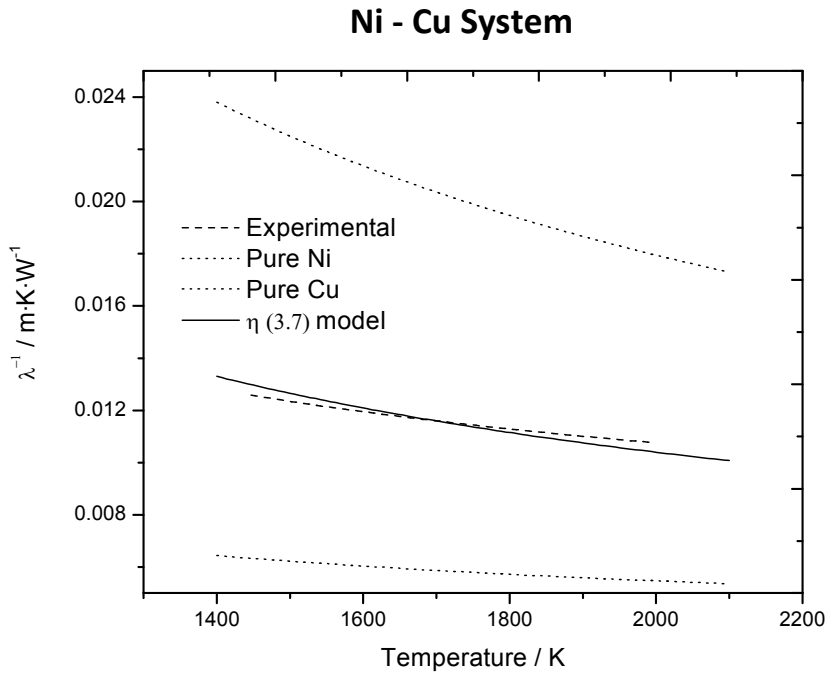

Figure 7.33. Comparison of measured and predicted thermal conductivity values of Ni15Cu85 as a function of temperature along with pure Ni and pure Cu [5-7].

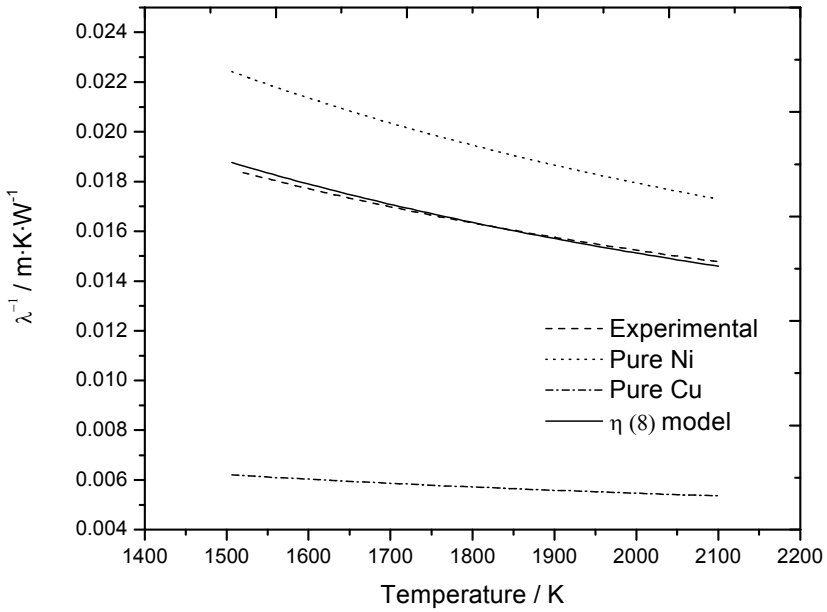

Figure 7.34. Comparison of measured and predicted thermal conductivity values of Ni30Cu70 as a function of temperature along with pure Ni and pure Cu [5-7].

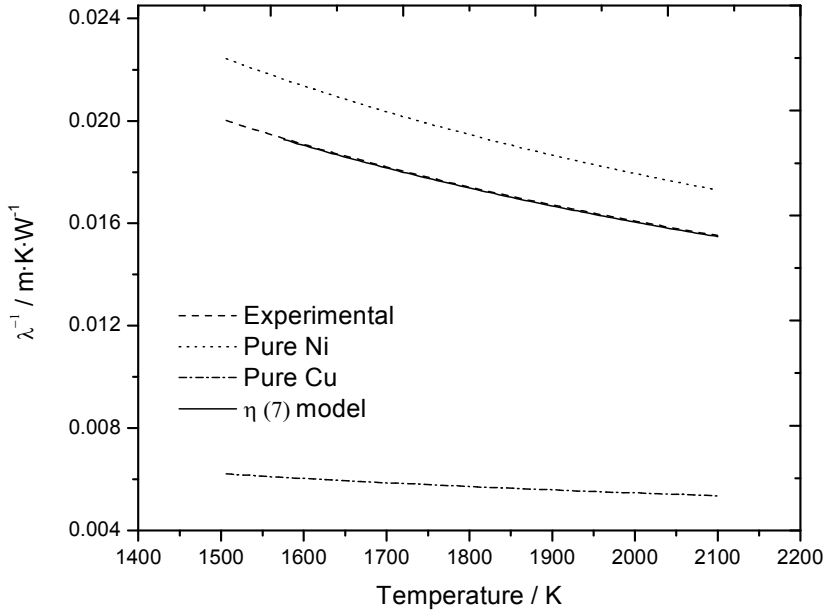

Figure 7.35. Comparison of measured and predicted thermal conductivity values of Ni45Cu55 as a function of temperature along with pure Ni and pure Cu [5-7].

Fe-Ni System

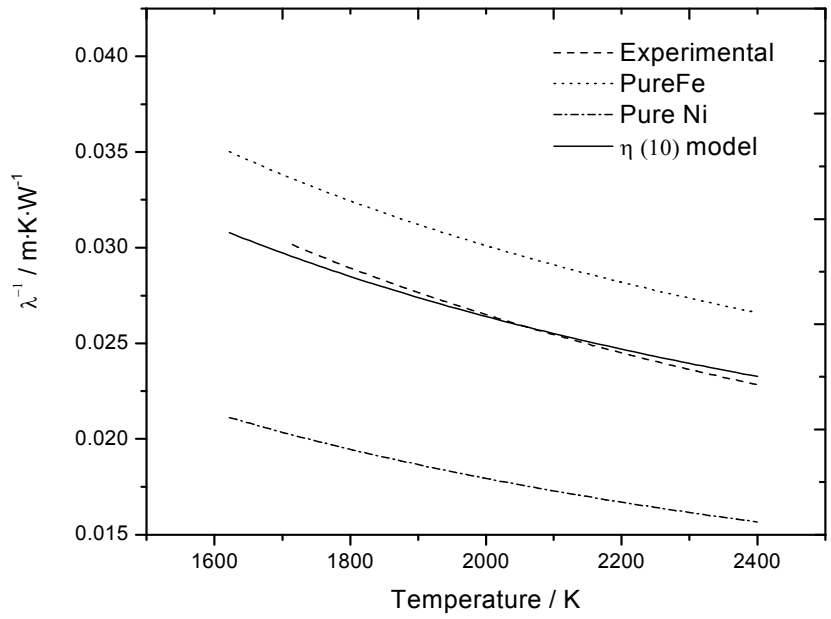

Figure 7.36. Comparison of measured and predicted thermal conductivity values of Fe20Ni80 as a function of temperature along with pure Fe and pure Ni [4, 6].

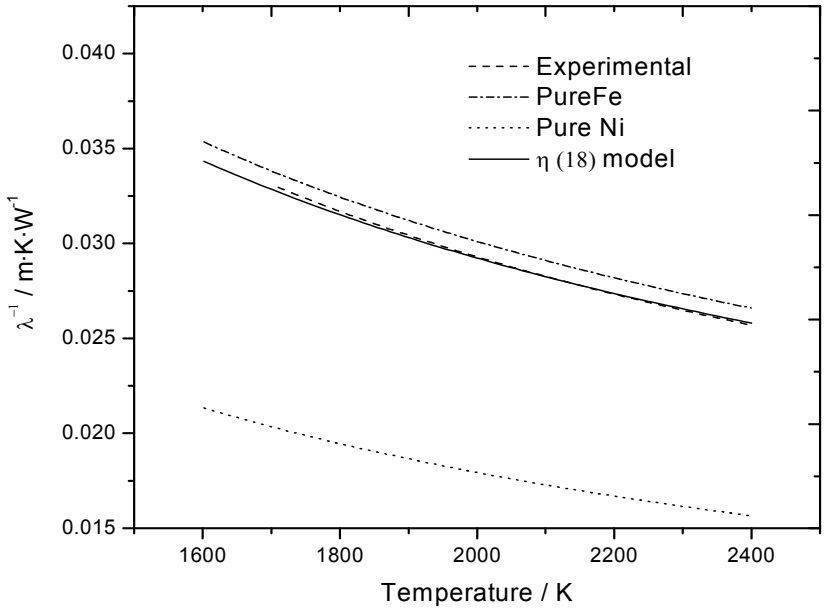

Figure 7.37. Comparison of measured and predicted thermal conductivity values of Fe40Ni60 as a function of temperature along with pure Fe and pure Ni [4, 6].

Conclusion

In this study a step is taken to establish empirical models taking into account experimental data of thermal conductivities of the constituent of binary alloys. To predict the thermal conductivity of alloy samples as a function of temperature previously proposed empirical model (Aurangzeb et al) has been exploited from corresponding liquidus point to several hundreds of Kelvin into the liquid region [1].

All models involve constraints to make them robust. Empirical models used here are as an alternate and they are generally satisfactory for a given suite of the alloy. All the three proposed models give convincing match with the experimental thermal conductivity values. In the case of T_0 - model has more deviation with maximum of 10 % whereas other two models, q and η model, have less deviations with the experimental values within maximum of 5 % and 2 % respectively.

References

[1] Aurangzeb, Mehmood S and Maqsood A, 2008 *Modeling of Effective Thermal Conductivity of Dunite Rocks as a Function of Temperature.* International Journal of Thermophysics, **29**(4): pp 1470-1479.

[2] Robert W Z, 1989 *Thermal conductivity of fluid-saturated rocks.* Journal of Petroleum Science and Engineering, **3**(3): pp 219-227.

[3] Aurangzeb, Ali Z, Gurmani S F and Maqsood A, 2006 *Simultaneous measurement of thermal conductivity, thermal diffusivity and prediction of effective thermal conductivity of porous consolidated igneous rocks at room temperature.* Journal of Physics D-Applied Physics, **39**(17): pp 3876-3881.

[4] Seifter A, Pottlacher G, Jäger H, Groboth G and Kaschnitz E, 1998 *Measurements of thermophysical properties of solid and liquid Fe-Ni alloys.* Berichte der Bunsengesellschaft für physikalische Chemie, **102**(9): pp 1266-1271.

[5] Hüpf T, Cagran C, Kaschnitz E and Pottlacher G, 2010 *Thermophysical Properties of Five Binary Copper-Nickel Alloys.* International Journal of Thermophysics, **31**: pp 966-974.

[6] Wilthan B, Cagran C, and Pottlacher G, 2004 *Combined DSC and Pulse-Heating Measurements of Electrical Resistivity and Enthalpy of Platinum, Iron, and Nickel.* International Journal of Thermophysics, **25**(5): pp 1519-1534.

[7] Cagran C, Seifter A, and Pottlacher G, 2000 Thermophysical properties of solid and liquid copper. Schriften des Forschungszentrums Jülich, Series Energy Technology, **15**: pp763–766.

Chapter 8

Specific Heat Modeling at High Temperature

In this chapter, specific heat values of the three different series of PtCu, CuNi, and FeNi alloys will be discussed from the theoretical point of view. Because we are mainly interested in an ab initio approach to the problem, we concentrate our intentions (i) on the phononic contribution to the specific heat in the harmonic approximation, and (ii) on the contribution of the valence electrons. In both cases, the theoretical quantity to be investigated is usually the specific heat at constant volume c_v, in opposite to the experimental situation where the specific heat at constant pressure is at the center of interest.

For this reason, we cannot expect to achieve a quantitative agreement between our experimental and theoretical results, but we are able to investigate whether or not the tendency of the specific heat of an alloy as a function of the mass contributions of its constituents.

8.1. Platinum-Copper Alloys

The experimental measurements of various alloys of the $Pt_{1-x}Cu_x$ system are investigated theoretically in this section. Experimentally, thermodynamical properties of copper alloys with mass percentage of copper x = 0.04, 0.32, 0.50, and 0.75 for the high-temperature region around the melting points are investigated. In the following Figure 8.1, the least squares (LSQ) evaluation of these data are summarized with respect to the specific heat at constant pressure $c_p(T)$ close below the corresponding solidus points:

For comparison, this figure also contains the values for pure Pt and for pure Cu [1, 2].

The following Table 8.1 shows the temperature regions of the LSQ analysis and the melting temperatures (both in K) of the materials investigated, where $x \in [0, 1]$ indicates the mass percentage of copper, divided by 100:

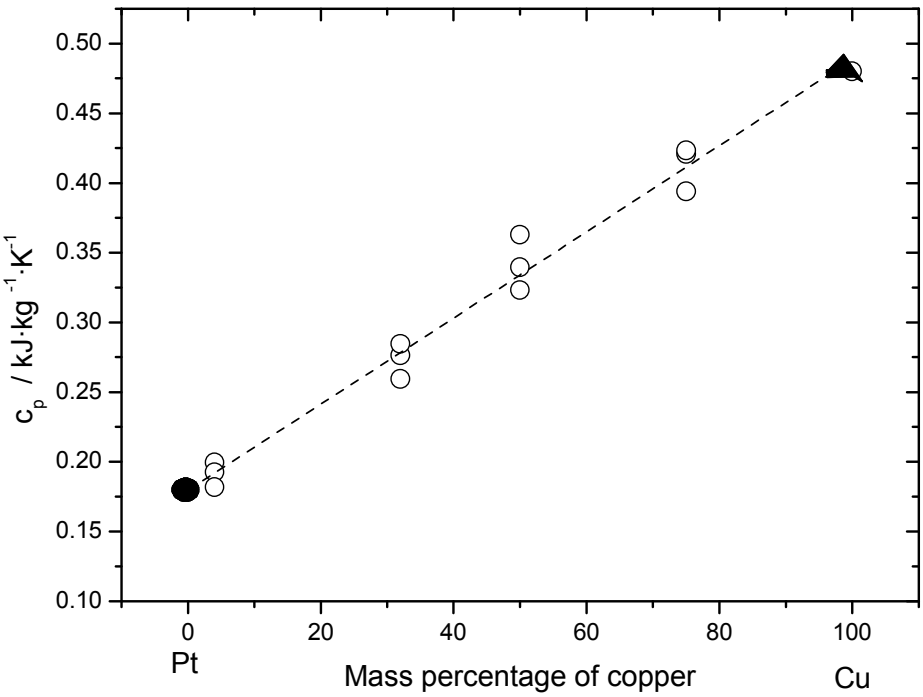

Figure 8.1. Specific heat at constant pressure $c_p(T)$ of copper alloys close below the corresponding solidus points vs. copper mass percentage. Open circle: Experimental values, dashed line: Least square fit, solid circle: Pure platinum, solid triangle: Pure copper [1, 2].

Table 8.1. The temperature regions of the LSQ analysis, the melting temperatures T_M (both in K) of investigated material; x is mass percentage of copper in alloy and c_p specific heat values.

material	x	LSQ region (K)	T_M (K)	c_p / kJ·kg^{-1}·K^{-1} (accord. line)
Pt	0.00	-	2041	0.180
Pt96Cu04	00.04	1450-1950	1953	01.92
Pt68Cu32	00.32	1250-1600	1650	0.276
Pt50Cu50	00.50	1250-1500	1530	0.330
Pt25Cu75	0.75	1150-1400	1450	0.405
Cu	1.00	-	1358	0.480

The experimental values for the alloys PtCu lie in good approximation on the straight line:

$$c_p = 0.180 + 0.300 * x \qquad 0 \leq x \leq 1 \tag{8.1}$$

Where x is mass percent of copper in the composition of alloy. Also in reasonable accordance with Neuman-kopp's rule [3]. As discussed earlier, we can theoretically evaluate the heat capacity at constant volume by using equations (3.16) and (3.19). It has to be noted that all calculations of heat capacities of alloy systems presented in this work are in the high-temperature region far above the Debye and the Einstein temperatures and in case of ferromagnetic constituents, also far above the Curie temperature.

Table 8.2. The melting temperature T_M and Debye temperatures θ_D of pure Pt and pure Cu.

Material	T_M (K)	θ_D (K) [4]
Pt	2041	240
Cu	1358	343.5

Under these circumstances, the heat capacity of the crystal lattices can be theoretically described by Dulong and Petit's formula using equation (3.16)

$$C_v^{DP}(T) = 24.9432\frac{r}{M} \tag{8.2}$$

For binary alloy consisting of 'molecules' with alpha (Pt atoms) and beta (Cu atoms), the above equation changes to

$$C_v^{DP}(T) = 24.9432\frac{r}{\alpha m_{Pt} + \beta m_{Cu}} \tag{8.3}$$

where, $r = \alpha + \beta$, means the number of atoms per unit cell and m_{Pt} and m_{Cu} are the atomic masses of the two constituents. According to equation (3.17), a relation between these quantities and mass percentage of Cu is given by

$$x_{Cu} = \frac{\beta m_{Cu}}{\alpha m_{Pt} + \beta m_{Cu}} \tag{8.4}$$

For typical theoretical models of ordered PtCu alloys, one gets:

Table 8.3. Some parameters representing typical theoretical models. α, β are number of atoms in a molecule, *r* is sum of α and β *and* *x* is value given by equation (8.4).

Molecule	α	β	r	x	x for $m_A = m_B$
A	1	0	1	0	00.00
A_3B	3	1	4	$m_B / (m_B + 3\ m_A)$	00.25
AB	1	1	2	$m_B / (m_A + m_B)$	00.50
AB_3	1	3	4	$3m_B / (3m_B + m_A)$	0.75
B	0	1	1	1	1.00

It is clear that the difference between the *mass* percentage and the *particle percentage* will be significant for alloys with a great difference between m_A and m_B. In this research work, this will especially be the case for the PtCu alloys where m_{Pt} and m_{Cu} amount to 195.08 and 63.546 g, respectively. For this special case, we have the following situation as in Table 8.4 and plotted in Figure 8.2:

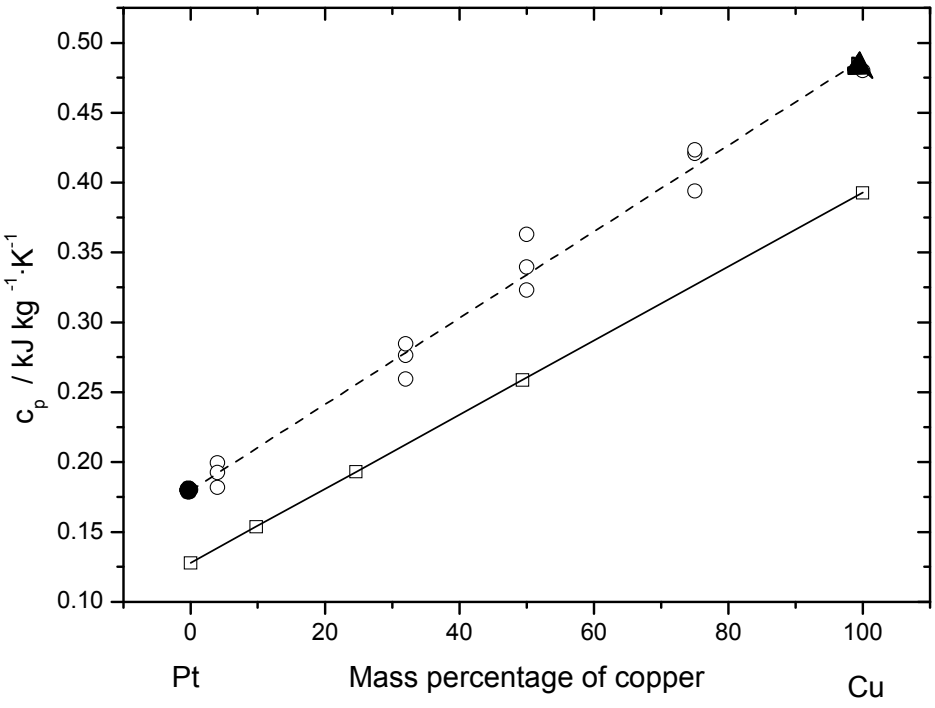

Figure 8.2. Specific heat of PtCu alloys vs. mass percentage of copper, Open circle: Experimental values, dashed line: Least square fit of experimental c_p values, open rectangle: c_v values by using equation (8.2), solid line: Line through open rectangles, solid circle: Pure platinum, solid triangle: Pure copper [1, 2].

Table 8.4. Some parameters representing PtCu alloys. α, β are number of atoms in a molecule, *r* is sum of α and β, *x* is value given by equation (8.4) and c_v is specific heat at constant volume

Molecule	α	β	r	x	$\alpha m_{Pt} + \beta m_{Cu}$/g	c_v / kJ·kg^{-1}·K^{-1}
Pt	1	0	1	0	195.080	0.1279
Pt_3Cu	3	1	4	0.098	648.786	0.1538
PtCu	1	1	2	0.246	258.626	0.1929
$PtCu_3$	1	3	4	0.494	385.718	0.2587
Cu	0	1	1	1	63.546	0.3925

As we already expressed in section 3.2.7, the contribution of the valence electrons to the heat capacity requires the numerical evaluation of the Equations (3.24, 3.25) or the evaluation of the Sommerfeld approximation (3.26).

In order to get the electronic density of states (DOS) of the valence electrons, one has to perform the corresponding band structure calculations. To make this task less complicated, we describe the binary system, PtCu, by its easy-to-handle ordered alloys Pt_3Cu, PtCu, and $PtCu_3$ [5]. The DOS curves, calculated using the FP-LAPW band structure program, are shown in Figure 8.3 [6]. The estimated values of electronic specific heat obtained by the numerical integration of Equation (3.25) and Sommerfeld approximation (3.26) are plotted in Figures 8.4 to Figure 8.8. In the following Table 8.5, *n* means the space group number of the corresponding crystal lattice:

Table 8.5. The ordered PtCu alloys along with mass percentage of copper, lattices, space group *n*, Bohr *a*, density *d* and estimated electronic contribution c^{elec} to specific heat.

Molecule	x	lattice	n	a / Bohr	*d* / kg·m^{-3}	c^{elec} / kJ·kg^{-1}·K^{-1}
Pt	0.000	fcc	225	7.5952	21450	0.0216
Pt_3Cu	0098	sc ($L1_2$)	221	7.4028	18916	0.0237
PtCu	0.246	stetra ($L1_0$)	123	7.2406	15890	0.0218
$PtCu_3$	0.494	sc ($L1_2$)	221	7.0575	12560	0.0167
Cu	1.000	fcc	225	6.8585	8960	0.0138

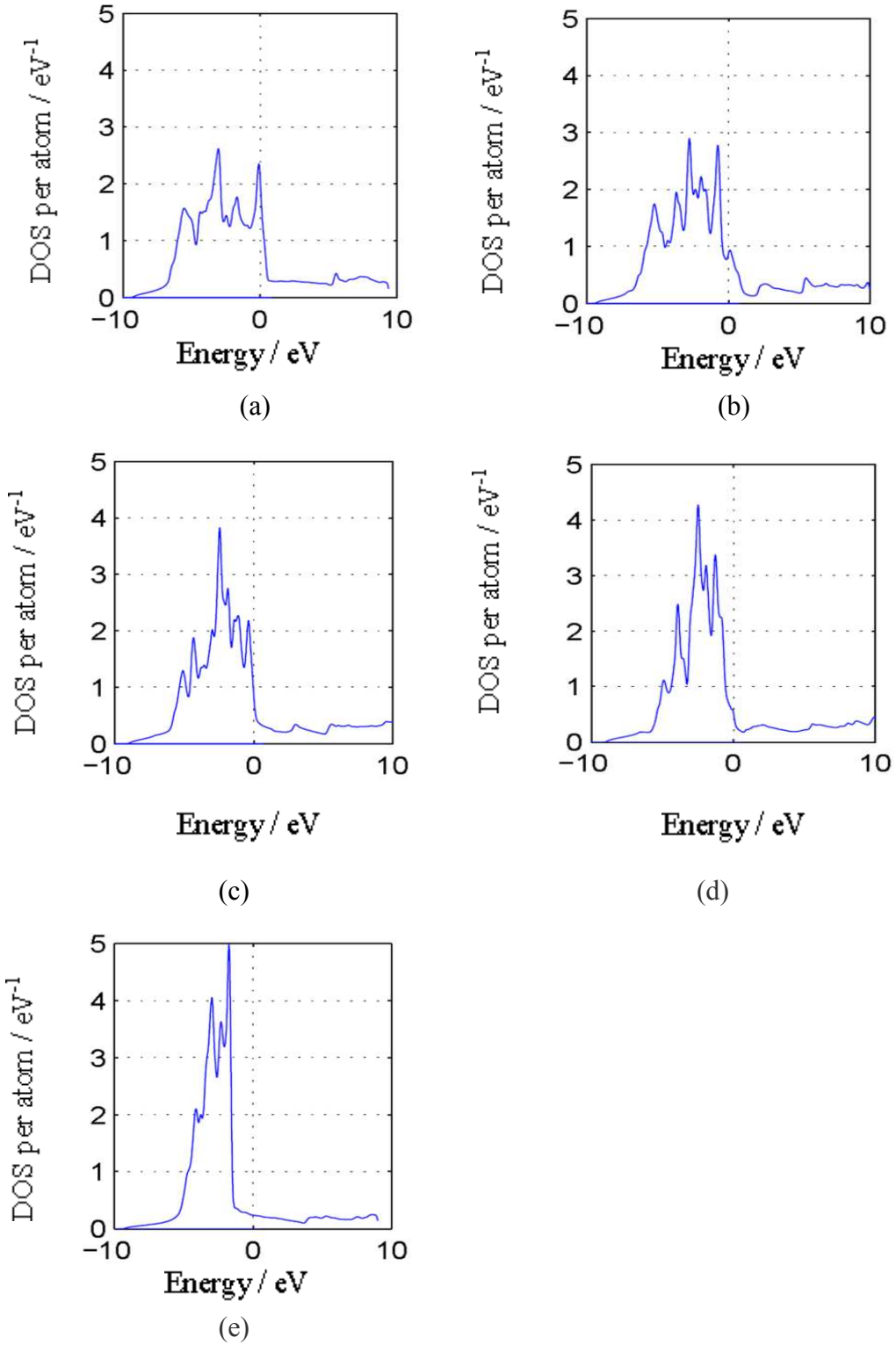

Figure 8.3. Density of state curves (a) Pt (b) Pt_3Cu (c) PtCu (d) $PtCu_3$ (e) Cu.

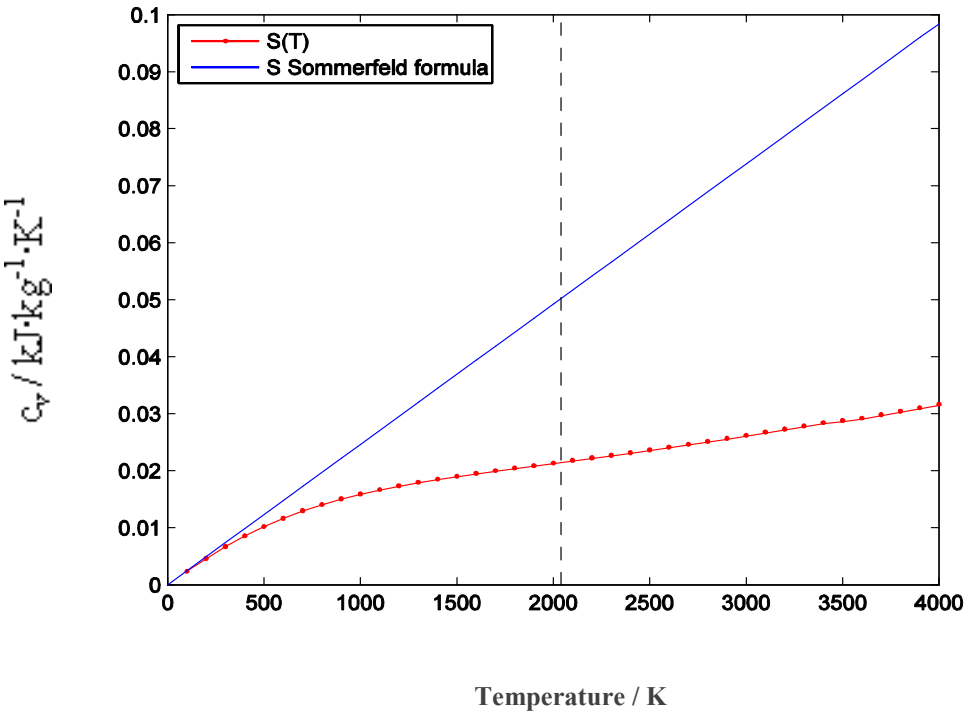

Figure 8.4: Heat capacity of Pt by valence electron using equation (3.25), red curves, and by Sommerfeld approximation equation (3.26), blue curve.

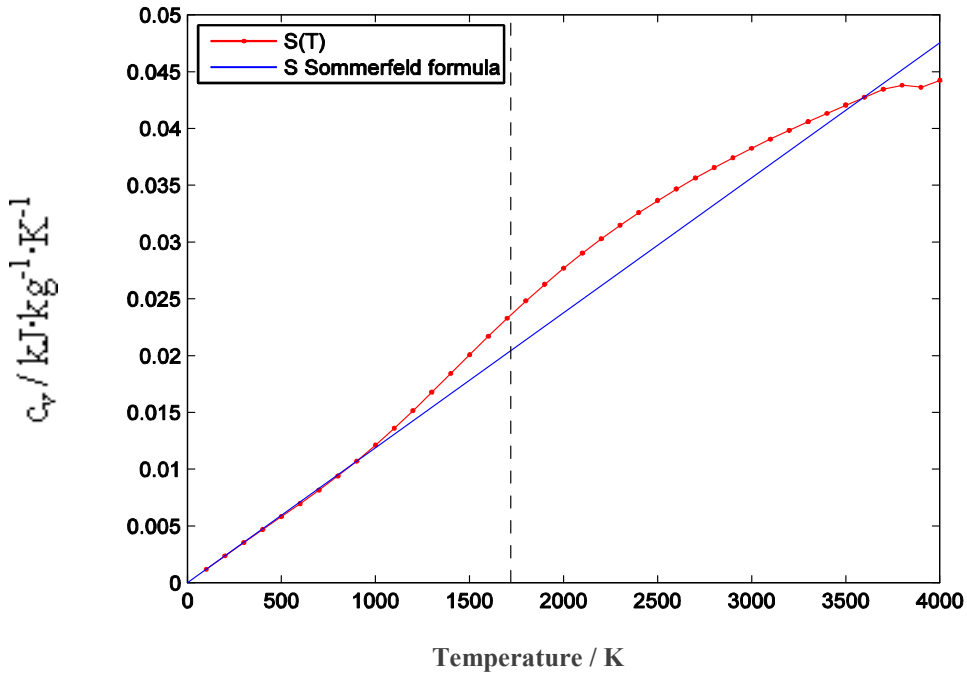

Figure 8.5. Heat capacity of valence electron in Pt_3Cu using equation (3.25), red curve, and by Sommerfeld approximation equation (3.26), blue curve.

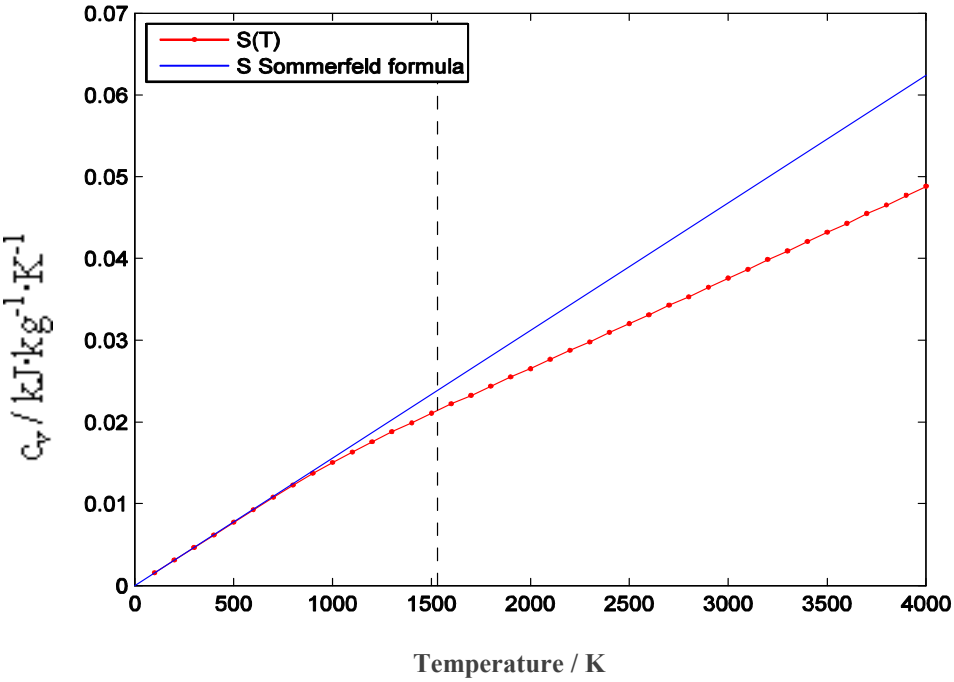

Figure 8.6. Heat capacity of valence electron in PtCu using equation (3.25), red curve, and by Sommerfeld approximation equation (3.26), blue curve.

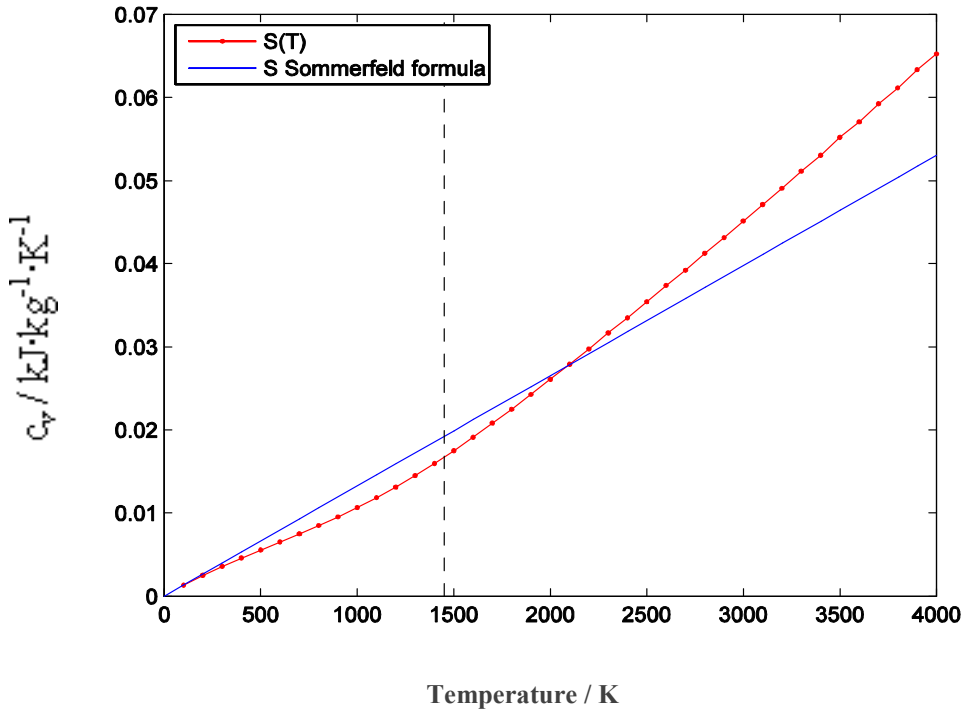

Figure 8.7. Heat capacity of valence electron in $PtCu_3$ using equation (3.25), red curve, and by Sommerfeld approximation equation (3.26), blue curve.

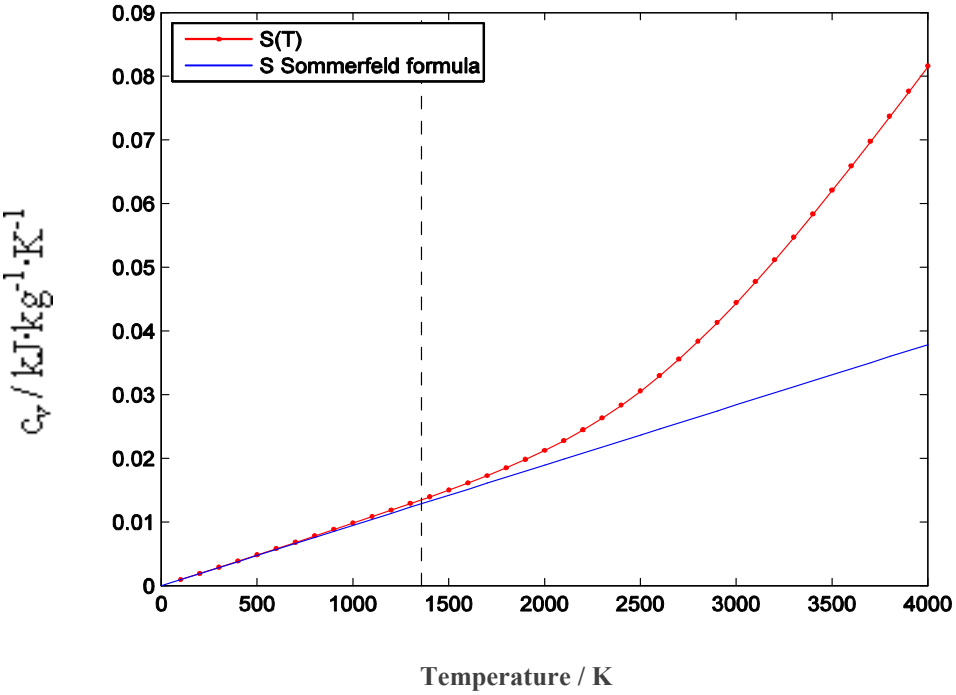

Figure 8.8. Heat capacity of valence electron in Cu using equation (3.25), red curve, and by Sommerfeld approximation equation (3.26), blue curve.

For almost all materials under investigation - for temperatures close to the melting points, the simple Sommerfeld formula (3.26) that only includes the DOS value at the Fermi energy is a rather good approximation for the heat capacity due to the valence electrons. The only exception is pure platinum where (at the melting temperature of 2041 K) the Sommerfeld formula gives an electron contribution to the heat capacity ($\approx 0.05 kJ \cdot kg^{-1} \cdot K^{-1}$) which is more than twice as big as the corresponding value obtained by a numerical evaluation of the integral (3.25) ($\approx 0.02\ kJ \cdot kg^{-1} \cdot K^{-1}$).The values of c^{el} at $T = T_{M,}$ taken from the exact integral (3.25), can be found in the last column of the Table 8.5.

The following Figure 8.9 summarizes the experimentally determined c_p results, the theoretically obtained c_v values of the lattice contribution, solid line, and the sum of lattice contribution and the corresponding valence electrons contribution, dotted line. As one can see, the electronic term goes into the right direction, i.e., it reduces the gap between the theoretical and the measured values of the specific heat. Nevertheless, the difference between theory and experiment remains rather large. It is clear that a great part

of disagreement between experiment and theory comes from the fact that the measured data are c_p values (= constant pressure), and the theoretical results are c_v values (= constant volume). As already discussed by equation (3.11), this difference is mainly dedicated to anharmonic lattice vibrations which play a great role in our investigation and will be studied carefully in the immediate future.

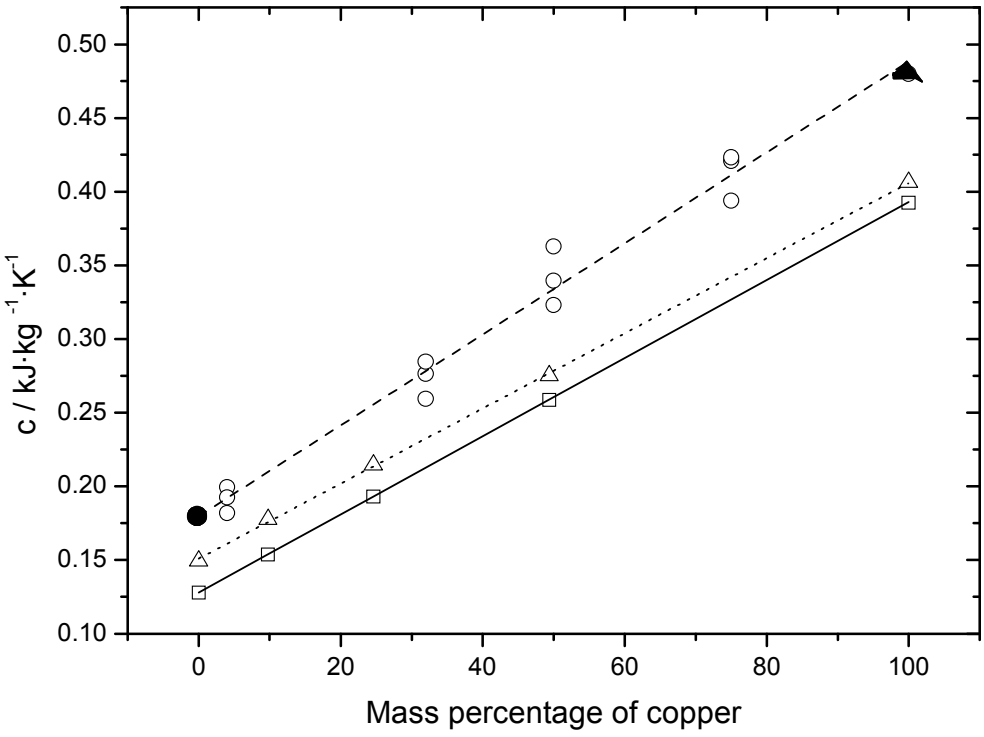

Figure 8.9. Specific heat of PtCu alloys vs. mass percentage of copper, open circle: Experimental c_p values, dashed line: Least square fit of experimental c_p values, open rectangle: Theoretically obtained c_v values of the lattice contribution, solid line: Least square fit of the lattice contribution, open triangle: Sum of lattice and the corresponding valence electrons contribution, dotted line: Least square fit of lattice and the corresponding valence electrons contribution.

8.2. Copper-Nickel Alloys

In this section, a series of alloys of the Cu_{1-x} Ni_x system is investigated. From the experimental side, we use enthalpy data of alloys with x = 0.15, 0.30, 0.45, 0.65, and 0.80, measured within the temperature region close to the melting points [7].In the following Figure, the LSQ evaluation are summarized of these data with respect to the specific heat at constant pressure $c_p\,(T)$ for $T \approx T_M$.

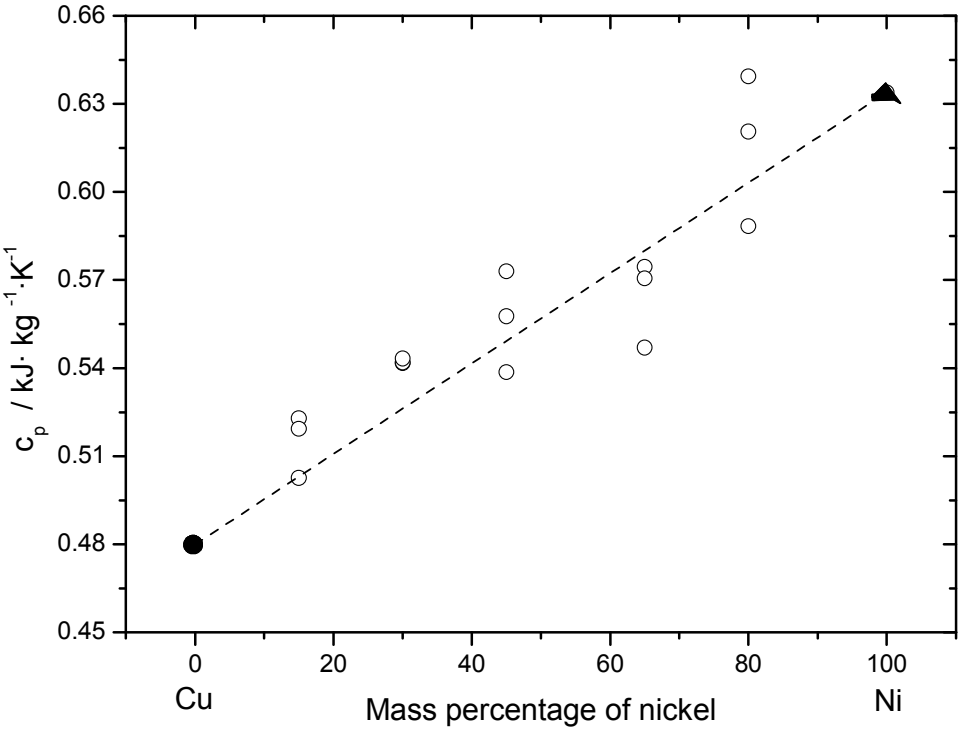

Figure 8.10. Specific heat at constant pressure $c_p(T)$ of CuNi alloys close below their corresponding solidus points vs. mass percentage of nickel. Open circle: Experimental c_p values, dashed line: Least square fit of experimental values, solid circle: Pure copper, solid triangle: Pure nickel.

The open circles in the above Figure show the c_p values, obtained by least-squares evaluations of the given enthalpy data [7]. Their mean values are given by the dashed line with the corresponding c_p values of pure copper and nickel.

Taking into account the relatively large uncertainties of the experimental data, one can say that the Neumann-Kopp rule is at least approximately fulfilled.

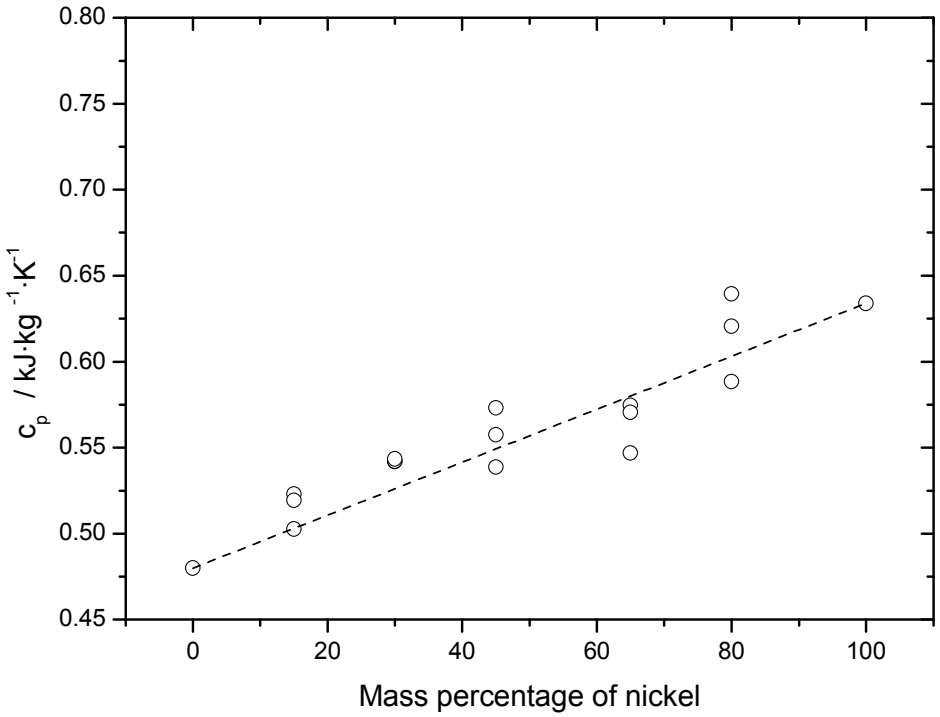

Figure 8.11. Specific heat at constant pressure $c_p(T)$ of CuNi alloys close below the corresponding melting points vs. Nickel mass percentage in same scale as that of PtCu system.

In order to allow a direct comparison of the CuNi alloys with the results PtCu of the previous section, the Figure 8.11 above shows the results for CuNi the at the same scale as in the case PtCu. The following Table 8.6 shows the temperature region of the LSQ analysis, the melting temperature (in K), average values of c_p by LSQ and their literature values of the investigated materials:

Table 8.6. The temperature region of the LSQ analysis, melting temperature T_m and c_p values of the investigated materials [7].

Material	LSQ region (K)	T_M (K)	c_p / kJ·kg^{-1}·K^{-1} (dashed line)
Cu	-	1358	
Cu85Ni15	1100-1417	1432	0.515
Cu70Ni30	1100-1472	1496	0.542
Cu55Ni45	1100-1528	1552	0.556
Cu35Ni64	1100-1599	1619	0.564
Cu20Ni80	1100-1656	1667	0.616
Ni	-	1728	

In order to properly compare the Dulong-Petit values for the materials, one has to evaluate a formula equivalent to Equation (8.5) but with $m_{Cu} = 63.55$ g and $m_{Ni} = 58.69$ g:

$$C_v^{DP}\left[Cu_{1-x}Ni_x\right] = 24.9432\left[\frac{1-x}{m_{Cu}} + \frac{x}{m_{Ni}}\right] \tag{8.5}$$

What concerns the contribution of the valence electrons to the specific heat for the PtCu alloys, the situation is in contrary to the PtCu alloys somewhat more complicated. The CuNi alloys do not build ordered crystalline structures but realize so-called disordered alloys [8]. Consequently, the corresponding density of states cannot be yielded by conventional band-structure calculations. For such systems, it would be necessary to use the so called coherent potential approximation. For this reason, we discuss the electronic part of the specific heat of CuNi alloys by assuming a linear connection between the values of $c^{el}(T_M)$ for pure Cu and pure Ni. The DOS profiles of Ni, calculated by WIEN2k are shown in Figures 8.12 [6]. The corresponding functions of $c^{el}(T)$, both obtained by evaluations of the integral (3.25) (red curves) and of the Sommerfeld formula (3.26) (blue curves), are shown in the following Figures 8.13.

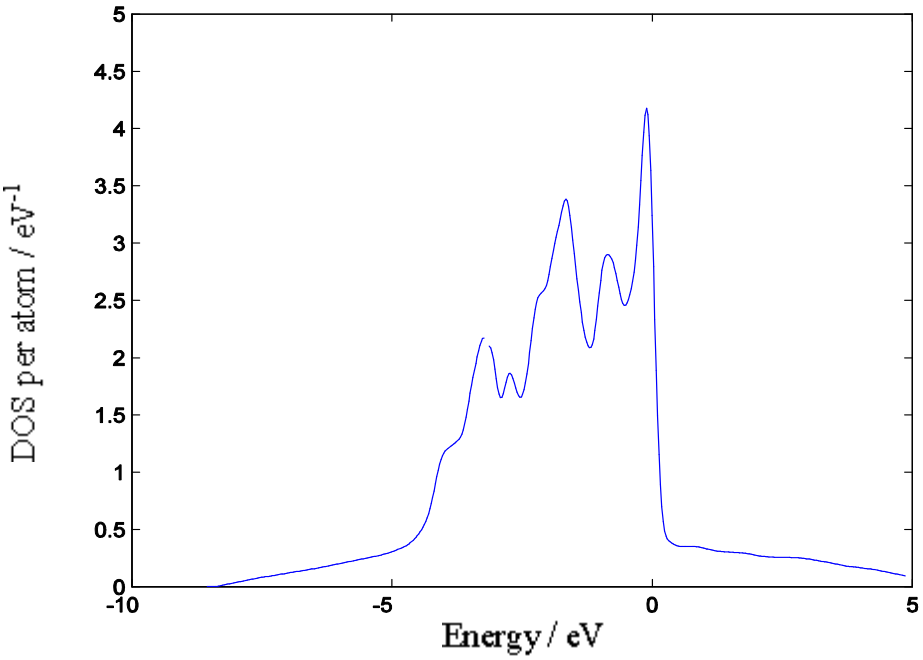

Figure 8.12. Density of state curve for pure Ni.

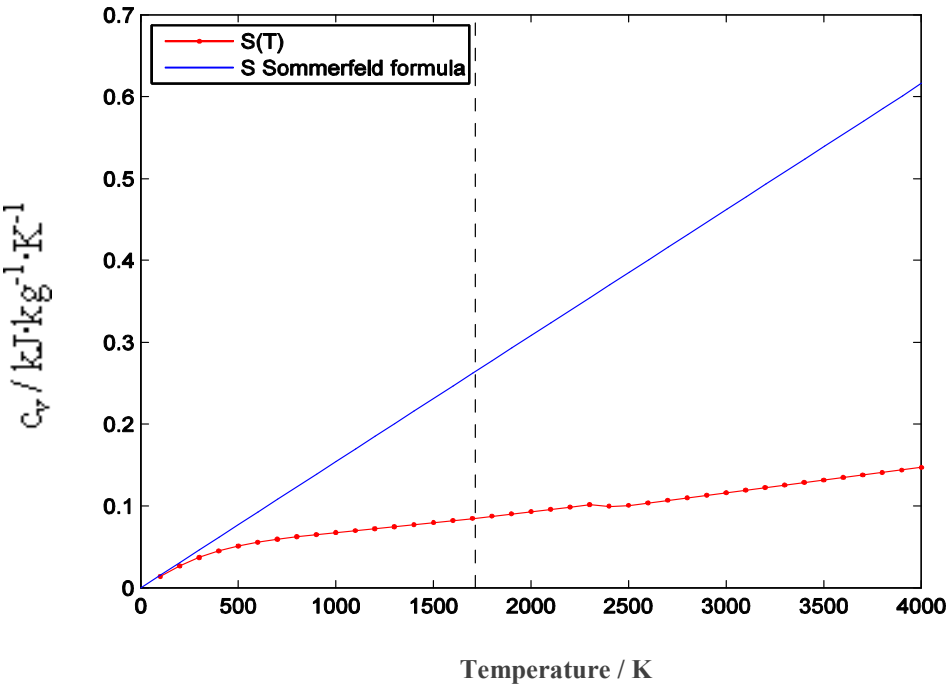

Figure 8.13. Heat capacity of valence electron in Ni using equation (3.25), red curve, and by Sommerfeld approximation equation (3.26), blue curve.

As it has been already discussed, Cu is an example where the Sommerfeld formula gives for T_M almost perfect result for the heat capacity of the valence electrons: $c^{el}(T_M) = 0.0140\ kJ \cdot kg^{-1} \cdot K^{-1}$. This is by no means the case for the typical (3d) transition metal Ni where the Sommerfeld formula exaggerate the heat capacity at $T_M = 1728$ K by nearly a factor of 3. A numerical evaluation of the integral (3.25) obtains $c^{el}(T^M) = 0.085\ kJ \cdot kg^{-1} \cdot K^{-1}$. In the next Figure 8.14, the results of this section are summarized: the experimental c_p data are the same discussed before, the solid line means the Dulong-Petit curve of the CuNi system, and the dotted line marks the sum over the harmonic lattice contribution and the valence electron contribution to c_v:

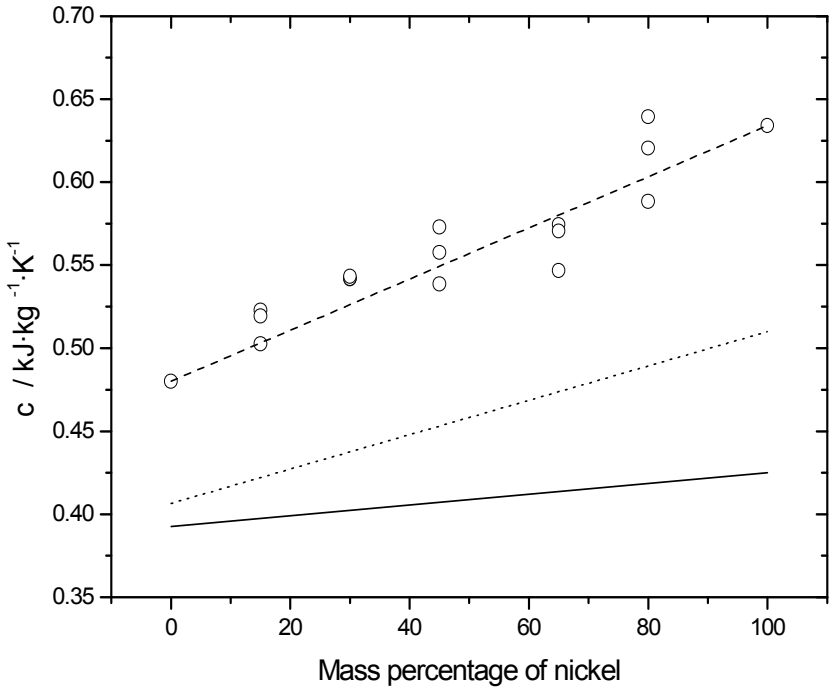

Figure 8.14. Specific heat at constant pressure c_p vs. Nickel mass percentage. Open circle: Experimental c_p values, dashed line: Least square fit of experimental values. Solid line: Theoretically obtained c_v values of the lattice contribution, dotted line: Sum of lattice contribution and the corresponding valence electrons contribution.

Here it is obvious that the inclusion of the electron contribution significantly improves the performance of the theoretical results. There is a relatively good agreement of the slopes of the dotted line and of the black dashed line, which connect the c_p and c_v values of pure Cu and pure Ni and this agreement quite convincingly describes the tendency of

the alloys. The absolute difference between the experimental values c_p and the theoretical results c_v is, probably, due to anharmonic lattice effects.

8.3. Iron -Nickel Alloys

From the theoretical point of view, the experimental results concerning the specific heat of a series of Ni_xFe_{1-x} alloys is quite strange, especially if one looks at the c_p values of pure Ni and Fe and their relation to FeNi alloys [9, 10]:

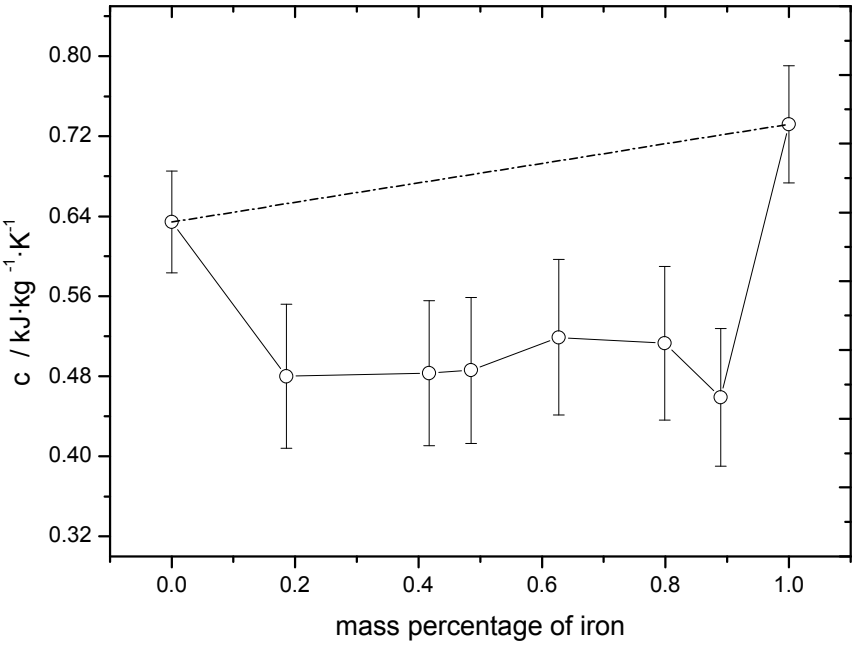

Figure 8.15. Specific heat at constant pressure $c_p(T)$ of FeNi alloys close below the corresponding solidus points vs. iron mass percentage.

For the two examples of binary alloys (PtCu and CuNi) discussed in the previous sections, we observed an almost perfect (PtCu, see Figure 8.1) or at least approximately (CuNi, see Figure 8.10) fulfillment of the Neumann-Kopp rule [3]. This is by no means the case for FeNi alloys, as it can be seen in the Figure 8.15 where the dashed-dotted line corresponds to Neumann-Kopp rule:

$$c_p(x) = (1-x)c_p\,(Ni) + xc_p(Fe) \qquad 0 \leq x \leq 1 \tag{8.6}$$

Where x is mass percent of iron in the composition of alloy. The experimentally determined c_p values of the alloys are rather well described by an almost constant behavior (if the large experimental error bars are taken into account) around roughly 0.5 $kJ \cdot kg^{-1} \cdot K^{-1}$. However, for x → 0 and x → 100, this line-up switches to the corresponding values of the pure metals Ni and Fe. This effect stays so efficient that if one takes into account the experimental errors of the c_p which are reported to be 8 percent for the pure metals and 15 percent for the alloys [9, 10].

Table 8.7. The temperature region of the LSQ analysis, *d* density, *x* is mass percent of iron and c_p is specific heat capacity at constant pressure [9, 10].

Material	x(Fe)	LSQ region / K	d /kg·m $^{-3}$	c_p / $kJ \cdot kg^{-1} \cdot K^{-1}$
Ni	0.000	1200 - 1715	8902	0.6344
FeNi alloy	0.186	1200 - 1712	8734	0.480
FeNi alloy	0.417	1200 - 1707	8583	0.483
FeNi alloy	0.485	1200 - 1709	8328	0.486
FeNi alloy	0.627	1200 - 1717	8000	0.519
FeNi alloy	0.799	1200 - 1740	8038	0.513
FeNi alloy	0.890	1200 - 1763	8150	0.459
Fe	1.000	1420 - 1790	7874	0.732

The calculations of the c_v^{DP} values for the (theoretical) test crystals of $FeNi_3$, FeNi, Fe_3Ni and Fe, have been done using the following relation:

$$C_v^{DP}(T) = 24.9432 \frac{\alpha + \beta}{\alpha m_{Ni} + \beta m_{Fe}} \tag{8.7}$$

with m_{Ni} = 58.6934 g and m_{Fe} = 55 847 g, respectively, gives the results as shown in Table 8.8. The values then obtained by Dulong-Petit presented in the Figure 8.21. Now for the part of electronic specific heat of the FeNi series which again starts with band structure and DOS calculations:

. **Table 8.8.** Some parameters representing FeNi alloys. α, β are number of atoms in a molecule, *r* is sum of α and β, *x* is value by equation (8.4) and c_v^{DP} is specific heat at constant volume by equation (8.7)

Molecule	α	β	r	x (Fe)	$\alpha m_{Ni} + \beta m_{Fe}$ (g)	c_v^{DP} / kJ·kg^{-1}·K^{-1}
Ni	1	0	1	0	58.6934	0.4250
Ni3Fe	3	1	4	0.2408	231.9272	0.4302
NiFe	1	1	2	0.4876	114.5404	0.4355
NiFe3	1	3	4	0.7406	226.2344	0.4410
Fe	0	1	1	1	55.8470	0.4466

Table 8.9. The ordered FeNi alloys along with mass percentage of copper, lattices, space group *n*, Bohr *a*, density *d* and estimated electronic contribution c^{elec} to specific heat.

Alloy	x(Fe)	lattice	n	a / Bohr	d /kg·m^{-3}	c^{el}, / kJ·kg^{-1}·K^{-1}
Ni	0	fcc	225	6.7000	8902	0.0847
Ni_3Fe	0.2408	sc ($L1_2$)	221	6.6012	8700	0.1198
NiFe	0.4876	($L1_0$)*	123	6.6357	8327	0.1347
$NiFe_3$	0.7406	sc ($L1_2$)	221	6.6101	8025	0.1477
Fe	1	bcc	225	5.4200	7874	0.1795

The DOS curves, calculated using the FP-LAPW band structure program WIEN2k [6], are shown in Figure 8.16. It is, of course, no surprise that the DOS of all materials investigated in this section are dominated by the 3d electrons of Ni and Fe. It is interesting to observe that the pure metals show a somewhat narrower distribution than the three alloys $FeNi_3$, FeNi and Fe_3Ni.Using the DOS curves, there is no problem to calculate the electronic part of the specific heat (at constant volume) of all members of the NiFe series by using the equation (3.25) and (3.26). It is clearly to be seen that, in all cases, the Sommerfeld result significantly over estimates c^{el}_v. The results obtained by numerical evaluations of the integral in equation (3.25) are given in the last column of the Table 8.9.

The following Figures 8.17 to 8.20 are showing c^{el}(T) for Ni, Ni_3Fe, NiFe, $NiFe_3$, and Fe. The red curves are the results obtained by the numerical integration of

equation (3.25), and the blue ones belong to the Sommerfeld approximation equation (3.26).

In fact, we observe a strong contradiction to our results shown in Figs. 8.4 to 8.8 for the PtCu series: for all those materials (except pure Pt), the Sommerfeld formula (3.26) did a remarkable good job. However, the Figs. 8.17 to 8.20 show very significant deviations of the Sommerfeld result in comparison to the exact numerical integration (3.25) for all members of the FeNi family. These strong differences are shown in the following table:

Table 8.10. Comparison of the electronic contribution to the specific heat, calculated by using the exact integration (3.25) or the Sommerfeld formula (3.26).

Alloy	**c / kJ·kg^{-1}·K^{-1}**	
	Exact integral Eq. (3.25)	**Sommerfeld formula (3.26)**
Ni	0.085	0.267
$FeNi_3$	0.120	0.186
FeNi	0.135	0.206
Fe_3Ni	0.148	0.168
Fe	0.180	0.276

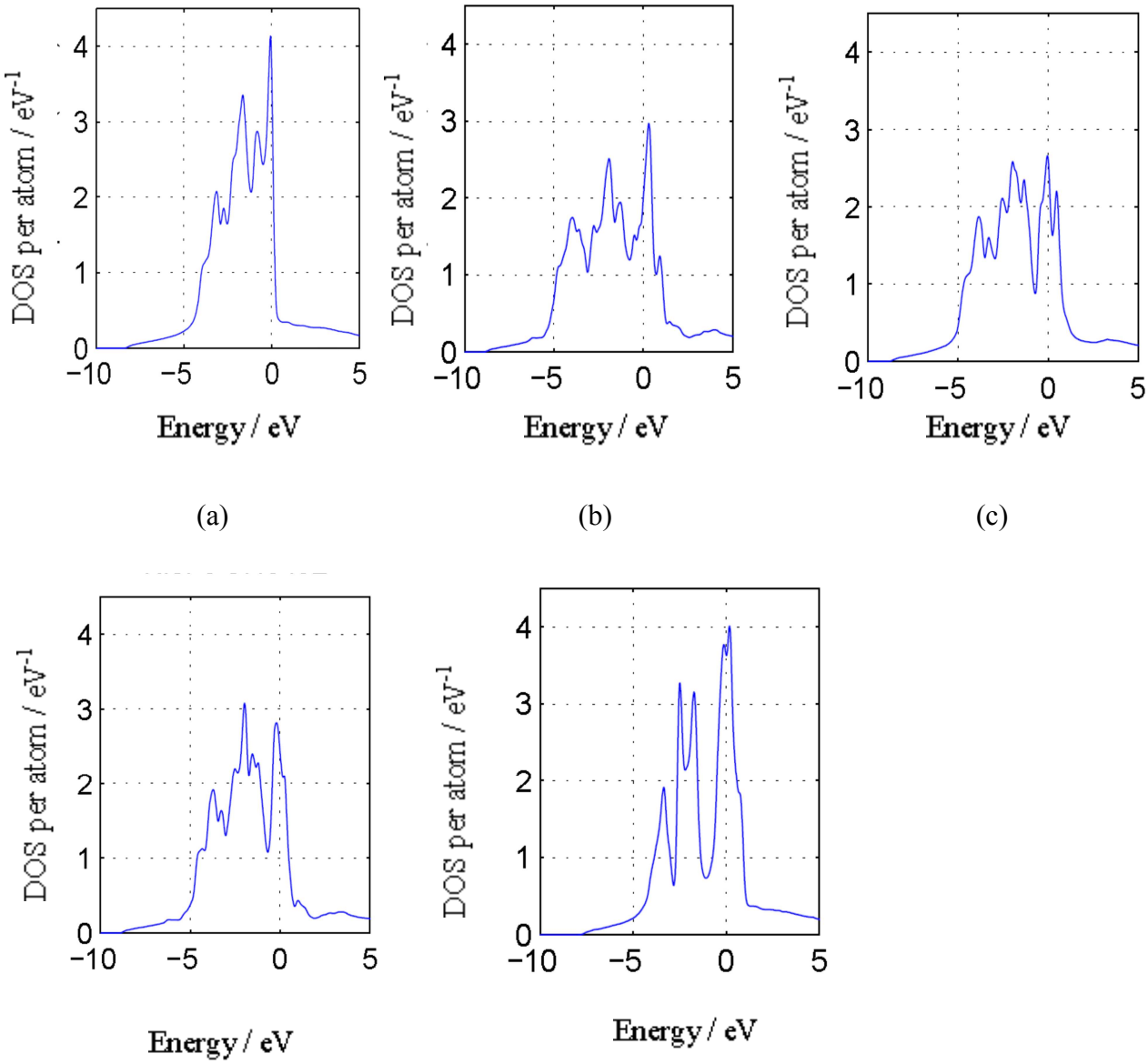

Figure 8.16. Density of state curves (a) Ni (b) $FeNi_3$ (c) NiFe (d) Fe_3Ni (e) Fe.

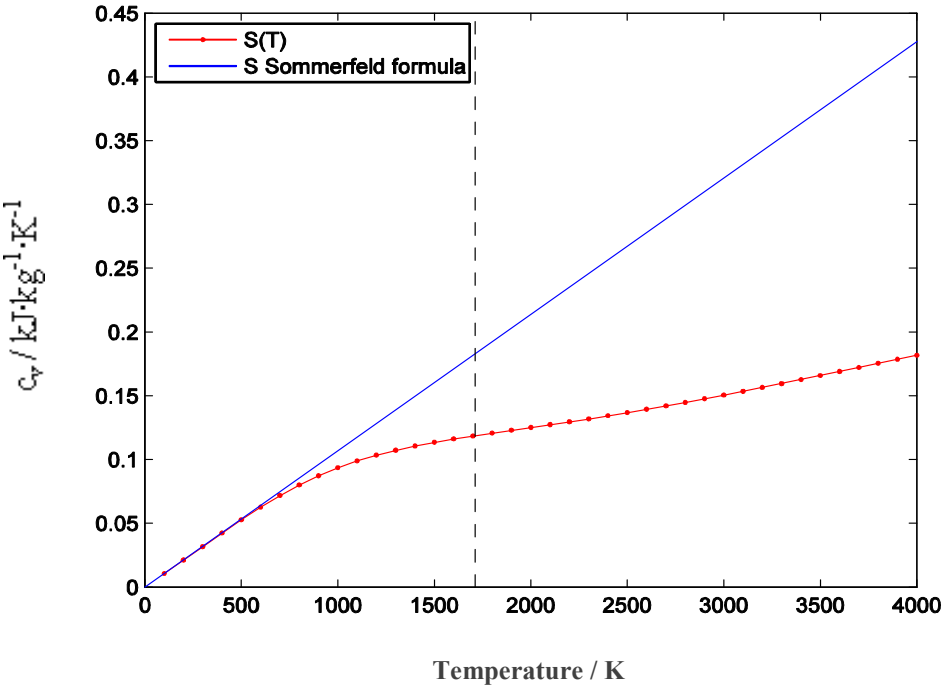

Figure 8.17. Heat capacity of valence electron in Ni_3Fe using equation (3.25), red curve, and by Sommerfeld approximation equation (3.26), blue curve.

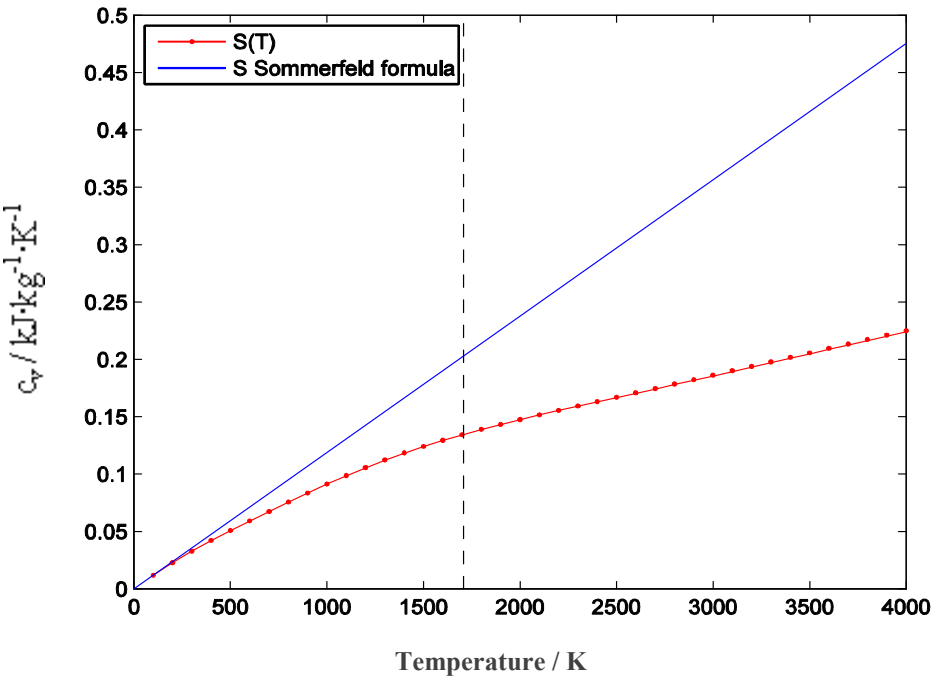

Figure 8.18. Heat capacity of valence electron in NiFe using equation (3.25), red curve, and by Sommerfeld approximation equation (3.26), blue curve.

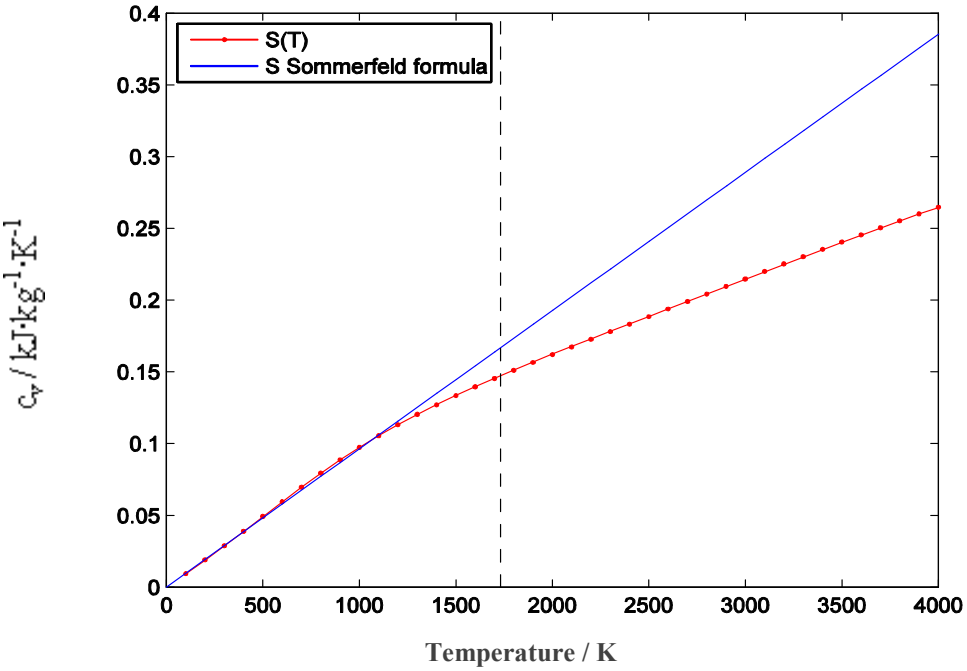

Figure 8.19. Heat capacity of valence electron in $NiFe_3$ using equation (3.25), red curve, and by Sommerfeld approximation equation (3.26), blue curve.

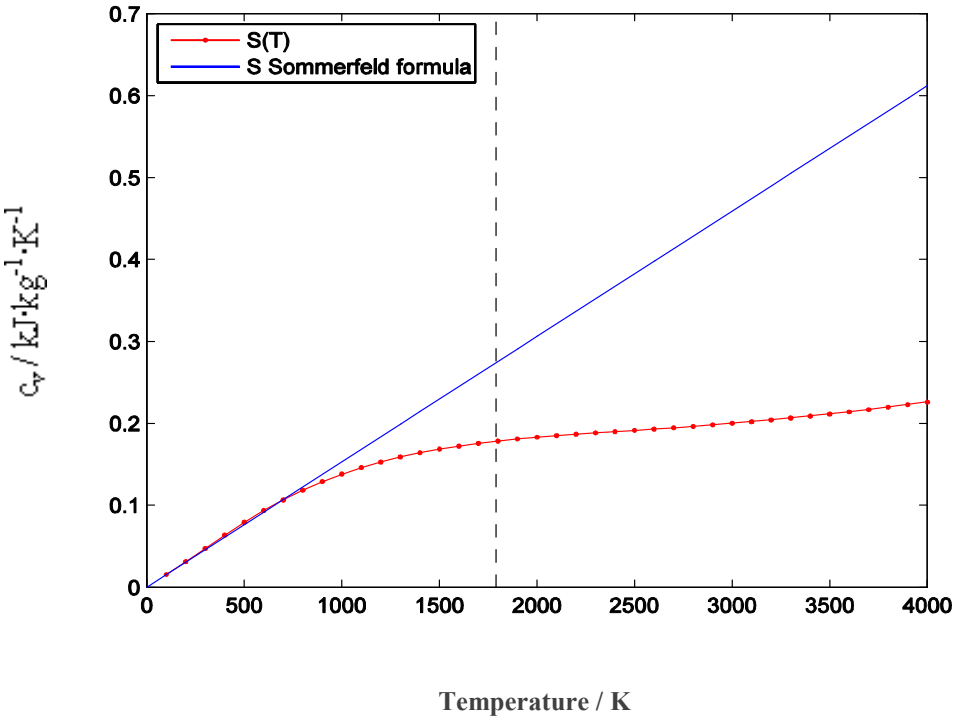

Figure 8.20. Heat capacity of valence electron in Fe using equation (3.25), red curve, and by Sommerfeld approximation equation (3.26), blue curve.

The following Figure shows a summary of the experimental and theoretical results of FeNi. As we argued at the beginning of this section of the NiFe series, the theory is not able to properly describe the relatively complicated profile of the measured c_p values. In fact, the sum of the Dulong-Petit and the electron parts of c_v give a kind of mean value through the experimental points.

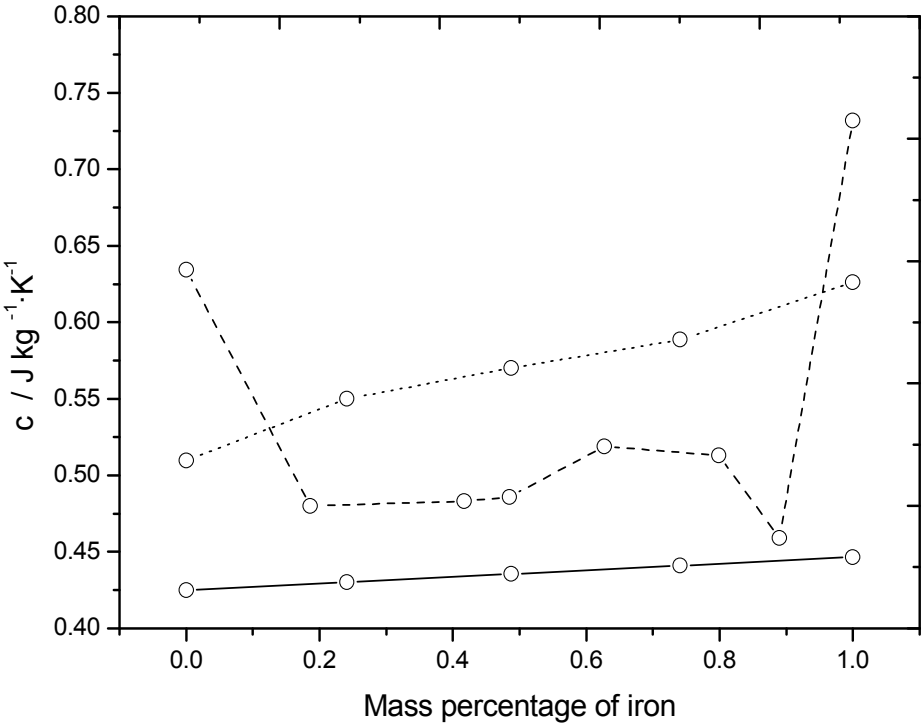

Figure 8.21. Specific heat at constant pressure c_p of FeNi vs. iron mass percentage. Dashed line Solid line: Experimental c_p values, solid line: Theoretically obtained c_v values of the lattice contribution, dotted line: Sum of lattice contribution and the corresponding valence electrons contribution.

Conclusions

Summarizing the discussions in the previous subsections on series of PtCu, CuNi, and FeNi alloys, we found a significantly different behaviour of the PtCu and the FeNi series: In the PtCu case, both the experimentally and theoretically obtained values of the heat capacity show a more or less convincing linear relation between c_p (experiment) and c_v (theory) and the mass percentage of one of the constituents, i.e., the Neumann-Kopp rule is reasonable fulfilled. Apart from the difference c_p - c_v which is mainly due to anharmonic lattice effects, the (qualitative) agreement between the experimental and theoretical curves is satisfying. Theoretically, one observes a dominant "harmonic-lattice" contribution to c_v, much larger than the relatively small contribution of the valence electrons.

The FeNi case shows a completely different and somewhat irritating behaviour (see Figures. 8.15 and 8.20): The experiments show more or less (note the relatively large uncertainty bars) constant c_p values (around 0.50 $kJ \cdot kg^{-1} \cdot K^{-1}$) for the alloys, in very strong contradiction to the two pure metals Ni (0.64 $kJ \cdot kg^{-1} \cdot K^{-1}$) and Fe (0.73 $kJ \cdot kg^{-1} \cdot K^{-1}$). That means, for this series, the Neumann-Kopp rule is completely out of the game. This behaviour is, however, not at all reflected by our theoretical results which appear quite Neumann-Kopp-like. It is also interesting to observe that - for FeNi - the contribution due to the valence electrons is much larger than it was the case for PtCu.

What concerns the series of CuNi alloys discussed in Section 8.2, these materials show, from the experimental point of view, a similar behaviour as PtCu, namely, an approximate Neumann-Kopp characteristic (compare Figures 8.10, 8.11). Due to the non-existence of ordered CuNi crystals, we were not able to do c_v calculations for these alloys, but our results for pure Cu and pure Ni lead to the rather satisfying theoretical results shown in Figure 8.14: The harmonic-lattice contribution to c_v is far away from the experimental curve. However, an inclusion of our band-structure based results for the valence electrons leads (i) to a significant reduction of the difference between the c_p and c_v curve and (ii) to a steeper theoretical curve which is (almost) parallel to the experimental result.

References

[1] Wilthan B, Cagran C, and Pottlacher G, 2004 *Combined DSC and Pulse-Heating Measurements of Electrical Resistivity and Enthalpy of Platinum, Iron, and Nickel.* International Journal of Thermophysics,. **25**(5): pp 1519-1534.

[2] Cagran C, Seifter A, and Pottlacher G, 2000*Thermophysical properties of solid and liquid copper*, Schriften des Forschungszentrums J¨ulich, Series Energy Technology **15**: pp 763.

[3] Cezairliyan A and McClure J M, 1973 Journal of Research **78**, 1.

[4] Kittel C, 1996 *Introduction to Solid State Physics*, New York: John Wiley and Sons, 7th edn.

[5] Takizawa S, and Terakura K, 1989 Journal Physical Review B **39**, 5792.

[6] Blaha P K, Schwarz GK, Madsen D K, and Luitz J, in WIEN2k, An Augmented Plane Wave + Local Orbitals Program for Calculating Crystal Properties, edited by K. Schwarz (Technical UniversityWien, Wien, Austria, 2001).

[7] Hüpf T, Cagran C, Kaschnitz E and Pottlacher G, 2010 *Thermophysical Properties of Five Binary Copper–Nickel Alloys.* International Journal of Thermophysics, **31**(4): pp 966-974.

[8] Vernes A, Ebert H and Banhart, 2003 Journal Physical Review B68, 134404.

[9] Pottlacher G, 2010 High *Temperature Thermophysical Properties of 22 Pure Metal* Graz, Austria: Keiper.

[10] Seifter A, Pottlacher G, Jäger H, Groboth G and Kaschnitz E, 1998 *Measurements of thermophysical properties of solid and liquid Fe-Ni alloys*. Physical Chemistry, **102**(9): pp 1266-1271.

Chapter 9

Derived Relation of Bulk Modulus

Experimental investigations have shown that the ratio of stress σ_b to strain ε_b is a constant for a given material, provided the external applied force is not too high. This constant is called modulus of elasticity and mathematically can be written as:

$$\frac{Stress}{Strain} = \frac{\sigma_b}{\varepsilon_b} \tag{9.1}$$

Since strain ε_b is a dimensionless quantity, the units of modulus of elasticity are same as that of stress $N \cdot m^{-2}$ or Pa. For three dimensional deformations or strain, where volume is considered, the ratio of stress to strain is called Bulk modulus which is measure of how a substance changes its volume by a uniform compression or expansion, it is denoted by the symbol *K* and its relation is [1]:

$$K = \frac{\frac{F}{A}}{\frac{\Delta V}{V}} \tag{9.2}$$

Where ΔV is the change in original volume V. The elastic constants for some materials are given in Table 9.1 [2]. In this work, a modified relationship of bulk modulus has been derived, while using some of the available parameters from pulse heating setup. To derive this relationship, let us consider a wire of length *l* (our sample wire) with diameter D_0 ($2r_0=D_0$, where r_0 is radius) and cross sectional area *A* clamped from both ends and stretched to the point where there are no kinks in the wire. This wire expands as time passes, the cause of its expansion is the electrical energy $I^2 R t$ given to it, where *I* is current passing through it, *R* is the resistance of the sample wire and *t* is the time for which the expansion occurs. It is important to note that the expansion occurs only laterally not longitudinally (length is constant $\Delta l = 0$) because its ends are properly clamped and fixed. The sketch of sample wire has been shown in the Figure 9.1. The energy supplied to the sample wire work as the main agent to do any kind of stress which

result changes in volume ΔV and hence strain ε_b. In our case, bulk modulus is being measured because of volumetric effects and its relation as mentioned before is:

$$K = \frac{Stress}{Strain} = \frac{\sigma_b}{\varepsilon_b} = \frac{\frac{F}{A}}{\frac{\Delta V}{V}} \tag{9.3}$$

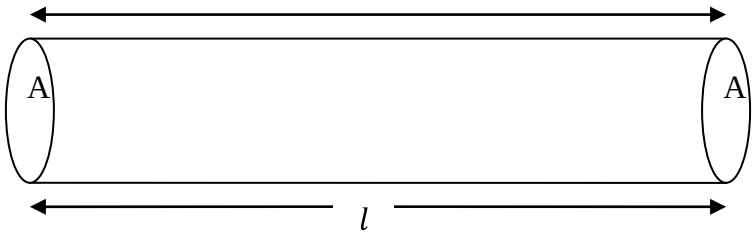

(a)

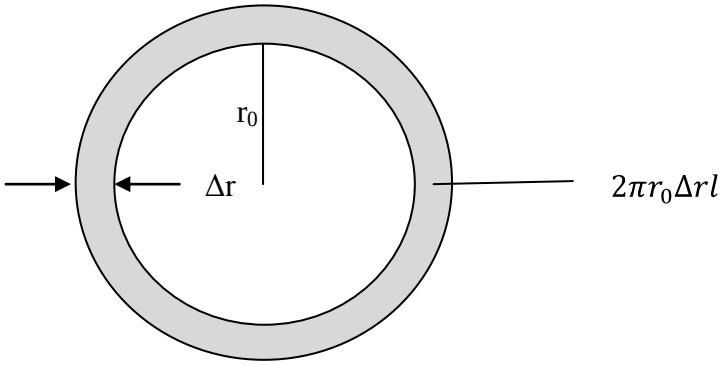

(b)

Figure 9.1. (a) A sample wire of length *l* and cross- section area *A* (b) cross- sectional view of wire sample with initial radius r_0, Δr change of radius and circumferential increase in cross- sectional area $2\pi r_0 \Delta r l$.

Let us take the denominator $\frac{\Delta V}{V}$ for further evaluation or conversion of Equation (9.3), where original volume $V = \pi r_0^2 l$ and change of volume is $\Delta V = 2\pi r_0 \Delta r l$, here r_0 and Δr

are initial radius and change in radius of the sample wire. Substituting these values in above relation we have,

$$\frac{\Delta V}{V} = \frac{2\pi r_0 \Delta r l}{\pi r_0^2 l} \tag{9.4}$$

Simplification of above equation (9.4) leads us,

$$\frac{\Delta V}{V} = \frac{2\Delta r}{r_0} \qquad \text{or} \qquad \frac{\Delta V}{V} = \frac{2\Delta D}{D_0} \tag{9.5}$$

Where $D_0 = 2\ r_0$ and $\Delta D = 2\Delta r$. Here Δr and ΔD are changes in the radius and diameter and r_0, D_0 are original or initial radius and diameter respectively. Simplifying Equation (9.3) we have,

$$K = \frac{\frac{F}{A}}{\frac{2\Delta D}{D_0}} = \frac{F}{A} \cdot \frac{D_0}{2\Delta D} \tag{9.6}$$

Since we know $W = F \cdot dx$ where F is the force acting on the sample wire which causes the expansion and dx is lateral displacement, then we can rewrite it as $F = \frac{W}{dx}$ using this value in Equation (9.6) we have

$$K = \frac{W}{dx \cdot A} \cdot \frac{D_0}{2\Delta D} \tag{9.7}$$

In our cylindrical shaped sample wire, $dx = 2\pi\, dr = 2\pi\, \Delta r$ and area is, $A = 2\pi r_0^2 + 2\pi r_0 l$ using these values

$$K = \frac{\mathrm{W}}{2\pi\Delta r \cdot (2\pi r_0^{\,2} + 2\pi r_0 l)} \cdot \frac{D_0}{2\Delta D} \tag{9.8}$$

$$K = \frac{\mathrm{W}}{4\pi^2 r_0 \Delta r \cdot (r_0 + l)} \cdot \frac{D_0}{2\Delta D} \tag{9.9}$$

If we take $\mathrm{W} = \mathrm{I}^2\mathrm{Rt}$, where I is current passing through the sample during the experimental duration time t and R is the resistance of the sample being investigated.

$$K = \frac{\mathrm{I}^2\mathrm{Rt}}{4\pi r_0 \Delta r \cdot (r_0 + l)} \cdot \frac{D_0^{\,2}}{\Delta D^2} \tag{9.10}$$

or

$$K = \frac{\mathrm{I}^2\mathrm{Rt}}{\pi^2 \cdot (D_0 + 2l)\Delta D^2} \tag{9.11}$$

or $$K = \frac{\mathrm{I}^2\mathrm{Rt}}{G \cdot F} \tag{9.12}$$

where $G.F$ is geometrical factor which is equal to $G \cdot F = \pi^2 \cdot (D_0 + 2l)\Delta D^2$. Based on this Formula (9.11) and by using $\mathrm{W} = \mathrm{I}^2\,\mathrm{R}\,\mathrm{t}$ corresponding changes in diameter measured experimentally from our pulse heating experiments, one gets the solid lines in Figures 9.2 for Platinum and Figure 9.3 for niobium respectively. Compared to results in the literature, dashed lines in Figures 9.2 and Figure 9.3, the values based on Equation (9.11) are much high and their temperature dependence is very high too. The major reason for these higher values is the assumption that the Formula (9.11) includes the whole invested energy, coming from the current ($\mathrm{H} = \mathrm{I}^2\mathrm{Rt}$), into an increase of the volume. But this is not the case: only a part of this energy is utilized to increase the volume, another part is used to increase the internal energy ΔU_{int} of the sample. Therefore, the real or actual bulk modulus is given by the formula

$$K(actual) = \frac{(I^2Rt - \Delta U_{int})}{G \cdot F} \tag{9.13}$$

Comparing results of Equation (9.12) and Equation (9.13), one obtains the percentage of real or actual work done as:

Percentage of real work of the metal under investigation $\frac{K_{actual}}{K_{estimated}} * 100\%$ (9.14)

Similarly percentage of internal energy is $\left[1 - \frac{K_{actual}}{K_{estimated}}\right] * 100\%$ (9.15)

It is concluded that if it is possible to subtract from the above derived Relation (9.11) part of internal energy ΔU_{int} and have only some value of work done W then there is more likely to get the accurate value of bulk modulus.

Despite the higher results of the above derivation, this relation is still useful in the sense that if we take some known (experimental or real) value of bulk modulus in Equation (9.14) then we are able to get percentage of work done by or on the sample. Similarly by using Equation (9.15) one can obtain percentage of internal energy being stored in the sample during expansion and heating.

It has been seen from these evaluations that, in comparatively low temperature, internal energy has much higher values and these values decrease with the rise of temperature, which seems logical, contrary to work done which increase with the increase of temperature. The estimated values of work and internal energies, at different temperatures, for platinum and niobium are shown in Table 9.2 by using experimental values of bulk modulus [3, 4]. The wire explosion after certain time can be understood from the explanation that most of the energy would be utilized to expand the wire at higher temperature which finally results in an explosion of the sample wire.

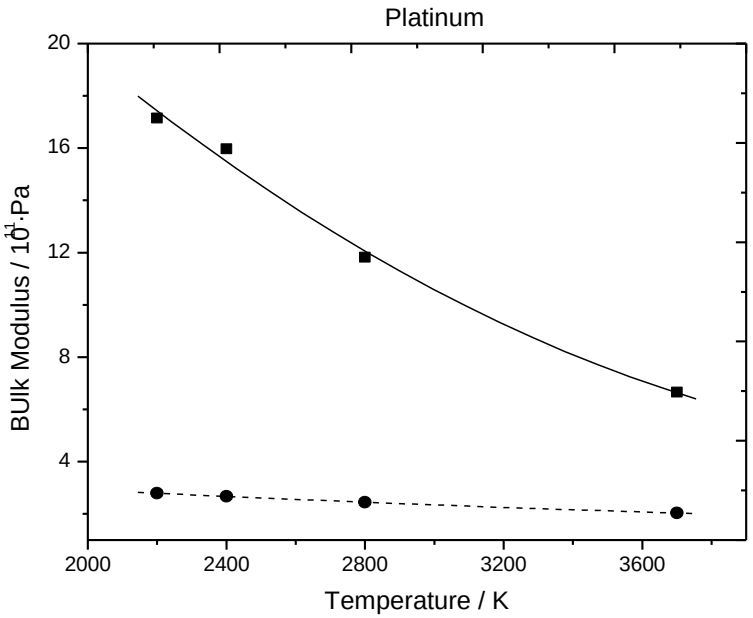

Figure 9.2. Comparison of experimental and estimated Bulk moduli of platinum, dashed line shows literature value and solid line shows estimated value using equation (9.11) [4].

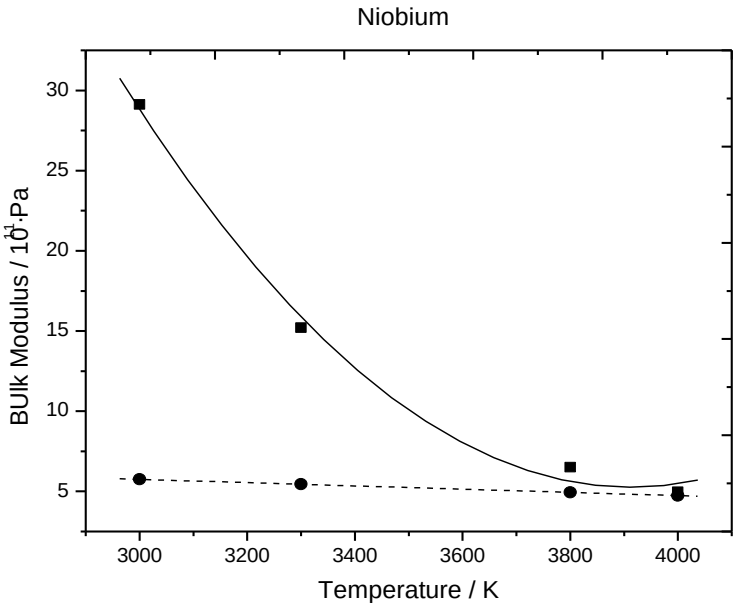

Figure 9.3. Comparison of experimental and estimated Bulk moduli of niobium, dashed line shows literature value and solid line shows estimated value using equation (9.11) [5].

Table. 9.1. Elastic constants for some materials [2].

Elastic constants for some materials			
Materials	Young's Modulus 10^9 N·m^{-2}	Bulk Modulus 10^9 N·m^{-2}	Shear Modulus 10^9 N·m^{-2}
Aluminum	70	70	30
Bone	15	-	80
Brass	91	61	36
concrete	25	-	-
Copper	110	140	44
Diamond	1120	540	450
Glass	55	31	23
Ice	14	8	3
Lead	15	7.7	5.6
Mercury	0	27	0
Steel	200	160	84
Tungsten	390	200	150
Water	0	2.2	0

Table. 9.2. Estimated values of work and internal energies, at different temperatures, for platinum and niobium.

	Platinum			Niobium	
Temperature/ K	Work done in %	Internal energy in %	Temperature /K	Work done in %	Internal energy in %
2200	12.28	87.72	3000	19.76	80.24
2400	16.57	83.43	3300	35.83	64.17
2800	20.72	79.28	3800	67.86	32.14
3700	30.53	69.47	4000	95.22	4.78

References

[1] Halliday D, Resnick R and Walker J 1992, *Fundamentals of Physics*, 9th Edition, John Wiley & Sons, Inc.

[2] *Physics* 2002 Punjab Text Book Board Lahore.

[3] Hixson R S and Winkler M A 1990, *Thermophysical properties of liquid niobium.* High Pressure Research, **4**(1-6): pp 555-557.

[4] Hixson R S and Winkler M A 1993 *Thermophysical properties of liquid platinum.* International Journal of Thermophysics. **14**(3): pp 409-416.

Chapter 10

Uncertainty Analysis

In this section the problem of determining the accuracy of our results and the related uncertainty will be discussed. Most of the known systematic errors have been taken into consideration during data evaluation and they are properly compensated. On the other hand, unknown systematic errors of our measurements are not included within the given uncertainty ranges. Systematic errors can be estimated from the deviation of our result from proven literature data. As our results match very well with literature data and recommended values, most of these errors seem to be corrected. The indicated uncertainties either come directly from the measurements or from the evaluation processes.

There are generally two approaches to estimate uncertainties in measurements: GUM method and (traditional) statistical method [1]. In the former case, the uncertainty is estimated by considering the propagation of the respective uncertainty of each input parameter and in later case the uncertainties are estimated by looking at the distribution of results. The selection of, either of the above mentioned, method for better estimation of uncertainty depends on the experimental setup and data acquisition system.

The uncertainty calculated in this work is according to GUM and a comprehensive detail of the uncertainty analysis of the measurement is discussed in the thesis of Wilthan [2]. A detailed description is omitted here because it is beyond the scope of this work; However, the final estimated maximum uncertainties with a coverage factor of $k = 2$ for each quantity will be stated instead.

As an elaboration, the results of the temperature-dependent uncertainty analysis for the uncompensated resistivity ρ_{IG} of Pt32Cu68 are shown in Figures 10.1 and 10.2. Figure 10.1 shows the expanded ($k = 2$) and relative expanded uncertainties vs. temperature, whereas Figure 10.2 gives an overview of individual contributions of different factors to the total uncertainty in uncompensated resistivity ρ_{IG}. It can be seen in Figure 10.2 that uncertainty in temperature and accuracy of the diameter are the main contributors to total uncertainty. The uncertainty in temperature is due to the fact that at

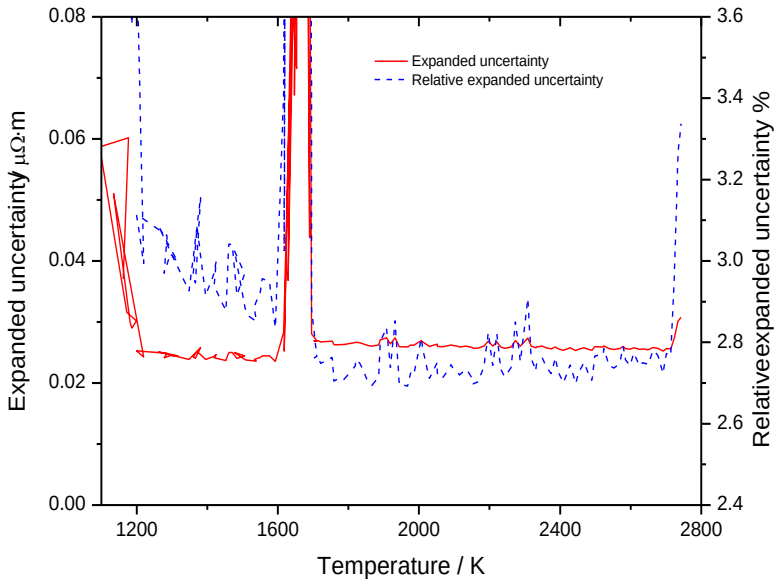

Figure 10.1 Expanded (k = 2) uncertainty estimation for uncompensated resistivity of Pt32Cu68 according to GUM. Red: Expanded uncertainty; Blue: Relative expanded uncertainty.

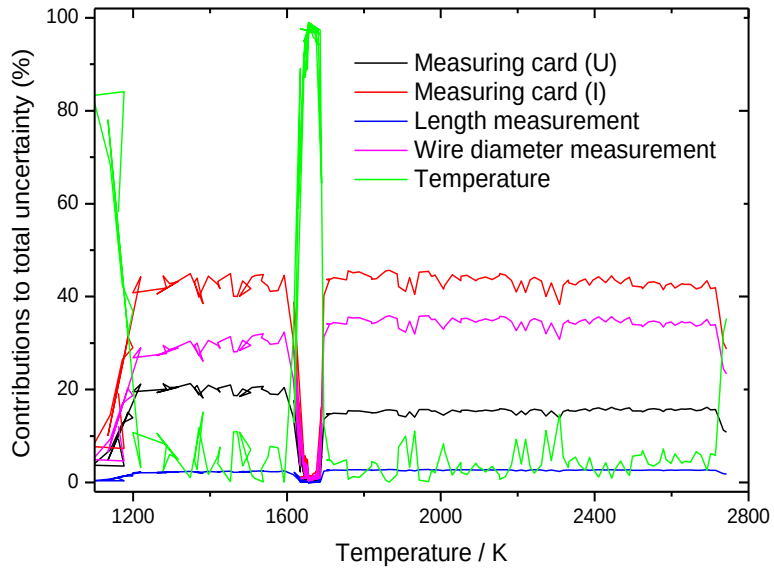

Figure 10.2 Individual contributions to the total uncertainty. Black and red : A/D interface cards in the PC (U, I measurements); Blue: Length of wire; Magenta: Diameter of wire; Green: Temperature.

low temperatures there is a weaker signal-to-noise ratio of the pyrometer signal which is much better at higher temperatures. This uncertainty tends to infinity in the neighborhood of the melting transition which is due to temperature-derivative. This outcome is very sensitivity to the actual uncertainty in temperature although the uncertainty in the temperature signal is constant at melting. Accordingly, the uncertainty analysis for platinum alloys yields the following uncertainties which are shown in Table 10.1 and Table 10.2. The calculated uncertainties which are shown in the Tables are valid for individual measurement values, a reduction of such uncertainties are due to the fact that the mean values were reported as the measured values.

Table 10.1. Relative expanded uncertainties (%) for expansion $D_0^2/D^2(T)$, specific enthalpy H (T), heat capacity c_p(T), uncompensated and compensated resistivity ρ_{IG} (T), ρ_{com} (T), thermal conductivity λ (T) and thermal diffusivity a (T) in the solid phase by a coverage factor $k = 2$.

Solid Phase							
Alloy	$D_0^2/D^2(T)$	H (T)	c_p(T)	ρ_{IG} (T)	ρ_{com} (T)	λ (T)	a (T)
Pt96Co5	3.2	4.2	5	4.1	5.5	6.2	10
Pt68Ru5	3.1	4.8	7.2	3.8	4.6	8.4	11.6
Pt96Cu4	2.1	4.3	7.5	4.1	5.2	8.1	10.2
Pt68Cu32	3.5	6.2	4.3	3.2	7.9	8.6	11
Pt50Cu50	2.2	8	8.6	3.4	4.6	8.2	11.1
Pt25Cu75	2.5	7	7.4	3	3.6	7.6	9.2

Table 10.2. Relative expanded uncertainties (%) for expansion $D_0^2/D^2(T)$, specific enthalpy H (T), heat capacity c_p(T), uncompensated and compensated resistivity ρ_{IG} (T), ρ_{com} (T), thermal conductivity λ (T) and thermal diffusivity a (T) in the liquid phase by a coverage factor $k = 2$.

Liquid Phase							
Alloy	$D_0^2/D^2(T)$	H (T)	c_p(T)	ρ_{IG} (T)	ρ_{com} (T)	λ (T)	a (T)
Pt96Co5	5	4.6	4	3.6	4.2	7.8	10.5
Pt68Ru5	3.2	4.4	4.2	4.2	6	9.2	11
Pt96Cu4	6.8	3	6	3.1	5.6	8	10.6
Pt68Cu32	6.3	4	4.4	2.9	8.1	8.5	8
Pt50Cu50	6	6	6.8	3	4.2	8.8	11.2
Pt25Cu75	5.9	6.4	8.1	2.8	3.8	8	10

References:

[1] GUM 1993 *Guide to the Expression of Uncertainty Measurement*, Geneva, ISO.

[2] Wilthan B, *PhD Thesis* (Technical University Graz, 2005).

Chapter 11

Conclusion

Platinum containing simple binary alloys with different compositions were chosen for this work to investigate and compare the results to the properties of both pure constituent elements of binary alloys, which have been extensively investigated by different authors. According to our knowledge, the data presented for PtCu alloys are new and will be used to solve different problems being faced in jewellery and casting industry. Ideal mixing behavior is confirmed in the investigated PtCu alloys by differential thermal analysis.

It has been observed that the thermophysical properties of binary alloys are greatly influenced by the pure constituent elements. Comparison of experimental results with the literature values shows a quite good match of some of the quantities while for others there are some discrepancies. The measurements of specific heat at constant volume using insulating capillary tubes have been done for the first time for pure copper which gives close agreement to literature values. It seems more appropriate to use sapphire capillary tubes rather than glass capillary tubes due to their higher melting point and less reactivity.

Theoretical investigations have been done for the calculation of specific heat at constant volume and thermal conductivity in the solid and liquid regions respectively for the deeper insight of thermodynamical behaviour of investigated alloys. Theoretically estimated specific heat at constant volume includes both lattice and electronic contribution and gives quite convincing outcome. Anharmonic lattice effects are most likely the cause of the absolute difference between the experimental values of c_p and the theoretical results of $c_{v.}$ Whereas the model proposals given for the prediction of effective thermal conductivity of three different alloy series namely: PtCu, FeNi and CuNi are suitable in the liquid region. It is noted that the experimentally obtained thermal conductivities λ_{exp} and predicted thermal conductivities λ_e by the proposed empirical model are in agreement within 10%.

Future work involving this μs pulse-heating technique will be undoubtedly to focus on more pure metals and alloys. On one hand, thermophysical properties of industrially significant alloys in their liquid phase are of great interest in many applications related to

high temperature technologies, particularly in the casting industry. On the other hand, such measurements on complicated systems can provide important insight into the physics of high speed melting of alloys.

Acknowledgments

The completion of this dissertation is simply because of Creator of the universe, **Allah Almighty**, the most gracious, compassionate and beneficent to His creature, Who blessed me with knowledge and potential to plan my research work. Countless prays for his holy prophet **Muhammad** (P.B.U.H), who is forever, a torch of guidance and knowledge for me and for all humanity.

I owe my indescribable special indebtedness to my teacher and research advisor **Prof. Dr. G Pottlacher**, for supervising this research work and who was very affectionate and cooperative during this research work. He always helped and boosted me whenever I contacted him. I am sure that his guidance will prove valuable source of inspiration throughout my life. Under his continuous kind guidance, creative support and encouragement it became possible for me to complete this research work.

I also extend my gratitude and thanks to **Prof. Dr. H Sorman**, who is with the Theoretical Institute of Physics at TUG, for valuable guidance, suggestions and much needed advices, which assisted me throughout the theoretical part of my research work.

I am very much thankful to the head of the institute, **Prof. Dr. W E Ernst** for giving me this opportunity and pleasant environment to work here as a PhD researcher. I would like to extend my thanks to **Dr. U E Klotz** for providing material and support with experiments at fem, Schwäbisch Gmünd Germany. A word of gratitude to my entire lab fellows, Dr. Claus Cagran, Dr. Boris Wilthan, Dr. Thomas Hüpf, Dr. Harald Reschab, Baric Pavao, Peter Kerschenbauer, Kirmanj Aziz, Alexander Schmon, Andreas Sanbach, Markus Kurz, Richard Romirer Maierhofer who helped and cooperated with me. I thank all the members of the institute for their help at various occasions in offices and elsewhere.

No words to describe my sweet sensation of respect about my parents and family, who supported me throughout my carrier, and without their shadow of love, perhaps, it could be impossible to attain this goal. Finally, I would like to acknowledge the Higher Education Commission, Pakistan, for supporting the doctoral studies.

SHAHID MEHMOOD